Sustainable
Energy & Fuels

ROYAL SOCIETY
OF CHEMISTRY

REVIEW

View Article Online
View Journal | View Issue

Check for updates

Cite this: *Sustainable Energy Fuels*, 2021, **5**, 5366

Redox flow batteries: a new frontier on energy storage†

P. Arévalo-Cid, * P. Dias, A. Mendes and J. Azevedo*

Received 3rd June 2021
Accepted 12th September 2021

DOI: 10.1039/d1se00839k

rsc.li/sustainable-energy

With the increasing awareness of the environmental crisis and energy consumption, the need for sustainable and cost-effective energy storage technologies has never been greater. Redox flow batteries fulfill a set of requirements to become the leading stationary energy storage technology with seamless integration in the electrical grid and incorporation of renewable energy sources. This review aims at providing a comprehensive introduction to redox flow batteries as well as a critical overview of the state-of-the-art progress, covering individual components, economic analysis and characterization techniques.

1. Introduction

Energy consumption is increasing on a daily basis, in response to a growing world population and a booming industrial development, particularly in densely populated countries such as India and China. Energy production still relies mainly on fossil fuels that urgently require a substitute, given their finite resources and negative environmental impact. Renewable energies, such as solar or wind, are the alternative to reduce their usage. Renewables are predicted to become the primary energy source by 2050, with an average annual percentage growth rate of 3.6%,[1] with solar and wind energies responsible for 70% of total renewable production.[1] However, the intermittent nature of both sources demands the development of safe, environmentally-friendly and low-cost energy storage systems to bridge the gap between generation and consumption.

Energy can be stored by separation of electrical charges or converted to potential, kinetic or electrochemical energy.[2] Separation of charges is the working principle of capacitors and supercapacitors, which have a rapid response, but low energy density, being used basically for power management.[3,4] Sodium-ion batteries are proposed to compete with lithium-ion batteries, due to their lower price and the apparition of new materials for high-voltage and high-capacity systems.[5] However, they maintain some common problems of safety and recyclability, as well as the necessity of specific electrodes with high Na storage, still in the first stages of development.[6] Pumped hydro and compressed air storage systems can accumulate large quantities of energy, but are limited by geographical aspects and produce a remarkable environmental impact due to the land use and the indirect specific CO_2 emissions, especially related to the construction of the reservoir.[7] Kinetic energy can be saved by using flywheels, which possess rotating disks connected to an electrical machine acting as motor or generator, depending on the load angle;[8] flywheels can reach peaks of high power and energy density, but low overall efficiency for prolonged periods, and are useful for their implementation in rapid energy response necessities, such as vehicles.[9]

Electrochemical devices offer elevated variability and adaptability, meeting the requirements of each application. Among the different possibilities, several authors highlight redox flow batteries (RFBs) for their interjection with renewable energy resources with peak-hour load leveling, presenting a high efficiency and low cost per unit energy and cycle[10] for large working lifetimes, providing the ability to enhance the stability of the grid.[11] RFBs offer great versatility and are especially interesting for their use in stationary applications, that require a great quantity of energy. However, before their massive scale-up and implementation, some aspects require further research, such as the energy density, the development of low-cost components, with special attention to the separators, and the optimization of the flow system.

This review offers essential guidelines needed for the investigation on RFBs, covering from fundamental principles, requirements and state-of-the-art research for each component of the system to characterization techniques. Finally, the authors propose a group of research topics with the potential to introduce a new step on the evolution of RFBs and help the scientific community to advance renewable energy storage systems.

LEPABE, Laboratory for Process Engineering, Environment, Biotechnology and Energy, Faculty of Engineering of the University of Porto, Rua Dr Roberto Frias, 4200-465 Porto, Portugal. E-mail: pabloarevalo@tecnico.ulisboa.pt; jcazevedo@fe.up.pt

† Electronic supplementary information (ESI) available. See DOI: 10.1039/d1se00839k

2. Redox flow batteries

2.1. Working principle

Electrochemical storage is carried out through reduction and oxidation reactions of chemical species. The particularity of RFBs is that the active species are dissolved in liquid electrolytes, with the reaction occurring in the solid–liquid interface between the active solution and an inert electrode, as a difference with other batteries as Li-ion batteries or solid-state batteries, where the reaction takes place in the solid electrodes. Fig. 1 shows a general scheme of a RFB, consisting of a cell (marked with a blue dashed rectangle), flow system (electrolyte tanks, pumps, pipes) and electrical controls (black). Active species (A and B) are dissolved in a liquid and are separated by an ion-exchange membrane (IEM) (grey). Both half-cells are connected by conducting electrodes (black), which are chemically inert. For this example, it will be considered that $E^0(\mathrm{B/B^-}) > E^0(\mathrm{A/A^-})$ and both reactions involve one-electron exchange. Accordingly, A/A$^-$ and B/B$^-$ are the negative and positive redox pairs and their electrolytes are known as anolyte and catholyte, respectively. Electrochemical processes take place on the electrode–electrolyte interface. Reactions are summarized in eqn (1).

Considering $E^0(\mathrm{B/B^-}) > E^0(\mathrm{A/A^-})$:

$$\begin{array}{lll} & \text{Charge} & \text{Discharge} \\ \text{Catholyte} & \mathrm{B^- \rightarrow B + e^-} & \mathrm{B + e^- \rightarrow B^-}\ \text{(a)} \\ \text{Anolyte} & \mathrm{A + e^- \rightarrow A^-} & \mathrm{A^- \rightarrow A + e^-}\ \text{(b)} \\ \text{Global} & \mathrm{B^- + A \rightarrow B + A^-} & \mathrm{B + A^- \rightarrow B^- + A}\ \text{(c)} \end{array} \quad (1)$$

During the charge (red arrows), B$^-$ is oxidized to B, losing one electron which is driven to the other half cell where reacts with A, reducing it to A$^-$. B and A$^-$ are the charged species in this system. State-of-charge (SoC) for the battery is defined as the percentage of species in a charged state in respect to the discharged species, B$^-$ and A. Cations X$^+$ pass through the membrane to maintain the charge neutrality. The solution in the cell is continuously renewed because of the flow of the electrolyte, maintained by pumps, which are connected to an external tank that acts as an electrolyte reservoir. Discharge entails the inverse process, which is spontaneous and results in a potential difference equal to the difference between both reduction potentials, $E^0(\mathrm{B/B^-}) - E^0(\mathrm{A/A^-})$. This potential value is directly related to the energy quantity that a battery can store.[12,13] Thus, the selection of redox couples is a critical

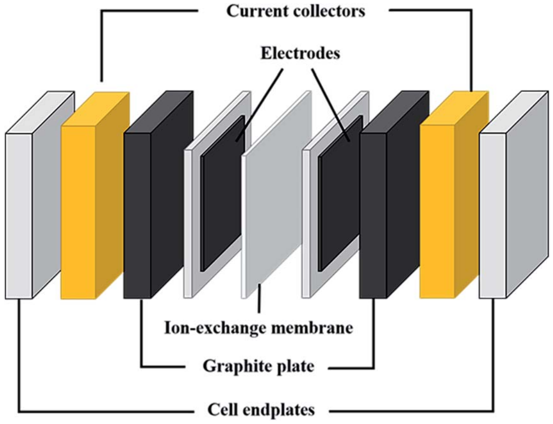

Fig. 2 Scheme of the main components of a RFB cell.

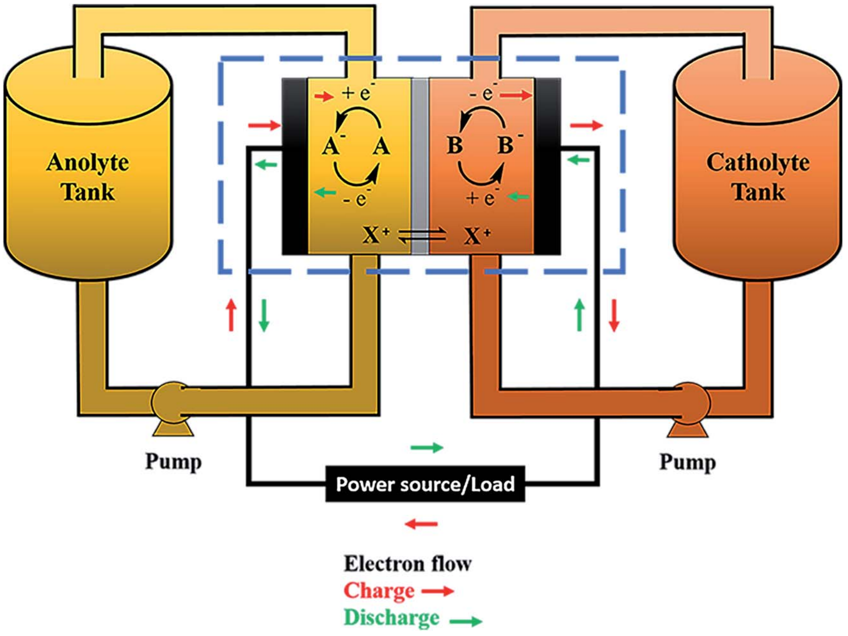

Fig. 1 General scheme of a RFB. Redox reactions take place inside the cell (marked with a blue dashed rectangle) on the surface of the electrodes (black rectangle). The electrolyte is continuously renewed by pumping the solution from the tanks. The direction of electron flow (charge or discharge) is managed by the electrical components, acting as a power source or loading the energy from the battery.

parameter on the battery design and researchers have tested a wide range of these pairs, as will be discussed in Section 4.

Fig. 2 shows a scheme of the main components of a general cell for RFBs (marked with a blue square in Fig. 1). Along with the cell endplates and the current collector, which are common components of most electrochemical devices, some specific characteristics from these types of systems are remarkable. The graphite plates define the pattern of the flow in contact with the electrodes; the serpentine and interdigitated flow fields are the typical flow fields used in the RFBs, as will be described in detail in Section 7.1. The electrodes appear in the scheme inside a gasket that provides fixed support for their attachment into the cell. Finally, the IEM, situated between the two symmetric half-cells, acts as the separator of both electrolytes; it is responsible for avoiding, as much as possible, the crossover of active species, but with the ability to exchange charged species to maintain charge balance on both sides. These three elements (graphite plates, electrodes and membrane) are suitable for systematic optimization studies, as previously reported in the literature,[14–19] and thus, will be treated more extensively in subsequent sections of this review.

Exist a series of parameters that serve for the evaluation of the performance of a RFB. The most commonly employed are described below.

Capacity (C) is a measure of the quantity of energy stored in the battery is defined as a product of the current that is drawn from the battery while the battery is able to supply the load until its voltage is dropped to lower than a certain value for each cell.[20] C is calculated as:

$$C = \frac{Q}{V} = \frac{It}{\Delta V} \tag{2}$$

where I is the applied current in A, t is the time in s and ΔV makes reference to the voltage interval defined for the experiment in V. The working lifetime of a battery is commonly estimated by the evolution of C with the number of charge–discharge cycles. It is expressed as the percentage of C that remains after a certain number of cycles. This parameter is known as capacity retention.

Coulombic efficiency (CE) represents the usable charge with respect to the total charge stored by the battery. CE is calculated as the ratio between total electrical charge drawn during the discharge and charge (eqn (3)). Gives information of the storage capacity loss during the charge–discharge process. Main losses of capacity are the result of the active species crossover and side reactions. The coulombic losses can be reversible or irreversible depending on the reaction and nature of electroactive species.

$$\mathrm{VE} = \frac{V_{\mathrm{Disc}}^{\mathrm{cell}}}{V_{\mathrm{Char}}^{\mathrm{cell}}} \tag{3}$$

Losses due to resistance, overpotential and polarization of the battery are measured as voltage efficiency (VE).[21] A reduction of the discharge voltage range is produced by ohmic losses. VE is defined as the ratio of cell discharge voltage *versus* the cell charge voltage (eqn (4)).

$$\mathrm{CE} = \frac{Q_{\mathrm{Disc}}^{\mathrm{total}}}{Q_{\mathrm{Char}}^{\mathrm{total}}} = \frac{\int I_{\mathrm{Disc}}\mathrm{d}t}{\int I_{\mathrm{Char}}\mathrm{d}t} \tag{4}$$

The effect of all the losses on the final performance of the battery is included in the energy efficiency (EE), which is the product of CE and VE, also called round-trip energy efficiency in a battery system (often excluding system losses, *e.g.* pumps, electronics, *etc.*).

2.2. Tecno-economic benefits

The capacity of static electrochemical energy storage devices is determined by cell construction. In contrast, RFBs can store large quantities of energy independently of the size of the cell, by increasing the volume of electrolytes in the external tanks. In such a way, the volume can be adapted depending on the application, providing power for periods from a few hours to several days.[2,22] Even more, the same system can be upgraded, depending on the demand, without substituting the entire battery – just changing the size of the reservoirs – substantially reducing the cost of modification and increasing versatility.

The configuration of a RFB containing different compartments offers the possibility of selective substitution of the components, that could present fails or degradation, reducing the cost of maintenance and enlarging the useful life of the system. This is not an option for classic batteries, where the system needs to be entirely disassembled to separate a central component.

Batteries with solid-state electrodes as active materials present increased capacity decays when forced to a deep charge/discharge,[23,24] with degradation of the electrodes.[25] This is not a risk for flow batteries, where the electrodes act as a medium for redox reactions, not as active species. In the case of redox pairs degradation, the electrolyte can be renewed directly from the tanks, and in some cases regenerated.

General use of non-rare metallic electrodes entails a reduction of the total price, removing heavy metals like nickel, cobalt or cadmium, constituents of other types of batteries. Alternative carbon-based electrodes together with iron, bromine or organic molecules, such as anthraquinones, based electrolytes with prices lower than \$5 kg^{-1},[26] improve the perspectives on a future scale-up for stationary energy storage.

As previously reported,[27,28] the most common energy storage systems, Pb and Li batteries, present security risks, not only of employment but also procurement, refining and manufacturing processes. During cycling, these systems can lead to internal short-circuits due to the formation of lithium dendrites by the inhomogeneous current density distribution during charging,[29] which represent the most dangerous failure due to its difficult external control. The self-heating causes thermal runaway that could be enough to reach the decomposition temperature of active species or the ignition point of the solvents, promoting combustion or, in the worst of the cases, explosion.[30] The possible appearance of internal short-circuits in RFBs, which is an unusual concern, was studied by Whitehead *et al.*[31] After forcing an internal short-circuit in the stack of a RFB, the temperature of the system only slightly increased (around 1 K); the volume of the tanks is always higher than that inside of the cells, so heat can be slowly transferred to the electrolyte, without risk of smoke or fire.

A low rate of recycled batteries, as in the case of Li, supposes an increasing environmental impact.[32] The introduction of new materials, like graphene oxide, has been studied as an alternative to reduce the damage of classical systems, but fossil fuel depletion or water eco-toxicity still remain as major concerns.[33] The global warming potential of a typical vanadium redox flow battery (VRFB) is lower than those of the classical systems, as exposed by Rydh *et al.*[34] Additionally, RFBs can increase their environmental-friendly character by the use of metal-free redox pairs or even natural products as active species, as will be developed later in the review.

3. Types of RFBs

3.1. All liquid flow batteries

In this configuration, both electrolytes are liquids and do not suffer any phase change during the entire charge/discharge process. Electrodes provide the support for redox reaction and conduction for the released electrons (Fig. 3a). A classic example of these systems is the VRFB.

3.2. Solid or gas hybrid RFBs

At least one of the active species is found as a solid or a gas, usually accompanied by a phase change during the charge/discharge process. In the case of solids, the active species is electrodeposited on the electrode surface, generally during the charge, and is dissolved again during discharge (Fig. 3b). This produces a limitation due to the size of the electrodes, which are covered by the deposited solid. The electrolyte is composed of metallic ions, as Fe[35,36] or Pb,[37,38] but the most utilized are the Zn-based RFBs. Zn has a large negative potential ($E^0 = -0.76$ V *vs.* SHE), being useful as an anode, increasing the energy density of the cell.[39] At such low potentials, hydrogen evolution is usually found. However, Zn reactions as anode have been demonstrated as an efficient process in aqueous electrolytes (both acidic and alkaline) due to the large hydrogen overpotential for zinc electrodeposition on inert substrates.[40]

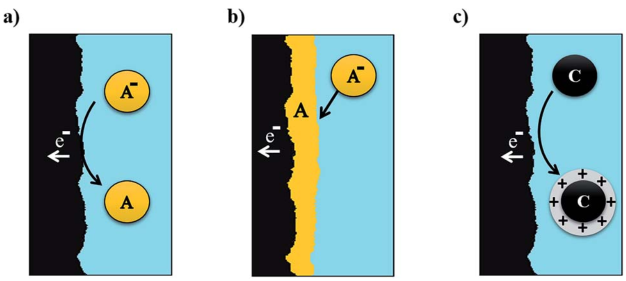

Fig. 3 Schematic representation of the electron transfer phenomena for the different types of RFB: all liquid (a), metal hybrid battery (b) and semi-solid (c).

Substitution of one half-cell by gas offers new possibilities, improving costs and environmental impact. Catholyte can be exchanged by a flow of air or oxygen, but an electrocatalyst is needed on the surface of the electrode in contact with the airflow, in order to reduce oxygen reduction overpotential.[41–43]

3.3. Semi-solid flow batteries

In an effort to obtain the best features from all liquid and hybrid RFBs, semi-solid batteries combine both concepts. In semi-solid flow batteries, electrolytes consist of a slurry composed of a percolating network of electronically-conducting particles and charge-storing active particles in a liquid electrolyte (Fig. 3c). Electronic exchange is produced with the intervention of a solid phase, but in this case, it is carried out on the surface of conducting material that is introduced in the form of a suspension.[44] Stability and adequate flow dynamics are required for the use of these slurries. The active material is stored in the external tank, as for pure RFBs. Nevertheless, in this case, species are not limited by their solubility, showing improved volumetric capacity.[45]

4. Electrolytes

4.1. Electrolyte requirements

According to the working principle of RFBs, the electrolyte is responsible for the electrochemical energy storage, being the carrier of the electroactive species. Several physical and chemical criteria need to be met for an efficient device. The desirable characteristics are here summarized:

4.1.1 **Wide potential window.** One of the factors that dictates the energy density of a RFB is the cell potential (potential difference between the two standard potentials of the redox couples involved). The separation between the redox potential of anolyte and catholyte species should be maximized to obtain a high cell potential, but it is limited by the electrochemical stability range for the solvent. As an example, for water in normal conditions, this gap cannot exceed 1.23 V, which is the difference between water oxidation and reduction. Consequently, the larger the window, the wider the range for the optimization of new redox species.

4.1.2 **High solubility.** Besides the cell potential, the solubility of redox couples also determine the energy density. An elevated effective concentration, calculated as the solubility multiplied by the number of electrons transferred in the redox reactions,[46] will lead to a high energy density.

4.1.3 **High ionic conductivity.** Within the charge/discharge process, active species must migrate from the bulk electrolyte to the electrode–electrolyte interface to achieve the redox process. In the same way, counter ions must be driven through the membrane to conserve the charges on both sides. For both processes, great mobility is required in the form of ionic conductivity. This factor is determined as the main cause of ohmic losses in non-aqueous RFBs (NARFBs).[47]

4.1.4 **Fast kinetics electrolyte–electrode.** The electronic exchange associated with the charge/discharge of the electrolytes takes place on the electrode surface. Elevated reaction rates minimize side reactions, such as recombination or gas evolution (oxygen, hydrogen),[48] and cell resistance,[49] leading to higher efficiencies. Improved charge transfer kinetics also avoid degradation of electrode surface.[50] A great effort is made by the scientific community on mechanistic studies, necessary for the improvement of reaction kinetics.[18] Developments, mainly focused on the optimization of electrodes, will be discussed in Section 6 (Electrodes).

4.1.4 Low viscosity. A constant flow of electrolyte is used to store energy in external electrolyte reservoirs. A higher viscosity supposes a greater effort from the pumping system, reducing EE and pressure drops.[51,52] To decrease the energy spent on running the device, a low viscosity is desired. Additionally, as the RFB charges and the SoC increases, the electrolyte composition changes, affecting its properties. It is important to maintain a low viscosity independently of the level of energy storage.[53] Finally, mass transfers are directly related to viscosity. In this sense, Geoffroy *et al.*[54] found a relationship between the activation energy of viscous flow and ionic conductivity, with their product constant independently of the temperature. Hence, an increase in viscosity causes an instantaneous decay of conductivity.

4.1.5 High chemical and thermal stability. The design of a long-term energy storage device requires the stability of the electrolyte under working conditions. New species of reduced solubility/activity can be generated during the charge/discharge process, reducing the efficiency of the battery. The use of elevated concentrations, which provide high energy density, can promote this degradation, as in the case of negative electrolyte of VRFBs, resulting in the formation of non-soluble $V_2(SO_4)_3$.[55] For some organic structures, the formation of reactive intermediate species during the process of charge/discharge could lead to irreversible deactivation by the formation of dimers[56] or free radical reactions.[57] Thermal instability problems were detected also for VRFBs, resulting in the thermal precipitation of V(v) for temperatures above 40 °C, as was reported by Skyllas-Kazakos *et al.*[58]

4.1.5 Low cost. A potential real application of RFBs is determined by the final price of the technology. Economic models can assist in the selection of cost-driven materials for the preparation of electrolytes, based on their composition (solvent, redox pairs, supporting salt) and potential energy density, as proposed by Dmello *et al.*[26] Aqueous electrolytes present practically no costs due to the solvent but are limited by the potential window. Organic solvents overcome this limitation, adding the possibility of using low molecular weight redox pairs, minimizing the price per mass unit of active species. However, the cost of the solvent itself increases the investment required to develop the system. Darling *et al.*[59] defend with their model that NARFBs need at least an open-circuit potential (OCP) of more than 2 V to be economically viable.

4.1.6 Safe and environmentally friendly. Electrolyte must be safe not only during the functional stage but also during its manufacturing and disposal. Low flammability and toxicity of both anolyte and catholyte are desirable for their manipulation. One of the main advantages of RFBs, compared with other energy storage systems, is the possibility of replacing the electrolyte directly from the tanks, introducing previously charged species, useful for fast energy demands, or to solve possible degradation. This renovation process leads to the generation of residues, whose environmental impact must be controlled and minimized. Reduce polluting metals and the content of organic solvents[60] must be a trend in batteries research.

4.2. Solvents

The solvent provides the supporting media for the redox process evolution. Its nature determines factors such as potential window, solubility, ionic conductivity and viscosity. An evolution of the selection of solvents for RFBs can be appreciated, from water to liquids with complex structures.

4.2.1 Classical solvents: aqueous *vs.* non-aqueous media. The first generation of RFBs were all based on aqueous electrolytes.[61] Water has clear advantages given its almost negligible price, great conductivity, high solubility of inorganic salts, used generally as supporting electrolytes, and charged species as Fe^{3+}, Br^-, Cr^{3+}, *etc.* As is well known, redox potentials of species that involve H^+ or OH^- on the reaction vary with pH value.[62] Modulation of these parameters is quite simple in aqueous media by the use of soluble acids, bases or buffer solutions. A moderated viscosity, a wide temperature range and no-environmental impact complete the benefits of water as a solvent. The main drawbacks are the functional incapacity for extreme temperatures (under 0 °C and over 100 °C) and the previously discussed limited potential window (1.23 V), due to the evolution of oxygen or hydrogen; the cell potential is, consequently, reduced. Few authors describe slightly greater potentials in aqueous media, given high over-potentials for hydrogen/oxygen evolution reaction at electrode surfaces[63] or using neutral pH where the kinetics of water electrolysis is not favored,[64] but always below the 2 V barrier.

To overcome this issue, in 1984, Singh *et al.*[65] proposed the use of organic solvents for RFBs. They provide a wider working potential (over 5 V) and temperature (more than 150 °C) ranges, even under 0 °C, where aqueous solutions are not suitable. New chemistries can be investigated with the incorporation of organometallic and organic compounds, with improved solubility in this kind of media. Nevertheless, non-aqueous solvents generally manifest low conductivities, being necessary the presence of supporting electrolytes, which are more complex than those used in aqueous solution and compete in terms of solubility with the redox pairs themselves,[66] decreasing the energy density. Additionally, solvents as acetonitrile, largely employed for these systems, possess elevated volatility, leading to losses of solvent and safety problems (flammability, toxicity).[67] Table 1 summarizes the properties of some of the most used organic solvents in electrochemistry, compared with water.

4.2.2 Novel solvents: ionic liquids and deep eutectic solvents. To avoid the problems associated with classical solvents, new liquid compounds have been proposed for their use in RFBs.[73–75] Room-temperature ionic liquids (ILs) are salts composed by large ions (at least, one of them) and a cation with

Table 1 Properties of the classical solvents employed for RFBs electrolytes

Solvent	T_{work} (°C)	Conductivity (mS cm^{-1})	Viscosity (cP)	$E_{\text{window}}{}^{a}$ (V)
Distilled water	0–100	1×10^{-3}	1.1^{b}	1.23
Acetonitrile (ACN)	-45–82^{b}	1.335×10^{-3c}	0.341^{c}	5.5
Propylene carbonate (PC)	-49–241^{d}	0.23×10^{-3c}	2.53^{c}	3.6
N,*N*-Dymethylformamide (DMF)	-61–153^{b}	0.69×10^{-3c}	0.802^{c}	4.4
1,3-Dioxolane	-95–74^{e}	0.036×10^{-3c}	0.6^{c}	4.0^{f}

[a] Extracted from ref. 68. [b] Extracted from ref. 66. [c] Extracted from ref. 69. [d] Extracted from ref. 70. [e] Extracted from ref. 71. [f] Extracted from ref. 72.

a low degree of symmetry. These geometries reduce the lattice energy of the crystalline form of the salt and hence lower the melting point, enough to be found as liquids at room temperature.[76] Properties of ILs depend on the structure of their ions, offering an elevated tunability for the final application. Especially important is their broad range of working temperatures, higher than water or common solvents. In this sense, 1-ethyl-3-methylimidazolium chloride-aluminum chloride is a reference, known as [EMIm]Cl–$AlCl_3$, which can be thermally stable from almost −100 °C to around 200 °C, depending on the molar ratio [EMIm]Cl:$A1Cl_3$.[77] ILs can dissolve substances within a wide range of polarities, providing new possibilities of combination of redox pairs. They present low flammability and low vapour pressure, reducing both the losses of the solvent by evaporation and the environmental impact. Nevertheless, they present several limitations, such as major viscosity,[78] sensitivity to the presence of water and high cost when compared with commonly used solvents.[79] An alternative can be found in deep eutectic solvents (DESs), which present similar features to ILs, but with improved stability and price.[80] A DES is liquid at room temperature, which is formed by the combination of a hydrogen bond acceptor, generally choline chloride, with hydrogen bond donors such as urea, carboxylic acids or polyols (see Fig. 4).[74,81] According to this, research on DES-based RFBs electrolytes is attracting more attention at the expense of ILs. Table 2 summarizes the studied RFBs containing ILs or DES so far.

Table 3 highlights the main advantages and drawbacks of the different categories of solvents.

4.3. Redox pairs

Active redox species determine the cell potential and energy density, turning them the object of a large number of research articles and reviews during the last few years.[46,91–93] To maximize both parameters, the redox potentials of the species involved must be as distanced from each other as possible (always within the potential window of the solvent). High solubility and stability are required of both oxidized and reduced forms, with minimum degradation of the species. Kinetics of the reaction on the electrode surface must be fast, only limited by mass transfer. At last, safety, price and abundance are considered important regarding a further scale-up.[94]

4.3.1 Inorganic species. Historically, metallic inorganic ions were the first group of tested species for RFBs. Most of them present at least two oxidation states with good solubility and stability in aqueous solution within a broad range of reduction potentials. The first successful RFB prototype was the iron–chromium flow battery, developed by the National Aeronautics and Space Administration (NASA) in the early 1970s.[95] The combination $Fe^{3+}/Fe^{2+}//Cr^{3+}/Cr^{2+}$ generates a standard potential of 1.18 V, exploiting the 1.23 V potential window of water. However, the reduced development of membranes led to a crossover of species, reducing critically the cell capacity. A revolutionary advance was introduced by Skyllas-Kazacos *et al.* in the 1980s with the development of the VRFB.[96,97] Vanadium possesses several stable oxidation states with a difference between their reduction potentials large enough to build two different redox pairs for their employment in RFBs, resulting in a theoretical cell potential close to the maximum available for aqueous solutions.

Catholyte:

$$VO_2{}^{+} + 2H^{+} + e^{-} \leftrightarrow VO^{2+} + H_2O,\ E^0 = 1.00\ \text{V} \tag{5}$$

Anolythe:

$$V^{3+} + e^{-} \leftrightarrow V^{2+},\ E^0 = -0.25\ \text{V} \tag{6}$$

Full reaction:

$$VO_2{}^{+} + 2H^{+} + V^{2+} \leftrightarrow VO^{2+} + H_2O + V^{3+},\ E^0 = 1.25\ \text{V} \tag{7}$$

Catholyte is composed by the pair $VO_2{}^{+}/VO^{2+}$, with oxidation states +5 and +4 respectively. In the anolyte, the active species are V^{3+} and V^{2+}. The advantages of this configuration are not only great potential but a solution to crossover problems. If V^{3+} goes through the membrane to the positive tank, is oxidized to VO^{2+} and then to $VO_2{}^{+}$ during the charging. In a similar way, if VO^{2+} passes to anolyte tank, is reduced spontaneously to V^{3+}, which is incorporated into the charge–discharge cycle, according to reaction (8).[98] The chemical combination of the VRFB results in reduced losses due to contamination of the electrolytes. However, the crossover is not removed and capacity fading appears as a consequence of concentration gradients, of each of the ions across the membrane.[99]

$$VO^{2+} + 2H^{+} + e^{-} \rightarrow V^{3+} + H_2O,\ E^0 = 0.34\ \text{V} \tag{8}$$

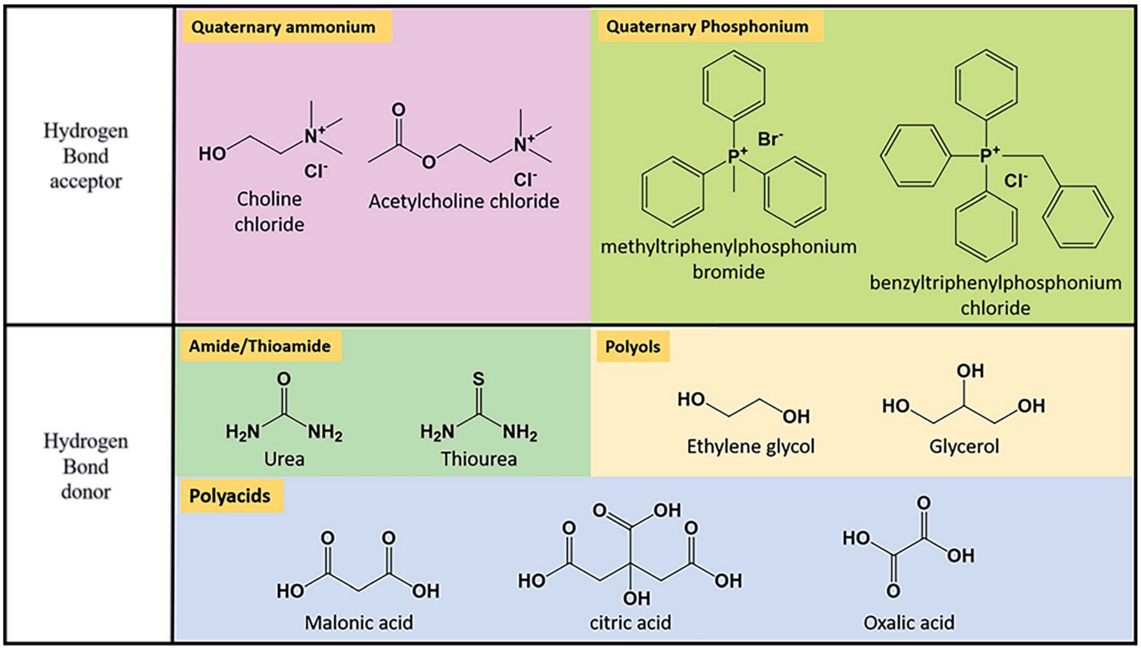

Fig. 4 Summary of typical hydrogen bond donors and acceptors for the preparation of DESs.

Authors continue their research on the application of different inorganic species due to the simple preparation of electrolyte, generally from metallic salts, and their good solubility in water. Some examples of these species are Mn^{3+}/Mn^{2+},[100–102] Ce^{4+}/Ce^{3+},[38,103–105] Fe^{3+}/Fe^{2+},[73,86,106,107] I_3^-/I^- (ref. 63 and 108–111) or S^{2-}/S_2^{2-}.[109,112] The focus has been increased for the use of inorganic electrolytes due to the development of metal-based hybrid RFBs. Generally, an electrode containing a solid metal is submerged in a solution of cations of the same metal, obtaining a solid–liquid redox pair. Due to the reduction potential of metals, they will act as the negative half-cell of the battery. Zn^{2+}/Zn couple is the most studied example for aqueous RFBs, due to its reduced price, good large potentials in both acidic and alkaline medium (eqn (9) and (10)) and high efficiency of electrodeposition process (charge), with current efficiencies of over 90%.[40] These properties have made the energy storage system orbit around the combination of Zn^{2+}/Zn pair with different nature species, such as other metals,[103,104] halogens as Br_2 (ref. 113–115) and I_2,[63,116] organic molecules[117,118] and even with gases,[119] with the Zn–air battery as the most representative case.[120,121]

Acid

$$Zn^{2+} + 2\,e^- \rightarrow Zn,\ E^0 = -0.763\ \text{V} \tag{9}$$

Table 2 Ionic liquids and deep eutectic solvents based RFBs

Solvent	Redox pair	E_{cell} (V)	η_e (%)	η_Q (%)	Reference
ILs					
$[C_2C1Im][N\ (Tf_2)]$	$[V(acac)_3]/[V(acac)_3]^-//[V(acac)_3]^+/[V(acac)_3]$	2.0	22	72.3	75
$[Cu(ACN)_4][Tf_2N]$	$[Cu(ACN)_4]^+/Cu/[Cu(ACN)_4]^+/[Cu(ACN)_4]^{2+}$	0.9	10–30	>80	82
DESs					
Ethaline (ChCl : EG 1 : 2)	$[CuCl_3]^{2-}/Cu//[CuCl_4]^{2-}/[CuCl_3]^{2-}$	0.773	52.1	94.3	74
Ethaline (ChCl : EG 1 : 2)	$[FeCl_4]^{2-}/Fe//[FeCl_4]^-/[FeCl_4]^{2-}$	1.24	41.5	85.9	73
Ethaline (ChCl : EG 1 : 2)	$[ZnCl_4]^{2-}/Zn//[FeCl_4]^-/[FeCl_4]^{2-}$	1.02	78.1	91.8	73
Ethaline (ChCl : EG 1 : 2) with 0.5 M $TEABF_4$	$[V(acac)_3]/[V(acac)_3]^-//[V(acac)_3]^+/[V(acac)_3]$	2.01	25–31	49–52	83
$[FeCl_2(urea)_4]Cl_2$	$Li+/Li//[FeCl_2(urea)_4]^+/[Fe\ (urea)_5]^{2+}$	3.4		∼100[a]	84
$[AlCl_2(urea)_n]^+$ + 0.5 M of LiCl + Dichloroethane	$[AlCl_2(urea)_n]^+/AlCl_4^-//I3^-/I^-$	0.9	78	∼100	85
Urea : EG 1 : 3 + EC/DMC	$Li^+/Li//[Fe(OD)_6]^{3+}/[Fe(OD)_5]^{2+}$	3.45		100	86
LiTFSI–NMePh–urea + DME/DCE	$Li^+/Li//NMePh/NMePh$	1.9		95	87
$[ZnCl(acetamide)_n]Cl$ + EC/DMC + LiTFSI	$[ZnCl(acetamide)_n]^+/Zn//[Fe(phen)_3]^{3+}/[Fe(phen)_3]^{2+}$		78	100	88
$AlCl_3$–urea	$[AlCl_2(urea)_n]^+/AlCl_4^-//H_2BQ/H_2BQred$	1.5	89	99	89
ChCl : urea 1 : 2	$V^{3+}/V^{2+}///Fe^{3+}/Fe^{2+}$	0.96	64.7	94.8	90

[a] After second cycle.

Table 3 Comparison of the most relevant characteristics of solvents for their use in RFBs

Solvent	Advantages	Disadvantages
Water	• High conductivity • Reduced cost • Good viscosity • No environmental impact	• Moderated liquid range • Limited potential range
Organic solvents	• Reasonable price • Large potential windows • Variable viscosity Large liquid range	• Low ionic conductivity Environmental risk • Flammable
Ionic liquids (ILs)	• Large potential range • High viscosity Great tunability • Wide liquid range • Low flammability	• Low ionic conductivity • High cost • Unstable in the presence of water
Deep eutectic solvents (DESs)	• Large potential range • Low cost • Great stability • Great tunability • Wide liquid range	• High viscosity • Low ionic conductivity

Alkaline

$$\mathrm{Zn(OH)_4}^{2-} + 2\ \mathrm{e}^- \rightarrow \mathrm{Zn} + 4\mathrm{OH}^-,\ E^0 = -1.260\ \mathrm{V} \qquad (10)$$

Lithium has been largely applied on this kind of batteries. Its negative potential ($E^0 = -3.0$ V) made Li a valuable candidate for RFBs, with theoretical large cell potential and energy density. However, its standard redox potential is out of the potential window of water and its reactivity with these media makes impossible its application on aqueous RFBs. This problem can be solved by changing to an organic, ionic liquid or deep eutectic solvent, that possesses a higher potential window as described above. It is possible to assemble a full non-aqueous battery[122] or a combination between a Li non-aqueous anode and an aqueous catholyte.[108,123,124]

In the last years, a new type of inorganic compounds has attracted increased attention due to its interesting electrochemical properties: polyoxometalates (POMs). POMs are polyatomic clusters with anionic character, formed by several transition metals atoms with high oxidation state (d^0 or d^1 electronic configurations) that act as nuclei of the structure, connected through oxygen anions. These complexes comprise an array of corner and edge-sharing pseudo-octahedral MO_6 (M = Mo, W, V, Nb) units that form an ionic core.[125] They can be described as metal oxides with well-defined size, structure and stoichiometry. The highly oxidised metals confer the capacity of accepting an elevated number of electrons per cluster, turning into electron-rich species. Some of these species are often recognized as electron reservoirs because of their high capacity to carry and release electrons.[126] The major example of this property was obtained by Wang *et al.*[127] for Keggin-type POM $[PMo_{12}O_{40}]^{3-}$. They demonstrated by X-ray absorption near-edge structure analyses demonstrate that all 12 Mo^{6+} ions can be reduced reversibly to Mo^{4+}, reaching a total amount of 24 electrons exchanged. Authors report a large capacity of *ca.* 270 A h kg^{-1} in a potential range between V = 4.0 V and V = 1.5 V when using POM as cathode active material with a lithium metal anode. According to these principles, the scientific community has focused on the application of POMs in energy storage,[125,128] generally for static applications in the form of solid nanocomposites with conductive material, such as nanostructured carbon[129,130] or conducting polymers.[131–133] The first-ever all-POM RFB was proposed by Pratt *et al.* in 2013.[134] The system was based on redox pairs $\mathrm{SiV^{V}{}_3W^{VI}{}_9O_{40}}^{7-}/\mathrm{SiV^{IV}{}_3W^{VI}{}_9}$-$\mathrm{O_{40}}^{10-}$ as catholyte and $\mathrm{SiV^{IV}{}_3W^{VI}{}_9O_{40}}^{10-}/\mathrm{SiV^{IV}{}_3W^{V}{}_3\ W^{VI}{}_6O_{40}}^{13-}$ as anolyte, with a three-electron exchange reaction. They tested the pair in aqueous (0.5 M H_2SO_4) and non-aqueous (0.5 M TBATf (tetrabutylammonium triflate) in PC) media. Aqueous battery demonstrated CE greater than 95% at 2 mA cm^{-2} with a cell potential of 0.8 V. Non-aqueous system had a higher operating potential (1.1 V) but at the expense of CE (87%). Low current densities were obtained, as a result of the small concentration of active materials (assuming mass transport limitations). Further research was carried out by the same group, using similar POMs structures, without earning much-improved results.[135,136] Chen *et al.*[137] introduced in their battery design a POM lithium salt, $Li_3PMo_{12}O_{40}$, obtaining high CE (>90%) up to 0.5 mA cm^{-2} and stability (>500 h) for the static cell. When an equivalent study was made in a RFB, efficiency was reduced to 68%, as a result of deposition of POMs on the electrodes, solvent loss in long-term cycling experiments and a slow crossover of the POM solution. In these terms, VanGelder *et al.*[138] prepared alkoxide-functionalized POMs with stoichiometry $[V_6O_7(OR)_{12}]$ with (R = CH_3, C_2H_5). The large size of these polyoxovanadates-alkoxide clusters makes them resistant to membrane crossover, especially with the use of ethoxyde moieties. Feng *et al.*[139] combined a POM, $H_3PW_{12}O_{40}$ (Fig. 5), as the active material for negative electrolyte with a classical redox pair, I^-/I^{3-}, for the positive electrolyte. As a result of the optimization process, they reach a 0.84 V cell with 99.6% and 80.1% of CE and EE at 100 mA cm^{-2}, respectively, and capacity retention of practically 100%. Friedl *et al.*[140] reported the first asymmetric all-POM RFB, employed for each side of the battery a completely different POMs. $[SiW_{12}O_{40}]^{4-}$ was proposed as anolyte and $[PV_{14}O_{42}]^{9-}$, as catholyte. The battery presented a CE of 94%, with a reduced VE of approximately 65% at 30 mA

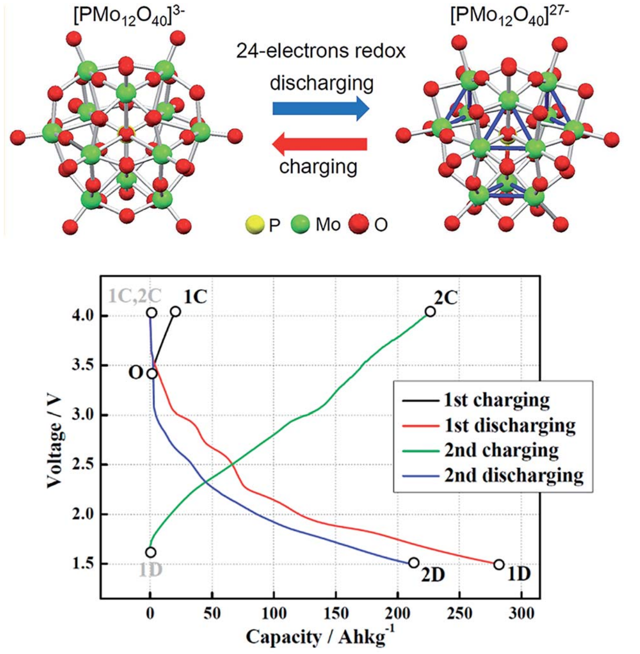

Fig. 5 Structures of POMs $[PMo_{12}O_{40}]^{3-}$ and $[PMo_{12}O_{40}]^{27-}$. Charging and discharging curves of a POM/Li battery. Extracted from ref. 127.

cm^{-2}, due to ohmic losses. In this case, the experiments were further for its potential application, being the first group to study the scalability of the battery.[141] The main objective was the upscale of membrane area from 25 cm^2 to 1400 cm^2. The new cell was cycling for 88 days (1400 cycles) with a loss of only 0.53 $\times$ 10^{-3} A per h per cycle. Additionally, the resulting CE and VE at 4 mA cm^{-2} for the scaled system, 99% and 86% respectively, improved the results obtained for the lab-scale cell, demonstrating its operativity.

4.3.2 **Metal complexes.** A metal complex is the union of a metal atom with free orbitals able to accept an electronic pair or electronic density with one/several molecules able to act as a donor of these electrons, known as ligands, generating a coordinated covalent bond. The number and structure of the complexes are determined by the nature of the metal and the ligands.[142] The most commonly employed organic/organometallic structures can be consulted in Table S2.† The use of these compounds in RFBs arises from the necessity of the application of new solvents. As described before, water has a limited working potential range and the substitution by organic solvents appears to be a solution. Classical inorganic ions, employed previously for the electrolytes, possess poor solubility in non-aqueous media. Coordination chemistry opened a new horizon in this sense, offering adaptability through the selection and modification of ligands. In contrast, the first report of a complex based RFB was an aqueous battery,[143] with the incorporation of ferricyanide, $[Fe(CN)_6]^{3-}$, in the positive electrolyte. It was not until 1988 that the first NARFB with coordination compounds as actives species were reported. Matsuda *et al.*[144] designed a symmetric cell based on $[Ru(bpy)_3]$ (bpy = 2,2′-bipyridine) with acetonitrile as solvent, obtaining an OCP of 2.6 V, double of the electrochemical window of water. Generally, redox activity of complexes comes from the metal ion, undergoing oxidation/reduction depending on their electronic configuration. Nevertheless, there are ligands that participate in electrochemical events separate from those of the metallic centre to which they are bound. They are known as non-innocent ligands[145] and are used to increase the energy density of a system, incorporating more electron-exchange processes and enlarging the active potential window. When studying a redox complex it is necessary to attend to the full molecule and not only on their independent elements, because of the decisive effect on their bonding, as was well evidenced by Popov *et al.*[146] In this work, it is described the theoretical study of iron complexes with different imine ligands (non-innocent). The reduction potential of the different ligands varies more than 0.5 V when comparing free molecules and complexed with Fe ion. On the other hand, the same reduction process can be moved until 1 V just with a slight variation of the attached ligand, demonstrating the interaction between the metallic ion and the complexing ligands.

A great effort has been made in the research of organometallic compounds for energy storage, as can be seen in Table S1.† Polydentate ligands are a useful tool for obtaining stable complexes, supported by the chelate effect.[147] In agreement with it, β-diketonates are known to form complexes with practically all the metals, with a great variability on their structure, size and properties.[148] Acetylacetone, the simplest of these structures, transform into an anionic ligand, acetylacetonate (acac) by the loss of one acidic proton. Octahedral complexes $M(acac)_3^{n+}$ present improved stability and elevated solubility in organic solvents.[149] Thus, it is one of the most investigated alternatives for the introduction of classical active metal ions to the NARFBs. Obviously, vanadium has attracted the attention, as a reference in traditional RFBs, for its accommodation in non-aqueous systems.[69,75,83,150,151] $V(acac)_3$ possesses a moderate solubility, close to 1 M in ACN. However, due to an oxidation process to $VO(acac)_3$, it can be affected, decreasing the efficiency of the cell.[151] To enhance its solubility, Suttil *et al.*[152] modified acetylacetonate structure by the incorporation of different organic moieties, reaching a solubility of *ca.* 2 M. Complex of the same family studied as electrolytes are $Cr(acac)_3$,[153] $Mn(acac)_3$ (ref. 154) or $Ru(acac)_3$.[144] Yamamura *et al.*[155] presented in their study the preparation of different diketonates with slightly varied structures with the participation of different ligands. They used UO_2 as the base of their work, proposing the symmetric uranium NARFB, utilizing its multiple oxidation states.

Bpy is a heteroaromatic compound formed by two pyridine rings bound through the C next to the N atom, that yields its pair of electrons, acting as a bidentate ligand and forming complexes with stoichiometry $M(bpy)_3^{n+}$. The differences with respect to acac are its non-charged nature and, mainly, a redox response, representing a classical example of a non-innocent ligand. These complexes present the oxidation potential/s of the metal, associated with its electrochemical characteristics, and a series of closely spaced, primarily ligand-centered reductions (3 signals for the normal stoichiometry) occurring at negative potentials, between −1.5 and 2 V, depending on the complex,[156] leading to large active potential windows. Bpy complexes present low to moderated solubility in organic solvents,[157] but with the advantage of easy synthesis and modification due to well-known controlled chemistry.[158] In this sense, Cabrera *et al.*[149,159] carried out a process of improvement of solubility by modification of ligands for $[Cr(bpy)_3]^{2+}$ complexes.

Metallocenes are complexes formed by a metal centre and two planar and parallel, or nearly parallel, sets of aromatic ligands, bound through the overlapping of the d orbitals of the metal and the π-orbitals of the ligands (also known as "sandwich structure"). Redox processes for this kind of molecules are generally reversible one-electron transfers,[160] making them an alternative as redox electrolytes. The most representative arene ligand is cyclopentadienyl anion (Cp), $C_5H_5^-$, which can be combined with most of the transition metals, obtaining stable complexes. Special attention was given to $FeCp_2$, called ferrocene (Fc), which is a robust molecule stable up to 400 °C, mild and reversible oxidation around +0.6 V *vs.* SHE and rich modification chemistry, based on electrophilic reactions on the aromatic cycles.[161] As in previous cases, this variability of the structure can be used to improve its solubility. Fc can be dissolved largely in a broad range of organic media,[162] but by a functionalization process, it can be adapted for application on aqueous batteries. The incorporation of charged moieties, commonly quaternary ammonium substituents, enhance its solubility in water, obtaining good values of concentration. Hu *et al.*[163] implemented the water-soluble ferrocenyl derivatives FcNCl and FcN_2Br_2, which contains one and two quaternary ammonium groups respectively. These compounds reached a molarity of at least 2.0 M even in presence of 2.0 M NaCl supporting electrolyte. The developed FcNCl/methyl viologen (an aqueous organic anolyte) battery exhibited long cycling stability, 99.99% of capacity retention after 700 cycles at 60 mA cm^{-2}, with an energy density up to 125 mW cm^{-2}.

Other families of ligands have been studied as potential electrolytes for RFBs. The classic ferrocyanide is still used, due to its great performance in aqueous media.[164] Macrocycles with presence of heteroatoms act as cations traps, complexing them strongly and resulting in an easy preparation. Nitrogen[165] and sulphur[166] containing cycles can be found as nickel chelates, promoting its solubility in organic solvents.

4.3.3 Metal-free organic species. The use of inorganic species or their complexes entails two main concerns: first, it is associated with the toxicity and environmental risk of certain metals, such as Cr, V or Co; second, metal-containing active species increase the global price of the RFBs, directly related with their abundance on earth, clearly higher than organic/carbonaceous based materials, as is reflected in the studies carried out by Dmello *et al.*[26] and Darling *et al.*[59] An alternative is the use of organic redox-active materials, which eliminate considerations regarding metals, especially in terms of extraction and abundance. The first attempt on the design of an all-organic RFB was proposed by Chakrabarti *et al.*,[167] with a symmetric battery with rubrene as active species. However, its poor solubility supposed the non-viability of the system. It was Li *et al.*[168] in 2011 who described the first successful RFB basic only on organic molecules as active pairs, with a combination of 2,2,6,6-tetramethyl-1-piperidinyloxy (TEMPO) and *N*-methylphthalimide as catholyte and anolyte respectively, using ACN as solvent. It was the beginning of growing research on organic active species, which is nowadays a trend on electrolytes for energy.

Quinones. Quinones are aromatic compounds that can be found in animals, plants, fungi or bacteria, participating in processes of critical biological relevance such as photosynthesis or cellular respiration.[169] They are integrated into electron transfer chains, due to their electrochemical behavior. Quinones are the oxidized form of aromatic compounds with two hydroxyl groups as substituents, known as hydroquinones (HQ).[170] Conversion between both molecules consists of a reversible two-electron redox reaction, whose mechanism depends on the pH according to the reaction described in Fig. 6b. For acidic media ($pH < pK_a$ (HQ)), reaction is slower due to the incorporation of protons to the structure, leading to two consecutive one-electron reactions, with an intermediate called semiquinone[170,171] (Fig. 6c).

In this section, all the structures which contain almost one quinone functionality are grouped, including those with fusion of cycles. The most common quinone derivatives (Fig. 6a) are benzoquinone (BQ), naphthoquinone (NQ) and anthraquinone (AQ).

Quinones are usually treated for their use in aqueous media, by adding polar substituents as sulphates, hydroxyls or amines. In the case of quinones, modifications on the structure not only determine solubility on the different solvents but have a critical impact on the reduction potential. Comparing with the metal complexes, where the metal or the ligands have a defined potential, that can vary slightly as a function of substituent on ligands, quinones possess a potential wide potential range. Wedege *et al.*[171] reflected on this situation, analysing the electrochemistry of a catalogue of 33 different molecules of this family, obtaining differences up to 2 V. AQs present negative potential values, especially significant at pH 13, and high stability and solubility for sulfonated or hydroxylated molecules. All these properties contribute to their use as anolyte in RFBs. However, they present problems of dimerization for both acidic and neutral conditions even for low concentration, leading to a reduced capacity.[172] Moderated potentials were found for NQs, low enough for the application of the hydroxyl-containing derivatives in alkaline conditions. Halogenated NQs present problems of irreversibility, excluding them for energy storage implementation. Positive potentials can be achieved by using BQs, but only in a moderated range. Higher positive potentials correspond to highly reactive BQs. These molecules are electrophiles with great affinity with nucleophiles, including water, undergoing Michael addition,[173] leading to irreversible reactions and decomposition. A potential solution is the design of substituted BQs that could reduce degradation *via* this reaction.[174,175] Regarding the developed work, hypothetically an all-quinone RFB can be as high as 1.1 V at pH 7, while at pH 0 and pH 13 it could be around 0.9 V. Nevertheless, only an anolyte can be feasible utilized nowadays, as AQs possesses

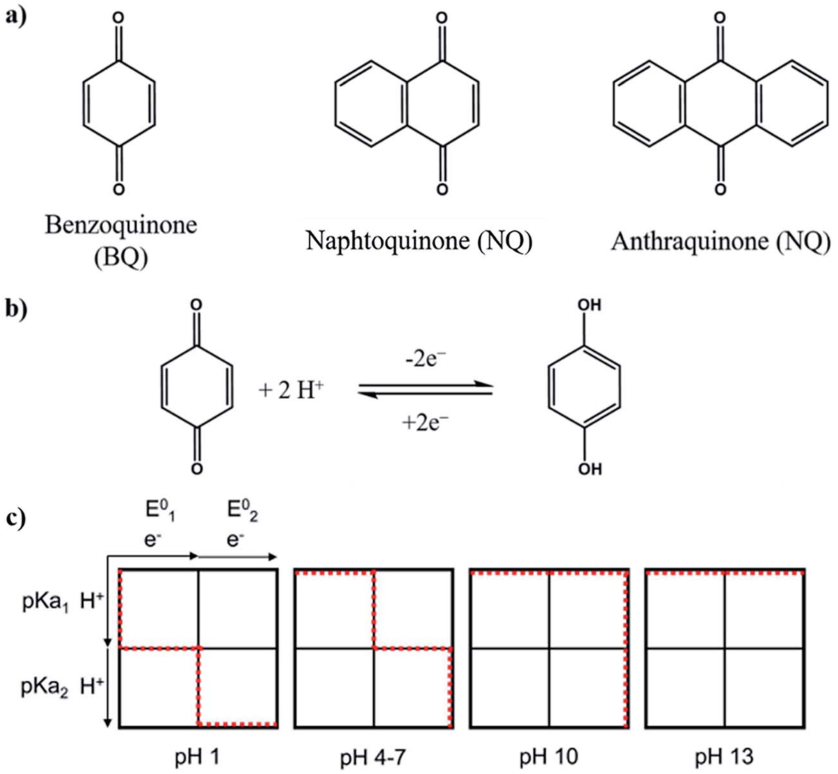

Fig. 6 (a) Structure of most common quinones. (b) Quinone-hydroquinone equilibrium. (c) Scheme-of-squares for pH-dependent reduction mechanism of ADQS. Horizontal movement indicates electron transfer and vertical indicates proton transfer. Extracted from ref. 171.

sufficiently low E^0 with high solubility and stability. Further effort is needed for the positive electrolyte, in terms of both potential and stability. Theoretical studies have been proposed to optimize the search of new redox-active quinones, as the one developed by Er *et al.*,[176] creating a complex library by combining different quinone cores (number of cycles, position of ketones) and substituents (18 groups) to obtain a total of 1710 quinone/hydroquinone pairs. One of the main results is the obtainment of a list of 300 candidates for positive electrolyte with a reduction potential above 0.7 V.

In the last few years, researchers have focused on the use of natural quinones as active species. Hu *et al.*[177] put their attention on the use of lawsone (a pigment isolated from the leaves of the henna plant) derivative as negative electrolyte for the assemble of a redox flow battery, due to its negative reduction potential of −0.454 *vs.* SHE. One step further was the application of its dimer, bislawsone, made by Tong *et al.*[178] Its use in energy storage was already proposed in 2018 by Miroshnikov *et al.*[179] for Li-ion batteries. Bislawsone suffered a 4 electron transfer process with a redox potential of −0.551 V *vs.* SHE. The system Bislawsone/$K_4[Fe(CN)_6]$ reached an OCP of 1.07 V at 100% SoC with a CE > 99% and capacity utilization > 90% at 100 mA cm^{-2}. Alizarin, originally obtained from the root of the common madder plant, Rubia tinctorum, was applied by Liu *et al.*[180] modified with a methyliminodiacetic group, improving peak current with respect to the original quinone. A RFB was built by using $K_4[Fe(CN)_6]$ as catholyte, obtaining an OCP of 1.38 V, EE of 84.9% at a current density of 0.1 A cm^{-2}, and a maximum power density of 0.49 W cm^{-2}. Nevertheless, alizarin presents another advantage. In its most stable configuration, possesses fused cycles of quinone and hydroquinone. Thus, it can suffer an oxidation to all-quinone molecule or a reduction to turn into a two hydroquinone compound, as described by Tong *et al.*[181] They exploit this possibility designing a symmetric all-quinone flow battery, with a two electron reaction in both sides of the cell, resulting in with 1.04 V of OCP, 163 mA h g^{-1} of capacity, and 100 cycles at 10 °C with 100% of depth of discharge.

Nitrogen-containing aromatics. Aromatic compounds with nitrogen forming a part of the aryl rings are redox-active species. An example of this structure is bpy, previously discussed as a non-innocent ligand. Most of the used molecules for RFBs contain two nitrogen atoms and can suffer two consecutive or simultaneous one-electron transfer reactions. Conversion from oxidized to reduced form, generally with charges +2 and 0 respectively, is conducted *via* a radical intermediate. As an

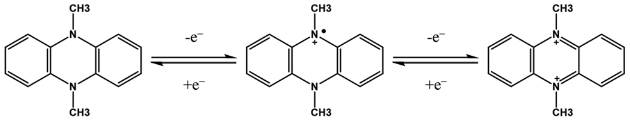

Fig. 7 Redox processes for 5,10-dihydro-5,10-dimethyl phenazine (DMPZ).

example, Fig. 7 shows the redox process for the 5,10-dihydro-5,10-dimethyl phenazine.

This family of nitrogen derivatives usually lose aromaticity when reduced, so generally present a negative reduction potential. The most studied and applied structure is 4,4-dimethyl bipyridinium, known as Methyl Viologen (MV). It possesses good stability, a low potential for its first reduction reaction and a great solubility in aqueous media, reaching 3.0 M in 1.5 M NaCl solution.[182] Even more, conductivity of MV solutions is relatively elevated (131 mS cm^{-1}, 25 °C), decreasing the quantity of needed supporting electrolyte.[183] There is a large number of studies that use this molecule as anolyte in RFBs.[163,182,184,185] Nevertheless, MV can suffer dealkylation in the presence of oxygen,[186] demanding the search for new derivatives with improved stability. Most of the proposed viologens present equivalent electrochemical reactions to MV, but with more positive potential or limited solubility.[183,187] A promising solution was found in bis(3-trimethylammonio)propyl-viologen (BTMAP-V). It maintains low reduction potential (−0.38 V *vs.* SHE) and a great solubility (2.0 M) in water, turning into the best alternative to avoid degradation problems. Beh *et al.*[188] found the capacity decay reduced by a factor of 40 when compared with the equivalent system with MV, obtaining retention of 99.9989% per cycle (Fig. 8). Similar values (99.993% per cycle) were found by Liu *et al.*[189] when using a nitroxide, TEMPO, as positive electrolyte. Li *et al.*[190] used the combination BTMAP-Fc/BTMAP-V for its application on a Solar Flow Battery, obtaining continuous operation time for more than 200 h and a capacity utilization rate of above 80%.

Directly related to viologen, diquat is a compound used in commercial herbicides, but also presents redox activity. Independently of the substitution with radicals, reduction potential is set around −0.403 V *vs.* SHE. Huang *et al.*[191] utilized a dimethyl-diquat as anolyte of a RFB with FcNCl as catholyte, showing problems of deposition of the organic radical on the electrodes, concluding the necessity of optimization of the structure. Fused benzene–pyrazine cycles have been studied as candidates since Brushett *et al.*[192] proposed a series of quinoxalines as negative counterparts for all-organic Lithium-ion RFBs. A more complex structure, phenazine, was selected by Hollas *et al.*[193] for optimization of an aqueous anolyte, resulting the most promising molecule the 7,8-dihydroxyphenazine-2-sulfonic acid, that reaches an elevated concentration (1.4 M in 1 M NaOH) and high material utilization of 90% and VE of 82% at a current density of 100 mA cm^{-2}. It is noteworthy the use of a modified phenazine, DMPZ, by Kwon *et al.*,[194] as positive electrolyte due to its high redox potential of 0.61. Additionally, this molecule presents different colour depending on the SoC, easy monitored by UV-Vis spectroscopy. All these features led the group to prepare a DMPZ/9-fluorenone RFB, with EE around 70% and capacity retention of 90% after 80 cycles. As for quinones, some authors put their focus on the adaptation of natural compounds based on nitrogen-containing aromatics. Is the case of Lee *et al.*,[195] which introduces alloxazine, an adenosine receptor antagonist, as active species. Assisted by carboxylic acid-carbon nanotubes as catalyst, the group earns a VE of 64% and a discharging capacity of 26.7 A h L^{-1} when combined with $K_4[Fe(CN)_6]$ as catholyte. An example of the most advanced investigation in this kind of compound is the development of a symmetric cell based on verdazyl radicals, a ring containing 4 nitrogen atoms. Their electrochemistry was previously described by Gylroy *et al.*[196] highlighting their potential for energy storage applications. Recently, Charlton *et al.*[197] described the use of 3-phenyl-1,5-di-*p*-tolylverdazyl, which can be reversibly oxidized and reduced in one-electron processes. However, it presents problems of capacity decay due to decomposition of the active material.

Nitroxides. Nitroxides are, in general, radicals with low stability. When presenting a hydrogen atom in α respecting to the nitrogen atom, they undergo disproportionation to form the corresponding hydroxylamine and nitrone.[198] Substitution of this H by alkyl or aryl groups stabilize the structure. However, if those groups are too big, there is a possibility of homolytic cleavage of a C–N(O) bond leading to a nitroso compound and alkyl radical. The structure of tetramethylpiperidine 1-oxyl (TEMPO) complies perfectly with these requirements, as hydrogen atoms are substituted by methyl moieties and the nitrogen is a part of a 6 atoms cycle, increasing stability. Energy storage with nitroxides is based on TEMPO structure, adding modifications to improve performance. TEMPO radical is oxidized *via* one-electron transfer to form an oxoammonium cation.[199] Major interest resides in the high positive reduction potential, around +0.8 V *vs.* SHE, unusual for the rest of organic structures. The main drawbacks of this nitroxide are the degradation of the molecule due to disproportionation reactions at strong acidic pHs and the instability of the oxoammonium (the oxidized form of TEMPO) in alkaline media.[200]

TEMPO without any modifications is soluble in polar and non-polar organic solvents, including water,[201] increasing the possibility of use in both aqueous and non-aqueous systems. Without any further functionalization, it reaches a concentration of 5.2 M in the mixture ethylene carbonate (EC)/PC/ethyl methyl carbonate, as exposed by Wei *et al.*[122] Even in the presence of a concentrated supporting electrolyte, 2.3 M $LiPF_6$, a 2.0 M TEMPO can be obtained. This group implemented this solution on the design of a Li/TEMPO NARFB, exhibiting an EE of ∼70% and a discharge volumetric energy density of 126 W h L^{-1}. With the purpose of increased solubility in water for aqueous systems, different variations of TEMPO were proposed. The first adapted structure was 4-hydroxy-TEMPO (TEMPOL), with a maximum concentration of 2.1 M. The performance of the MV/TEMPOL cell set by Liu *et al.*[182] demonstrated quite stable cycling retention with CE staying above 99% at 40 mA cm^{-2}, but capacity retention of 89% after 100 cycles. This decay can be explained by the reduction of pH during cycling, enhancing side reactions of TEMPOL.[202] Taking TEMPOL as starting point, alkyl ammonium derivatives have been prepared.[189,203] Liu *et al.* obtained a great solubility by exchanging the hydroxyl by 3-(trimethylammonio)propoxy group, leading to a maximum concentration of 4.62 M.[189] However, this solution possesses high viscosity, compromising the overall efficiency of the system because of pumping losses. For its test as catholyte, a 0.1 M solution was combined with BTMAP-V in the negative electrolyte, resulting in a 1.10 V battery

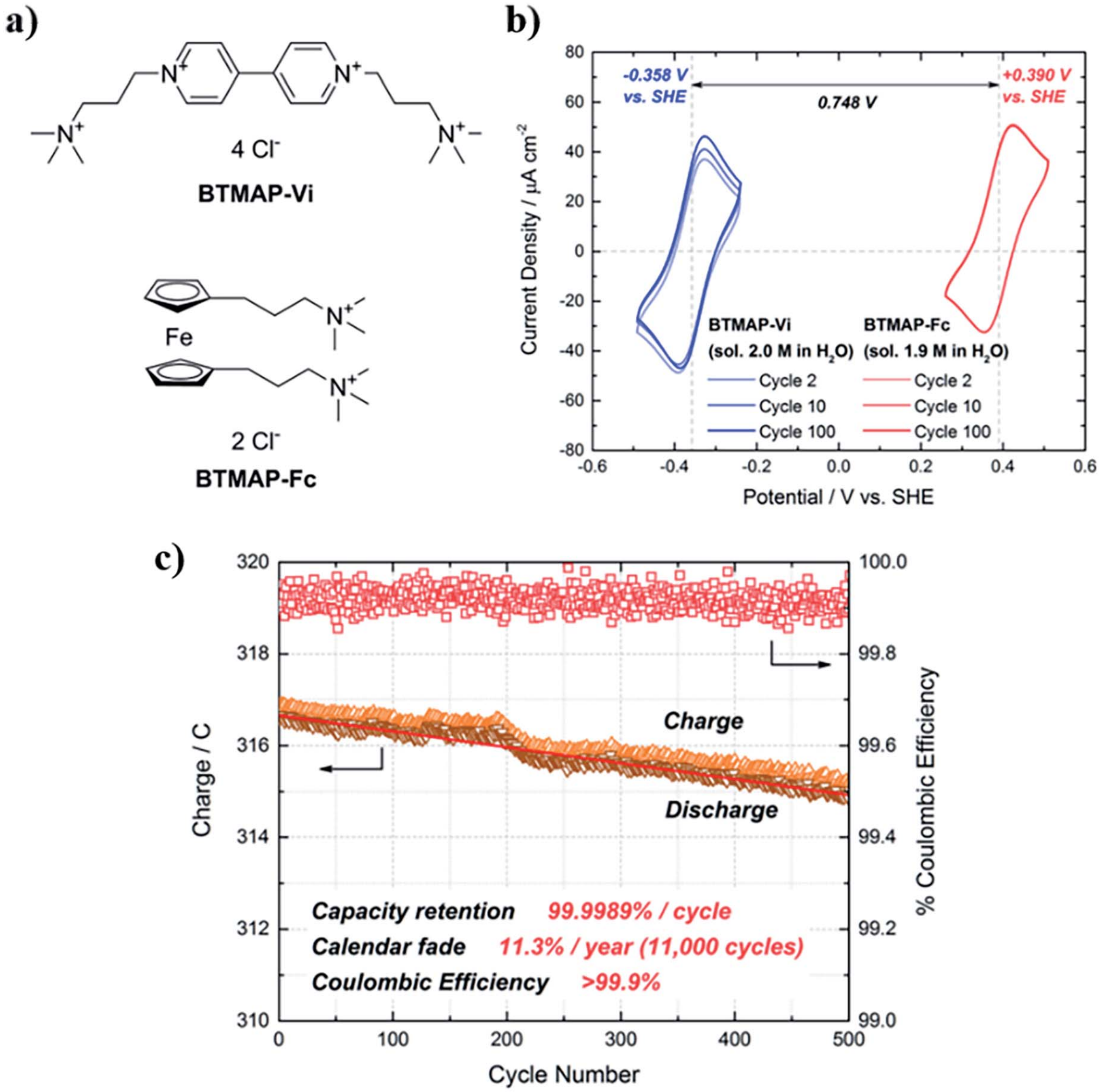

Fig. 8 (a) Chemical structures of BTMAP-Vi and BTMAP-Fc. (b) Cyclic voltammograms of BTMAP-Vi (blue trace) and BTMAP-Fc (red trace). The water solubilities and reduction potentials of both molecules *vs.* the standard hydrogen electrode (SHE) are indicated. (c) Cycling of a BTMAP-Vi/BTMAP-Fc pH 7 cell at 50 mA cm^{-2}. Extracted from ref. 188.

with capacity retention of 95% after 1000 cycles. An imidazolium-modified TEMPO was proposed by Chang *et al.*[204] with a reasonable solubility (0.5 M). A 1.64 V cell potential in aqueous media is noteworthy when it is coupled with Zn^{2+}/Zn negative half-cell, with a capacity fading of 0.15%·per cycle.

Other organic molecules. Different structures from the described above are proposed as electrolyte for RFBs. Kim *et al.*[205] studied *p*-phenylenediamine and its alkyl derivatives, highlighting *N*,*N*,*N*′,*N*′-tetramethyl-*p*-phenylenediamine as the best candidate for polycarbonate-based RFB, because of its increased solubility, reducing interaction *via* hydrogen bonding when removing H from amine, and improved chemical stability because of steric protection of the redox centre. Zhang *et al.*[87] developed a RFB containing *N*-methylphthalimide (NMePh), urea, and lithium bis(trifluoromethanesulfonyl)imide (LiTFSI). The active species, NMePh, is up to 4 M into the eutectic and presents a potential of −1.573 V *vs.* SHE. The Li/NMePh cell exhibited an OCP of 1.9 V, delivering a volumetric capacity of 28 A h L^{-1} with a concentration of 2.0 M. NMePh was also used by Wei *et al.*[206] as anolyte, with a catholyte based on 2,5-di-*tert*-butyl-1-methoxy-4-[2′-methoxyethoxy]benzene (DBMMB) which exhibit a +0.707 *vs.* SHE redox potential. This molecule is the result of the search for positive active species for organic batteries with dialkoxybenzene structure.[207,208] Due to the difficulty of finding new organic positive electrolyte material, DBMMB has been utilized extensively for all-organic RFBs.[57,209,210] Cyclic ketones are also applied for their use as electrolytes. A quinone-like ketone, 1,3-cyclohexanedione, was studied by Leung *et al.*[211] as negative electrolyte with moderate potential (−0.403 V *vs.* SHE) in an operating pH range 1–5. Conjugated ketones 9-fluorenone[57,194] and 2-methylbenzophenone[210] have been also proposed as anolyte for non-aqueous systems, standing out the latter due to its large potential (−2.457 V *vs.* SHE) and theoretical solubility (>5 M in ACN).

4.3.4 Polymers. Advances in new membranes for RFBs requires great effort and time, leading to the use of non-specific membranes. As a result, low control of species crossovers is achieved, which is one of the main causes of efficiency losses. A solution can be reached from electrolyte modification, by the use of redox-active macromolecules and polymers. High molecular weights are associated with large sizes, preventing crossover by a size-exclusion mechanism.[212] Electrochemical behavior can be controlled by the introduction of known electroactive moieties, as the polymer would exhibit equivalent current–potential responses to those obtained with the corresponding molecule containing a single centre, with current intensity proportional to the number of active units: the larger the chain the higher the current.[213] First-ever all-polymer RFB was reported by Janoschka *et al.* in 2015.[214] Electrolyte polymers consist of two components: a unit enhancing water solubility (quaternary ammonium) and a redox-active moiety, TEMPO for catholyte and viologen for anolyte. Performance test revealed an OCP of 1.1 V, energy densities of 10.8 W h L^{-1} (charging) and 8.0 W h L^{-1} (discharging) and capacity retention of 80% after 10 000 cycles. Since then, most of the work has been focused on these polymers and their optimization.[212,215–217] Winsberg *et al.*[218] substituted the classic bromine catholyte of Zn/Br$_2$ hybrid batteries by a non-aqueous derivative of p(TEMPO), incorporating vinylbenzene monomers. They also describe the first polymer/zinc RFB in aqueous media,[219] with an improved OCP of 1.7 V and a stable EE of 80%. BODIPYs, heteroaromatic structures containing N–B–N bonding, present two one-electron transfer reactions, offering the possibility of their use in a symmetric RFB. This concept was used through their introduction as electrolyte as poly(BODIPY), tested by Winsberg *et al.*[220] Even with a large theoretical cell potential (over 2 V), obtained capacities are very low, with EE of only 55%, concluding in a necessity of further research on the topic. In 2019, Hatakeyama-Sato *et al.*[221] introduced poly(AQ) nanoparticles for hybrid RFBs (Fig. 9), as an alternative of viologen-based polymer, founding a higher capacity for the polymer-particle electrolytes than the dissolved species (1.5 M) and a stable capacity during 50 cycles of approximately 6 A h L^{-1}.

4.4. Supporting electrolytes

As reflected in Section 4.2.1., pure solvents present low ionic conductivity, leading to ohmic losses during the charge–discharge process. The use of supporting electrolytes is the response to this necessity. It consists of a compound that can be ionized in the solvent into an anion and a cation, contributing both to improve ionic conductivity. The selection of supporting electrolyte must accomplish some requirements. The negative impact on the solubility of the active species needs to be as low as possible. It is well known that the solubility of a solute may be affected by the co-existence of other solutes, as a consequence of

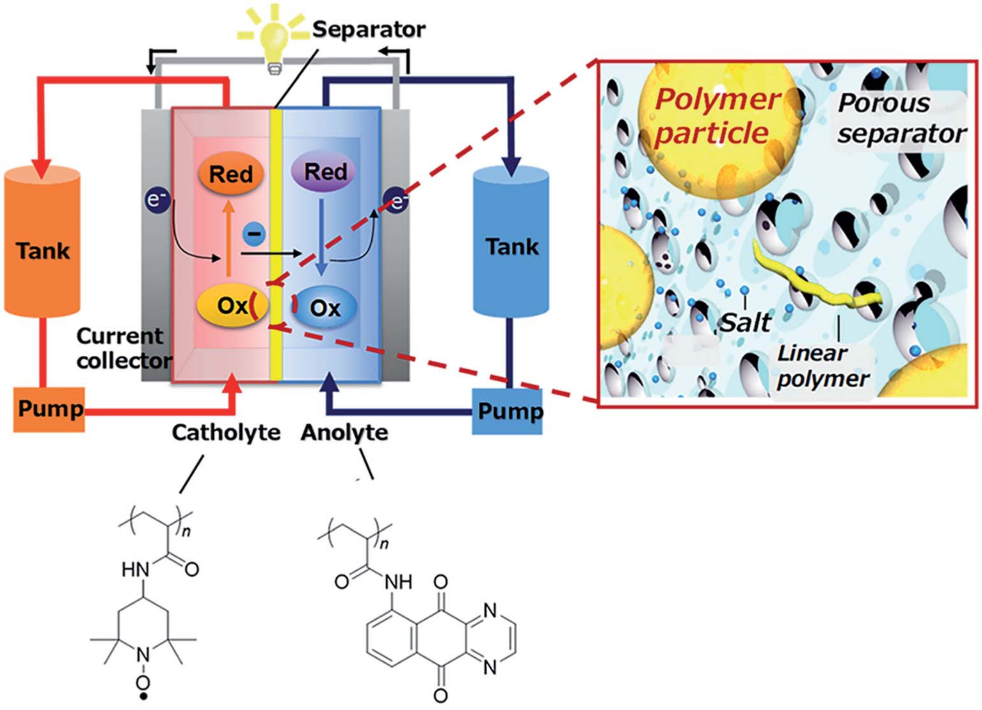

P1 P3

Fig. 9 Scheme of the RFB based on organic redox-active polymer nanoparticles developed by Hatakeyama-Sato *et al.* extracted from ref. 221.

excluded volume effects or changes in solution activity.[222] This effect is corroborated by Shinkle *et al.*[66] in the study of the solubility of the pair V(acac)/tetrabutylammonium tetrafluoroborate ($TBABF_4$). Interaction between active species and supporting electrolytes should be minimized, especially in terms of chemical stability. As an example, MV presents instability in strongly acidic media,[223] used as support in many designs of RFBs.

The use of the different supporting electrolytes is limited by their different solubility. Due to their ionic character, a broad range of possibilities appears when working on aqueous media. The use of cheap electrolytes in high concentrations is allowed, including inorganic salts, as NaCl,[163,182,214] strong bases as KOH[224–226] or NaOH[164] or acids. Sulphuric acid is extensively used as a part of the classical composition of VRFBs.[96] Nevertheless, other strong acids have been considered in a supporting role as HCl, such as the Fe/Cr battery developed by the NASA[95] or the V/Br developed by Vafiadis *et al.*[227] Kim *et al.* studied the viability of the introduction of hydrochloric acid as supporting electrolyte in VRFBs. They found improved thermal stability, even for high V concentration (3.0 M).[228] Following these results, the group design a prototype based in a H_2SO_4/HCl mixture as supporting electrolyte, reaching a high EE of 82% and energy content of 1.4 kW h.[229]

For non-aqueous solvents, the possibilities are reduced. Halogens present low electrochemical stability in organic solvents and the limiting molar conductivity of alkali metals is lower than expected by Stokes Law.[91] Tetraalkylammonium groups are the most used alternative as cations. Bibliography reflects the reduction of resistance of non-aqueous solutions due to the incorporation of salts containing this type of cation. Independently of the solvent, conductivity increases with the concentration of the supporting electrolyte[230] and the resistance increases with the length of the alkyl chain; it could be a result of the increase of viscosity, which evolves with the same trend when varying the substituents.[231] Another option of cation is Li^+, which possesses lower mobility than ammonium cations but good enough to be considered as supporting electrolyte, due to its small size.[200]

The selection of anions was focused on finding the higher mobility values in organic solvents. It is critically determined by the ionic size, favoured for smaller ions.[91] Typical examples are BF_4^-, ClO_4^- or PF_6^-. TFSI has also been applied in designs of RFBs as supporting electrolyte, as in the study developed by Wei *et al.*[57] This ion presents high mobility[91] and is typically used for the development of ILs.[232,233] Precisely, Zhang *et al.*[234] proposed the use of an IL composed by $TBAPF_6$ and 1-ethyl-3-methyl imidazolium hexafluorophosphate as supporting electrolyte for a non-aqueous VRFB.

5. Membranes

5.1. Membranes requirements

As it can be seen in Fig. 2, the IEM separates both half-cells, avoiding the mixture of both electrolytes and allow selectively the permeation of the ions needed to keep the electrical neutrality. Independently of the mechanism of ion exchange (Fig. 10), the membrane must fullfill the following characteristics:

5.1.1 High ionic conductivity. Ionic transportation through the membrane is a necessary step to keep electrical neutrality and close the electrical circuit started at the electrodes. To enable high efficiencies, it is thus necessary that ions can move without much resistance. Membrane conductivity is generally obtained from electrochemical impedance spectroscopy (EIS) using electrochemical system.

5.1.2 High ionic selectivity. Exchange of the charged ions is necessary for the cell performance, as commented above. Nevertheless, a non-controlled permeation results in crossover of active species between both electrolytes. The membrane must be permeable to the charge balancing ions and prevent diffusion of active redox pairs which leads to a self-discharge of the battery.

5.1.3 High mechanical strength. Cell assembly involves the manipulation of the membranes, which suffer mechanical stress. Additionally, during operation, the membranes are in direct contact with the electrolytes that causes swelling. Membranes require strong enough mechanical resistance to reduce the damage and enlarge the lifetime of the battery.

5.1.4 High chemical stability. The use of highly concentrated solutions of active species with large reduction potential (positive or negative) is one of the main strategies to maximize the energy density of the battery. In some cases, these conditions result in an aggressive media with capacity to degrade the membrane. A typical example is the catholyte of aqueous VRFBs, composed by a solution of VO_2^+/VO^{2+} ($E^0 = 1.00$ V) in concentrated sulphuric acid. Membranes need high chemical stability according to the type of electrolyte used to ensure a long cycle life.

5.1.5 Low cost. The price of membranes is one of the limiting factors for the implementation of this technology at large scale. As an example, Nafion®, the most used material for membranes, supposes up to the 40% of the price of the stack[15] and a 20% of the entire battery.[235] It is required to optimize the selection and development of membranes to minimize the economic impact of this component on the total cost.

5.2. Cation-exchange membranes (CEM)

A cation-exchange membrane (CEM) allows positively charged species to permeate. This permeation is achieved due to the existence of acidic groups in the membrane backbone, of which some of the most relevant are sulfonic and phosphonic acids, which can easily be dissociated, releasing the cation and favoring its mobility.[236]

Nowadays, the research on flow batteries is still dominated by Nafion®,[237–242] which is used as a reference for the development of new IEMs. It is composed of a random copolymer formed by a perfluoroethylene backbone with side chains of the same nature but functionalized with terminal sulfonic acid groups.[243] Besides its characteristics as a cation conductor, Nafion® stands out due to its good mechanic properties and its outstanding chemical stability, especially notorious for strong acidic media as those used for VRFBs.

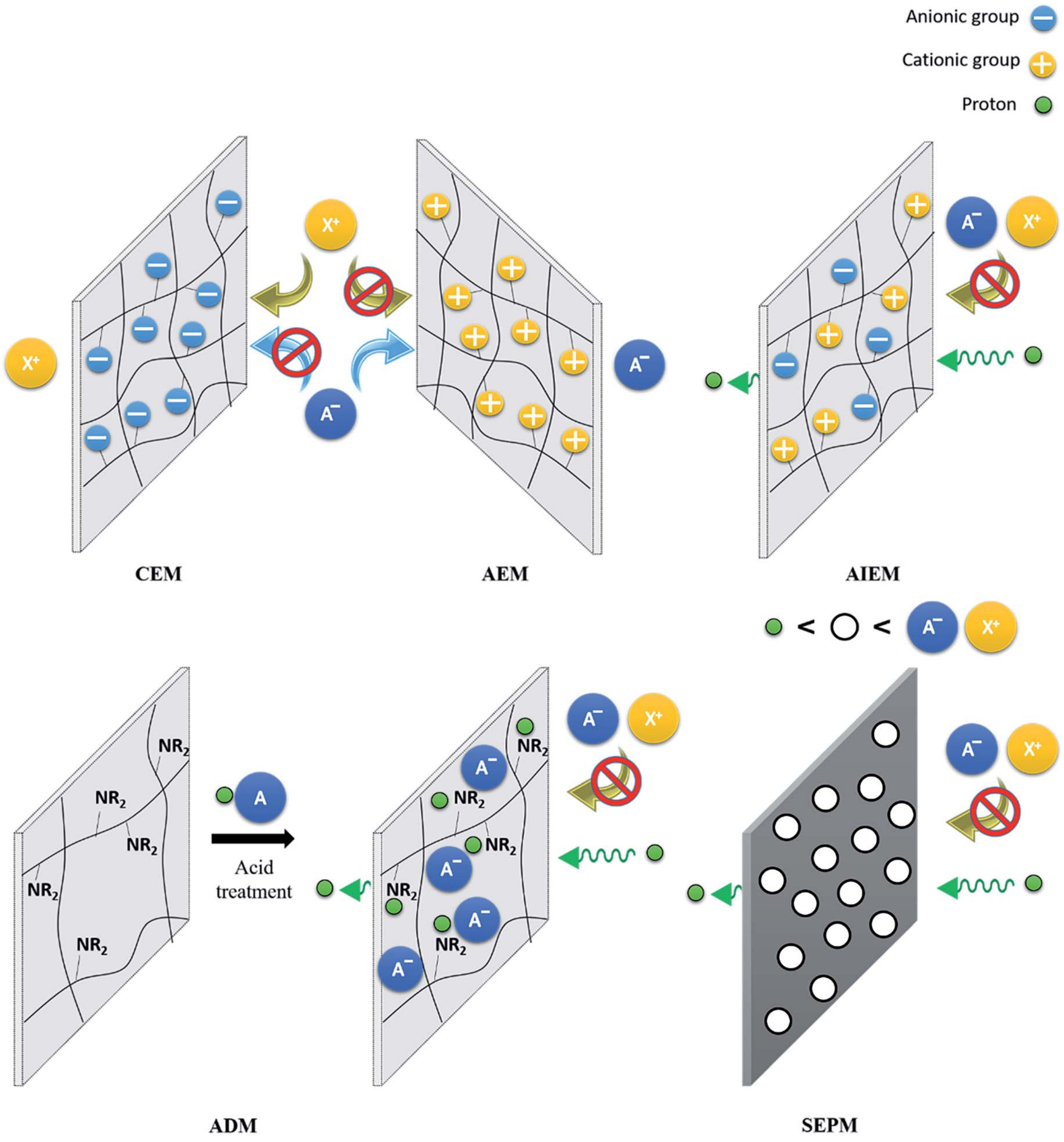

Fig. 10 Selectivity of the different IEMs employed in RFBs.

Nafion® is expensive and presents problems of ion selectivity, due to the large hydrophilic ionic clusters (4–5 nm) of hydrated Nafion®, which facilitates the crossover of vanadium ions and water molecules.[244] Because of this, new Nafion®-derivatives have been studied for their implementation. Teng *et al.*[245] used a Nafion®-covered porous polytetrafluoroethylene (PTFE); the introduction of a different polymer reduces the price and the tested 45 μm composite membrane, which displays higher VE than Nafion® N212, with reduced vanadium ions permeability. A different strategy to reduced crossover is the modification of the Nafion® surface: introduction of different oxides into the structure of the membrane, as silica[246,247] or TiO_2 (ref. 246 and 248) produce a block of polar clusters in the polymer structure, reducing the space available for the pass of vanadium ions. The reduction of the ions crossover leads to an increased CE and a lower self-discharge rate of the battery. It is interesting to highlight the article by Teng *et al.*[246] who obtained a CE of 94.8% and an EE of 77.9% at 30 mA cm^{-2} for a VRFB, increasing the values obtained from the pristine N117 of 90.8% and 77.0% at the same applied current. In this case, both organic silica and titanium oxide were the Nafion® modifiers, earning a stable membrane with no capacity decay during the first 100 cycles.

Poly(ether ether ketone) (PEEK) has been considered as a low-cost alternative to Nafion®. It can be easily functionalized in sulphuric acid to obtain sulfonated-PEEK (SPEEK),[249] which displays cation exchange properties, excellent chemical resistance and high ion selectivity.[235] Mai *et al.*[250] studied the performance of different SPEEK membranes as a function of the degree of sulfonation (DS), finding an optimum value of 40% for their use in VRFB. The CE and EE rose to 98.5% and 87.5% at 60 mA cm^{-2} respectively, compared with 91.7% and 84.7% for N115 in the same experimental conditions.

Equivalently to Nafion®, SPEEKs with high DS present higher permeabilities to vanadium, with additional low membrane stability. Li *et al.*[251] described the modification with mesoporous silica, optimizing the ratio SPEEK/silica in the process. A hybrid membrane with 20 wt% of silica shows the best performance in a VRFB of the studied samples, with a CE 96.3% and EE 88.1% at 60 mA cm^{-2} and slower discharge capacity decline during 120 cycles when compared with N117. Dai *et al.*[252] applied the well-known mechanical improvement of graphene-grafted polymers[253,254] in the preparation of a SPEEK/graphene (0.5–5 μm) composite membrane for VRFBs. Graphene reduces the permeation to V ions, leading to a higher CE and EE for SPEEK/graphene membrane compared with Nafion® 117 (96.4% *vs.* 92.8% and 83.8% *vs.* 79.5% respectively at 80 mA cm^{-2}) with a retention capacity superior on 30% than with N117, after 300 cycles.

With the aim of finding a positive synergy between both membranes, a combination of both Nafion® and SPEEK was also presented as a potential composite membrane by Luo *et al.*[255] The prepared separator displayed very low permeability to vanadium ions, but higher resistance per area than pristine Nafion®, even with a lower membrane thickness (100 μm for Nafion®/SPEEK and 175 μm for Nafion®). It resulted in an improved CE but lower VE, slightly reducing the final EE (85%, 84.8% and 83.3% for Nafion®, SPEEK and Nafion®/SPEEK membranes reported in this study at a current density of 50 mA cm^{-2}, respectively).

Daramic®, which consists of ultra-high molecular polyethylene (based on large polyethylene chains; presents high mechanical resistance), amorphous silica and mineral oil, is a microporous separator with low cost and good chemical stability. These characteristics attracted the attention of researchers as a starting point for their use in RFBs. To increase its selectivity and proton conductivity, further functionalization was needed. Mohammadi *et al.*[256] carried out a crosslinking of the polymer with divinylbenzene (DVB) to reduce the pore size, reducing the uncontrolled pass of species by size exclusion and a subsequent sulfonation to determine its behavior as CEM. Tian *et al.*[257] treated Daramic® with Nafion® solution, earning a composite membrane with proton exchange character. The incorporation of Nafion® also reduces the self-discharge rate when used for VRFBs. Fluorinated poly(arylene ether) (FPAE) possesses a structure that is similar to that of SPEEK, but with the introduction of fluoroaryl moieties as a part of the backbone of the polymer. A sulfonated-FPAE was proposed by Chen *et al.*[258] as CEM for VRFBs. Prepared membrane showed CE higher than 98%, VE higher than 92% and EE higher than 90% at discharge current densities ranging from 25 mA cm^2 to 100 mA cm^2. Additionally, capacity decay is 7 times slower than that of N212 membrane.

5.3. Anion-exchange membranes (AEM)

As a counterpart of CEMs, AEMs allow the permeation of negatively charged species. The main advantage of these membranes is the reduction of permeability to V cations, a major problem of CEMs. Commercial AEMs as AFN,[259] Fumasep®,[260] Neosepta® (ref. 261) or New Selemion® (ref. 262) have been tested for their use in RFBs.

Several efforts are being made to further improve the performance of AEM on RFBs. The most employed strategy for the construction of AEMs is the functionalization of polymer membranes with positively-charged ammonium groups. Yun *et al.*[263] prepared a quaternized-cardo-poly(ether ketone) as separator of the vanadium–cerium system. Practically null permeability was found for Ce^{4+}, while V(IV) had a 35-fold lower permeability through the AEM than through Nafion® 212. It results in CE between 97.5% and 100% depending on the applied current, without any remarkable behavior change during the first 50 cycles. A functionalized adamantane-containing poly(aryl ether ketone) (PAEK) was used by Zhang *et al.*[264] for a VRFB. The insertion of rigid hydrophobic adamantane in the backbone made the membrane display a lower water uptake and permeability to vanadium ions than that of N117. As a consequence, higher CE and EE (99.4% and 84.0% for studied membrane *vs.* 76.0% *vs.* 74.0% for N117 at 80 mA cm^{-2}) are obtained. As demonstrated by Jian *et al.*,[265] the presence of phathalazinone groups into the backbone of the polymer introduces quaternary groups without the need of a previous chloromethylation step, which requires the use of methylchloromethyl ether, a carcinogenic agent. Zhang *et al.*[266,267] prepared phathalazinone-containing PAEKs as AEM for VRFBs. Membranes present an improvement of the permeability to V ions respecting the Nafion® 117, with a mass transfer coefficient for V at least one order of magnitude less (1.19×10^{-4} cm min^{-1} for Nafion® 117 and in the range 6.53×10^{-5} to 5.94×10^{-6} cm min^{-1} for the different PAEKs-based membranes) and large stability, with no remarkable changes during 100 cycles.

Derivatives of poly(aryl ether sulfone) (PAES), a similar structure, have been also tested as AEM materials. A commercial PAES, Radel®, was quaternized by Chen *et al.*[268] for its use as AEM for VRFBs. It presented an improved IEC, but limited selectivity and the capacity decays due to the V ion permeability. Zhang *et al.*[269] functionalized the commercial Udel®, a similar poly(sulphone), with 1-methylimidazole and 1-(3-aminopropyl) imidazole to produce imidazolium cations and imidazolium–ammonium dications. It supposes not only the functionalization with positively charged groups but the crosslinking of the polymer chains. Vanadium cross-over was almost negligible, obtaining a CE of 99% at 80 mA cm^{-2} and stability over 900 cycles. The same effect was observed by Cha *et al.*[270] when crosslinked quaternized Udel® with diaminobenzophenone, reaching a CE of 100% at 50 mA cm^{-2}. Ren *et al.*[271] combined the ion exchange properties of modified Udel® with the mechanical and chemical stability of poly(vinylidene fluoride) (PVDF) to prepare a blend AEM with similar efficiencies of that of Nafion115® and improved mechanical behavior.

Simpler structures have been studied; Park *et al.*[272] focused on a quaternized-vinylbenzene as the base for new anion exchange materials. A copolymer with this monomer, styrene and hydroxyethyl acrylate was tested for its application in VRFBs. Adipic acid was used as crosslinker to reduce permeability to V ions, reaching a maximum value of CE and VE of 95.2% and 74.9% at 40 mA cm^{-2} respectively. Using poly(styrene) as the backbone, Maurya *et al.*[273] carried out a process of selection of the cationic group for the membrane surface, varying from ammonium to diammonium or phosphonium moieties. Ethylated quaternary ammonium was found as the best candidate due to its higher conductivity, oxidative stability and cell performance when tested in a non-aqueous vanadium acetylacetonate RFB. Hwang *et al.*[274] prepared a copolymer containing ethylated 1-vinylimidazolium, which has two positive charges per monomer. The obtained membrane was stable during 150 cycles, maximum CE, VE, and EE of 94.6%, 79.6%, and 85.3% at 40 mA cm^{-2}, respectively. A poly(arylene piperidinium)-based AEM with low V permeation was employed by Khataee *et al.*[244] for VRFBs. For the same conditions, the self-discharge time of the battery using this membrane doubles the time for Nafion® 212. Urushi is a mixture of catechol derivatives, mainly *o*-cathecol, substituted with a C15 unsaturated hydrocarbon chain with one to three double bonds.[275] It can be found in nature as a polymeric film with super-high durability, anti-corrosion properties, and toughness. These exceptional properties attracted Cho *et al.*, who studied the incorporation of Urushi for obtaining a new AEM for NARFBs. Its composites with chitosan[276] and poly(diallyldimethylammonium chloride)[277] presented high selectivity, reducing $V(acac)_3$ crossover.

An unexpected problem has been reported when using AEMs in VRFBs operating at high current densities, known as "power-drop effect". It was firstly described by Bhattarai *et al.*[278] They observed a discharge voltage sag when working at a current discharge of 130 mA cm^{-2}. It resulted from the electrolyte imbalance due to the low permeability of the membrane to vanadium ions. It led to a higher SOC in the positive tank, resulting in a higher concentration of V(v) in the positive half-cell compared to a fully balanced cell charged to the same voltage limit.

5.4. Amphoteric ion-exchange membranes (AIEM)

CEMs have in general high ionic conductivity, but in some cases present a lack of selectivity, leading to crossover problems. For AEMs, positively charged surfaces lead to a reduction of ions crossover, but present lower conductivities. To obtain the synergy of both types, authors proposed a combination of characteristics, with membranes containing the acid groups of CEMs and the quaternary ammonium of AEMs, leading to the construction of amphoteric ion-exchange membranes (AIEM). One of the first examples of their use for RFBs was reported by Mohammadi *et al.*,[279] who sulfonated a Selemion® Type 2 membrane with a sulphuric acid treatment and the introduction of poly(sodium 4-styrenesulfonate), reducing the capacity loss by decreasing the water transfer.

As a starting point, researchers used previously explored materials for AEM and CEM. Liu *et al.*[280] proposed the use of SPEEK combined with a quaternized poly(ether imide). They found that an increase in the content of the imide in the blend membranes reduced vanadium ion permeability effectively and improved the proton selectivity. Membrane showed a CE 96.1% and EE 88.45% at 50 mA cm^{-2}, with a capacity retention of 64% after 100 cycles, considerably larger than the 22.6% that N115 presented in the same conditions. Dai *et al.*[281] used a PTFE-reinforced quaternized poly(sulfone) as a complement for the SPEEK, obtaining a sandwich structure in a layer-by-layer disposition, a CE of 98.9% at a current density of 40–80 mA cm^{-2} was obtained, due to the controlled permeation of cations. However, it results in a low ionic conductivity that decreases the VE. Gan *et al.*[282] and Yan *et al.*[283] focused on the use of imidazolium as an anion exchange carrier. Their combinations with SPEEK resulted on the preparation of AIEM with low crossover and high VE of 97.1% (80 mA cm^{-2}) and 97.5% respectively (200 mA cm^{-2}).

Poly(styrene) has also been used as a polymer backbone for AEIMs. Sharma *et al.*[284] studied the functionalization of sulfonated-poly(styrene) with different quaternary ammonium groups. IEC is low due to the formation of ionic knots between the acidic and basic groups of the polymer chains. The best conductivity was obtained when *N*-methylmorpholine was selected as the quaternary agent, resulting in CE and VE of 89.8% and 84.5% at 116 mA cm^{-2}.

A new perspective of the AEIM concept is the use of bipolar membranes. They are a "sandwich" of an anion and a cation exchange layers. The use of these membranes was already known for water splitting and other applications.[285–288] Bipolar membranes allow the design of systems with different pH in each half-cell, with controlled permeation of H^+ and OH^-, avoiding the acid–base neutralization. This concept was extrapolated by Yu *et al.*[113] for a Zn–Br_2 RFB. The use of a pH gradient allows the tunning of the overall redox potential, since the redox potential of the active species is pH sensitive, and the catalysts often perform better at different pH for the anode and cathode this principle was used by Khataee *et al.*[289] for an anthraquinone-2,6-disulfonate (AQDS)-Br_2 RFB. However, in this case, Nafion® 117 was selected as separator, which is a CEM, and the difference of pH was maintained by the buffering character of the prepared electrolytes.

5.5. Acid-doped membranes (ADM)

Poly(benzimidazole) (PBI) appears as the first example of acid-doped membranes.[290] These membranes present moieties with basic behavior, generally amines. In presence of an acid as H_2SO_4 or H_3PO_4, these groups get protonated and the conjugated base is sorbed by the membrane as counter-ion. So, the membrane sorbs the entire acid molecule. The positive charge on the PBI polymer backbone effectively repels cations, while a surplus of acid allows high conductivity.

PBI is usually combined with sulfonated polymers, with the resulting membrane presenting an amphoteric character. Both materials create an ionic crosslinking due to the interaction between sulfonic groups and positively charged benzimidazole moieties. Liao *et al.*[291] used a sulfonated-PAEK as anionic counterpart of PBI for its employment in VRFBs. The high crosslinking leads to a low V crossover, obtaining CE close to 100% at 30 mA cm^{-2}. Similar results were obtained by Chromik *et al.*[292] by using a sulfonated-PAES-PBI composite membrane. As explained by Chen *et al.*,[293] an increase of the PBI/SPEEK mass ratio improves not only the CE, by the reduction of V crossover, but also the mechanical properties, enhancing parameters as elastic module and tensile strength. Oldenburg *et al.*[294] found that a thin film of PBI of 4 μm over Nafion® NR212 was enough to suppress the vanadium crossover, while a thickness over 6 μm is not recommendable since the electrical resistance per area would further increase without any benefits on vanadium transport. Xia *et al.*[295] proposed a copolymer containing both benzimidazole and arylsulfonic moieties as materials for AIEMs. The CE and EE of the assembled VRFB using this membrane reach 97% and 85% respectively at 60 mA cm^{-2} (maximum of 93% and 83% respectively for Nafion®117 in the same conditions), maintaining both values for at least 300 cycles with little decay.

Although PBI is the most studied material for acid-doped membranes, different amine derivatives have been proposed. Dimethylaminoethyl methacrylate (DMAEMA) is a molecule easy of polymerizing due to the double bond of the methacrylate structure. Qiu *et al.* reported the grafting of polyDMAEMA onto ethylene–tetrafluoroethylene, PVDF and its copolymerization along vinylbenzene and further sulfonation to obtain the amphoteric membrane.[296–301] It is noteworthy that the obtained membrane contains the three studied functionalities: sodium styrenesulfonate (CEM), DMAEMA (acid-doped) and quaternized DMAEMA (AEM).[296] The obtained membrane, which is produced by the grafting of the copolymer on PVDF films, exhibited similar conductivity and lower permeability of vanadium ions than N117.

Liu *et al.*[302] introduced ethylenediamine-modified graphene oxide (GO) to reduce the permeability of the membrane. The combination with SPEEK provided a narrow pathway for proton transport, which contributed to improve conductivity. Membrane exhibited CE of 97.2% and EE of 89.5% at 50 mA cm^{-2}, with a capacity retention of 92% after 100 cycles, while for N115 and SPEEK was only 22.6% and 32% respectively. Tests with poly(ethyleneimine)-grafted GO-based membranes were carried out by Cao *et al.*[303] This composite membrane, made of poly(ethyleneimine)–GO and a sulfonated poly(imide), presented values of CE and EE higher than those of the N117 under the same conditions (93% and 78% *vs.* 89% and 70% at 30 mA cm^{-2}). Liu *et al.*[304] used a poly(etherimide) as basic species, creating a SPEEK-poly(etheimide) composite membrane with CE of 97% at 50 mA cm^{-2} and stable without any capacity losses during the first 50 cycles. Other materials such as poly(-acrylonitrile) (PAN)[305] and g-C_3N_4 (ref. 306) have been also proposed to form acid-doped amphoteric membranes with SPEEK. Wang *et al.*[307] introduced both acid-doped and cation exchange moieties in the backbone of the polymer structure by using bis(4-fluoro-3-sulfophenyl)sulfone and a fluorene-derived amine. The best performance was obtained with a composition with 20% of the aminated monomer, obtaining an 88.1% of CE at 50 mA cm^{-2}.

5.6. Size-exclusion porous membranes (SEPM)

The selectivity of IEM is mostly determined by the chemical nature of its constituents, with a critical role of the functional groups, as seen above. However, some membranes use a size-exclusion mechanism to selectively allow the ionic exchange. These porous membranes control the exchange of species through the discrimination of ion size. As a typical example, protons are generally allowed to pass through porous structures because of their small size. So, pore dimensions lower than the diameter of (solvated) active species lead to a decrease in the crossover, increasing the battery efficiency.

The first use of commercial porous membranes can be attributed to Chieng *et al.*,[308,309] who used Daramic® for their implementation of in VRFBs. Although they finally modified the surface with an ion-exchange resin, which changes the exchange mechanism of the membrane, it is also reflected the effect of pore size. The use of DVB as crosslinker decreases the diameter from the 0.1 μm of the untreated Daramic® to less than 60 nm. However, as described by the authors, it was ineffective in blocking the migrating ions. A later study of the mechanism for ion exchange in VRFBs with porous membranes carried out by Zhou *et al.*[310] revealed that an effective decrease of V crossover is reached only when the pore size is below 15 nm.

Different polymers have been tested for preparing SEPM. Zhang *et al.*[311] prepared a membrane based on partially hydrolyzed PAN. Decrease of pore size results in a denser structure and a higher selectivity V/H. A battery assembled with this membrane presented high CE (95%) at 80 mA cm^{-2} and stability during the first 200 cycles. Nevertheless, low VE was observed, reducing EE to 76%. Cao *et al.*[312] studied the effect of the coagulation of PVDF on the morphology of the membrane. Increasing the quantity of ethanol during the preparation process results in a large porosity and elevated permeability to V ions. Authors found an optimum performance for a ratio water : EtOH 1 : 1, which presents lower porosity and a limited pass of species. The VRFB constructed with this kind of membranes reaches an EE of approximately 80%, maintaining it during 50 cycles at 80 mA cm^{-2} practically constant.

Since the main mechanism for ion selectivity is not related to the presence of organic functional groups on the surface of the membrane, porous inorganic materials appear as an alternative for the classical polymer-based membranes. Zeolites are porous inorganic structures based on aluminosilicates used in great scale in industry for separation or catalytic processes.[313] As described previously,[314] zeolites can be prepared with controlled pore size and topology, becoming candidates for their use in SEPM. Yang *et al.*[315] proposed the use of silicalite films as a potential separator for VRFBs. The 0.56 nm pore size was large enough for H_3O^+ permeation and to block vanadyl ions, leading to low crossover. However, the ohmic resistance was high and further improvements of the membrane was required. Yuan *et al.*[316] prepared a polysulfone-supported ZSM-35 zeolite, which presented porous smaller than 0.6 nm. The selected zeolite creates conduction channels for protons with low permeability to V. A VRFB using the zeolite-coated membrane showed a CE of 98.63% and an EE of 91.41% at 80 mA cm^{-2} with a stable performance during the first 100 cycles. Th incorporation of amorphous silica nanoparticles is also an established strategy to improve the selectivity of SEPM. SiO_2 is a material very easy to obtain by hydrolysis of alkoxysilane precursors.[317] In this case, silica does not form channels as in the case of zeolites, but partially blocks the pores of the supporting structure, reducing the permeability to V ion, as can be found elsewhere.[318–320] Yan *et al.*[321] proposed an all-inorganic membrane composed by a TiO_2 layer and a macroporous Al_2O_3 substrate for VRFBs. The membrane presented an average pore size 2.7 nm, reducing vanadium permeability and obtaining an elevated CE of 93.5% at 30 mA cm^{-2}.

6. Electrodes

6.1. Electrodes requirements

Different from the classic solid batteries, electrodes in a RFB do not suffer electrochemical changes in their composition during the charging–discharging cycling. However, they have a critical role in the charge/discharge processes, as they provide support for the electrochemical reactions and connect both half-cells, completing the circuit. These are some requirements for the materials for RFB electrodes:

6.1.1 High electroactive area. Electron exchange reactions take place on the electrode surface. Enlargement of specific area increases the number of reaction sites. Optimization of the microstructure and the use of porous electrodes are useful strategies for new designs.[322]

6.1.2 High electrical conductivity. As the responsible to collect and transport the exchanged electrons from the half-cells, electrodes require a high electrical conductivity to minimize the ohmic losses.

6.1.3 Ability to operate at high current densities. Increasing the current density has the effect of providing equivalent current, and therefore power, with a smaller cell stack.[323] However, it has been reported the degradation of battery electrodes for high current densities.[324] It is necessary an improved stability in these conditions.

6.1.3 Adequate mechanical properties. As in the case of the membranes, electrodes must adapt to the mechanical stress of a RFB, as well as supporting the cell assemble. Previous studies emphasize the critical impact of the response of the electrode to compression and the final performance of the battery.[325,326]

6.1.4 Electrochemical stability. Electrode surface is the area with the highest electrochemical activity, serving as support of the electron exchanges. In some conditions, side reactions as carbon corrosion or hydrogen/oxygen evolution can degrade the electrodes, leading to performance losses,[327,328] as well as mechanical damage on the reactor.

6.1.5 Fast kinetics. Enhancement of charge transfer kinetic in the solid/liquid interface could help to the stability due to the reduction of the corrosion of the electrode surface. It has been previously reported the performance loss as a consequence of the electrode degradation for VRFBs,[329–331] especially sensitive for the negative half-cell were the reaction is kinetically determined.[332] Recently, a new mechanism has been proposed for the anode kinetics degradation in VRFBs.[333] According to it, degradation could be a result of the V^{2+} adsorption on the electrode surface, blocking the V^{2+}/V^{3+} reaction. An employed for strategy the improvement of electrode kinetics is the use of electrodes with non-planar morphologies.[50]

6.1.6 Low cost. Typically, electrodes comprise between 25–40% of the cost of systems, like in Fe–V or Fe–Cr RFBs.[334] So, the price of both electrodes and surface modifiers as electrocatalyst is a parameter to take into account.

6.2. Carbon-based electrodes

Among all the potential candidates for electrode material, carbon is extensively used due to its high electrical conductivity, excellent chemical stability, wide operation potential windows and easy obtainment and modification with large electroactive areas.[18] It was already present in the first systems developed by NASA[95] and Skyllas-Kazacos *et al.*[96] in the form of clothes or felts.

Carbon-based electrodes present high porosity (>90%)[322] to increase the active surface and allow the flow of electrolytes. Electrodes morphology affect directly the performance of the battery, as exposed by Melke *et al.*[335] They compared the electrochemical behavior of graphite flakes, carbon-black and carbon fibre materials. Results show the dependence of electrochemical activity with the content of sp^2-carbon atoms on the surface. For materials with low content of sp^2–C, electron transport is less effective. This kind of C atoms is precisely the structural unit of graphene and related structures as carbon nanotubes (CNT) and carbon nanowalls (CNW). Gonzalez *et al.*[336] proposed CNW thin films as material for the positive half-cell electrode in VRFBs. They presented low overpotential and fast electron transfer kinetics for V(IV)/V(V) redox reactions, which can be attributed to the large amount of exposed reactive graphitic edge planes in this disposition. Munaiah *et al.*[337] used CNTs grown on glassy carbon electrode as the electrodes of a Zn–Br_2 RFB. A similar effect is observed, with remarkable electrochemical behavior in terms of peak current density and peak separation, because of the high number of basal planes and edge planes.

The authors found differences also in carbon obtained from different precursors. Zhong *et al.*[338] compared graphite felts derived from rayon or PAN. Surface microstructure modifications made the difference between both materials. Rayon-derived carbon presented low resistance to oxidation, while PAN-based graphite exhibited better electrical conductivity and electrochemical activity. Ulaganathan *et al.*[339] produced mesoporous carbon electrodes using biomass (coconut shell) as starting material, obtaining an electrode with 60% of mesoporosity, which was used during 100 cycles in a VRFB. Ribadeneyra *et al.*[340] use lignin, obtained from paper industry waste, as a precursor for the preparation of electrospun free-standing carbons for VRFB electrodes. The material possessed a good active area, but the presence of side reactions induced low CE and fast capacity fading.

6.2.1 Modification of C electrodes. C electrodes have been demonstrated to be a reference for the construction of RFBs. However, pristine C materials present low activities and slow kinetics.[48,341] For a potential application in commercial/industrial energy systems, an improvement of properties is necessary.

Various authors remark the influence of oxygenated groups on the surface on the electrochemical performance of electrodes.[18,342,343] Kim *et al.*[344] compared several oxidation methods, including mild oxidation by thermal treatment, oxygen plasma treatment and the use of gamma-ray irradiation. The best VE and EE values were found for the electrodes with mild oxidation, due to their larger number of surface modifications, which provide abundant reaction sites. In later years, the use of similar treatments has been selected by researchers for electrodes optimization. Liu *et al.*[345] activated both carbon felt and paper by the application of 400 °C during 30 h in muffle and tube furnaces. González *et al.*[346] proposed a chemical oxidation of graphite and further exfoliation and reduction, obtaining a graphene-like material. The critical impact of the presence of oxygen during thermal treatments was evaluated by Pezeshki *et al.*,[347] increasing the capacity of the system integrating oxygen-rich electrodes around 50% higher than that of the treated in pure nitrogen.

However, the introduction of N by treatment in the presence of NH_3 gas can lead to higher adsorption of metallic ions and an increase of activity due to the defects appearing by N-doping.[348] Shao *et al.*[349] obtained N-functionalized mesoporous carbon, improving kinetics and reversibility of VO^{2+}/VO_2^+ redox couple. Co-doping of graphite felt surface with both N and O was carried out by Kim *et al.*,[348] obtaining 2–3 times greater reaction kinetics than the only oxidized electrodes at similar atomic contents.

The incorporation of different C nanostructures has been proposed as an alternative strategy for electrodes surface modification due to their elevated electrochemical activity.[350] Tsai *et al.*[351] developed graphene-modified graphite as electrode for RFBs. Best results were obtained with the addition of 3% of graphene, which produced a well-dispersed morphology within the graphite matrix. Similar functionalization with graphene was tested by Li *et al.*,[352] but substituting the graphite by a carbon felt. The obtained material was used as electrode in VRFBs, with a retention of 90% of EE after the 100 first cycles and no visual degradation of the electrodes during 200 cycles.

CNTs have gained relevance through the years attending their properties, among which stands out the electrochemical behavior.[353] Li *et al.*[354] compared the behavior of multi-wall CNTs (MWCNTs) as electrodes for VRFBs. MWCNTs suffered several functionalizations to optimize their electrochemical response. An outstanding performance was observed for carboxyl MWCNTs, due to the high surface area and the possible role of the carboxyl into the adsorption of active species. Park *et al.*[355] grown CNT/nanofibers directly on the surface of carbon felts (CF), improving discharge capacity and EE by 64% compared to untreated CF electrodes (Fig. 11). The use of N-doped CNTs on carbon felts was proposed by Wang *et al.*[356] Equivalently to the C electrodes explained above, N doping improves the performance of CNTs, increasing active species adsorption, generating defects and enhancing the electrochemical accessibility of the non-doped structures.

6.2.2 Incorporation of metallic catalyst. Previous bibliography reflects the use of several metals or metal oxides as electrocatalysts in processes as hydrogen/oxygen evolution or fuel cells.[357–359] A series of metals have been tested as electrode surface modifiers, in order to increase electrochemical activity and reaction kinetics. Traditionally, noble metals suppose a reference due to their unbeatable stability, making them reasonable candidates for C modifications. Wang *et al.*[360] proposed the functionalization of a porous carbon felt with Ir by reduction of H_2IrCl_6. The resistance of the cell of the VRFB assembled with these electrodes decreased by 25% compared to the non-modified felts, increasing the EE by about 6% for the global process. A copper nanoparticle deposited graphite felt electrode was tested by Wei *et al.*[361] The use of this material enhances not only the EE but the utilization of the electrolyte due to the catalytic performance of Cu ions (Fig. 12). Flox *et al.*[362] selected $CuPt_3$ nanocubes as electrocatalyst for graphene and PAN-derived carbon. The cell which incorporates PAN–$CuPt_3$ electrode reached a maximum EE of 84% at 20 mA cm^{-2} for at least 20 cycles. Nevertheless, the use of noble metals is limited due to their availability and high cost. A problem with side reactions is also presented, since these elements catalyze other

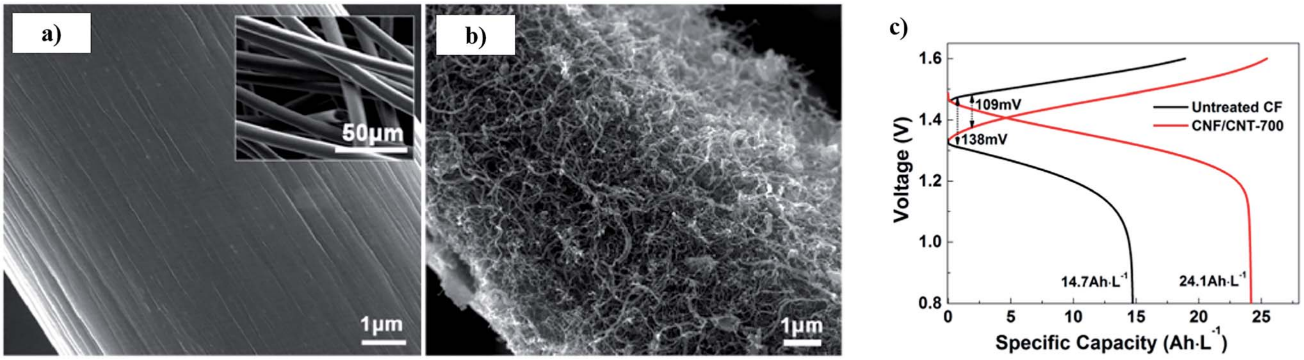

Fig. 11 SEM image of (a) untreated CF, (b) CNF/CNT grown CF surface. (c) Charge–discharge voltage profiles of VRFB employing untreated and CNF/CNT-T electrodes at 40 mA cm^{-2}. Extracted from ref. 355.

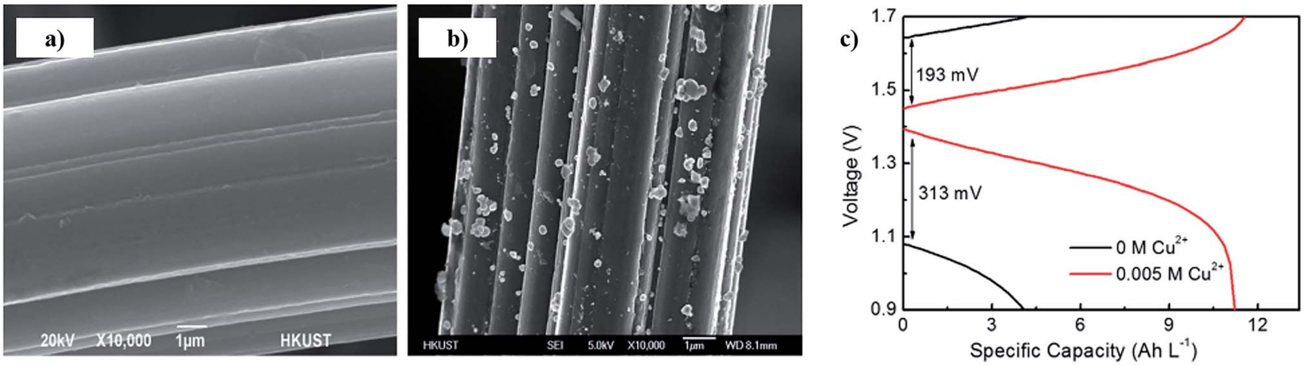

Fig. 12 SEM images of (a) original graphite felt and (b) the graphite felt decorated with copper nanoparticles. (c) Charge and discharge curves of VRFBs employing electrolytes containing different Cu^{2+} concentrations at 300 mA cm^{-2}. Extracted from ref. 361.

side reactions, as the hydrogen[363] or oxygen[364] evolution reactions, limiting the efficiency of the systems.[365]

Other metals were proposed as an alternative for the improvement of batteries performance. Special interest resides on the optimization of carbon electrodes for the negative size of VRFBs, since the $V^{2+/3+}$ transformation slower kinetics affect critically the final performance.[341] Ghimire *et al.*[366] employed a titanium carbide-decorated electrode in the negative half-cell with a 13% gain in energy efficiency (EE) at a current density of 100 mA cm^{-2}. Ti was also used by Vázquez-Galván *et al.*,[367] in the form of nitride–TiO_2, for the functionalization of a commercial carbon felt. This composite not only enhances the catalysis of the $V^{2+/3+}$ reaction but also inhibits the hydrogen evolution, the main drawback of the noble metals as previously described. Chen *et al.*[368] reduced the quantity of Pd by incorporation of TiO_2. Introduction of the sintered C–TiO_2–Pd electrode in a V–iodine system results in high efficiency values, with VE and EE of 96.56% and 81.23% respectively, maintaining them for at least 50 cycles. The introduction of Ti as titanium nitride was proposed by Yang *et al.*[369] Charge transfer resistance is much smaller for the Ti-modified electrode as compared to the original, obtaining a value of EE of 81.74% for the VRFB. MnO_2 is a material typically used in energy storage devices, as supercapacitor electrode. Jiang *et al.*[370] took advantage of the vast knowledge of this material for the construction of a Mn-functionalised carbon paper. The prepared electrodes improved electrochemical activity on the negative size, increasing the EE by 6% at 100 mA cm^{-2} regarding the pristine carbon paper. Li *et al.*[371] modified graphite felts with Bi nanoparticles for VRFBs. Their use led to an improvement on EE of 11% in respect of the pristine felt. Additionally, an applied current of 150 mA cm^{-2}, which is around 2.5 times higher than that without Bi, is feasible due to the catalytic effect of the metal. According to Suarez *et al.*,[372] this improvement is a consequence of the formation of BiH_x during the redox processes, which competes with the hydrogen evolution, responsible of CE losses. Li *et al.*[373] prepared W-doped Nb_2O_5 nanorods onto graphite fibers substrate for its application as VRFB electrode. Niobium oxide nanoarchitectures provide catalytic activity and elevated active area and the introduction of W salts in the preparation media allows the obtainment of a homogenous distribution and a smaller size of the nanorods. The introduction of these modifications increases the maximum applied current to 150 mA cm^{-2}, with a capacity of 14.4 A h L^{-1}.

7. Cell design

7.1. Construction materials

The optimization of the cell design and components, including electrode structure, electrolyte, membrane and architecture, is crucial for developing the next generation of high-performing and large-scale RFBs. The typical design of a redox flow cell is illustrated in Fig. 2; a battery stack is formed by connecting a number of unit cells. Briefly, a RFB is composed of a positive and a negative electrode and an IEM separating both; for avoiding electrolyte leakages, rubber gasket seals and steel tie-bolts are normally used to compress the cell. Metallic end-plates (*e.g.* aluminum and copper) are used as current conductors to provide electrical conductivity and flow distributors, and turbulence promotors are often employed to increase the mass transport and exchange of electroactive species between the bulk electrolyte and the electrode surface. Since the electroactive species used in RFBs are mostly highly oxidizing, no metallic component should be in contact with the electrolytes. Therefore, the cell components, excluding the metallic end-plate and the electrode catalysts, should be made of chemically resistant polymers, such as PTFE, PP, PE, ethylene-polypropylene-diene monomer (EPDM), polyvinylchloride (PVC), PVDF and acrylics (Perspex®).

7.2. Flow field architectures

Since Aaron *et al.*[374] reported for the first time in 2012 a serpentine flow field design, similar to those used in proton-exchange membranes (PEM) fuel cells, flow field designs have interested many researchers and engineers. Efforts have shown that RFBs with suitable flow field designs exhibit a more uniform distribution of the electrolytes through the electrode, particularly at smaller flow rates, and better electrochemical performance compared with those without flow field designs.[11]

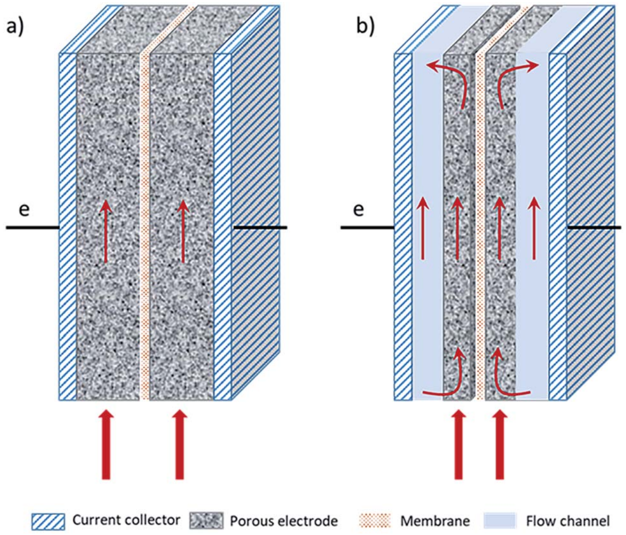

Fig. 13 Configurations of porous electrodes used in RFBs: (a) flow-through design and (b) flow-by design (adapted from ref. 509).

7.2.1 Flow-through and flow-by electrode configurations. Two basic architectures are used to flow the electrolytic solutions in the cell electrodes: (i) flow-through electrode configuration (Fig. 13a) and (ii) flow-by electrode configuration (Fig. 13b). In both configurations, the fluid flow is perpendicular to the current flow, but they differ from the design of the bipolar plates. In the flow-through, the bipolar plates have flat faces and electrolytes percolate transversally from one side to opposite one of thicker electrodes, while in the flow-by configuration the bipolar plates interposed between adjacent cells have flow channels on each face to promote a better distribution of the electrolytes into thinner electrodes. Therefore, the flow-through configuration requires extremely low flow rates and yields a lower return on investment, which makes it impractical for redox energy storage applications.[375] For these reasons, the flow-by electrode has been reported as the most suitable configuration for RFBs, demonstrating improved cell performance attributed to the smaller ohmic losses and the enhancement of localized mass transfer in the porous electrode.[376]

Besides the conventional RFB configurations, a zero-gap assembly has been increasingly adopted since the first work by the Zawodzinski's group.[374] This configuration employs structured flow fields that act as the current collector and compress the carbon electrodes (usually carbon felts) against a membrane, which dramatically reduces the ohmic drop in the cell, thereby displaying improved limiting current density and peak power density.

7.2.2 Flow field at the bipolar plate. Typical flow field designs used in RFBs are the serpentine flow field (SFF) and interdigitated flow field (IFF); their structures over the porous electrode are shown in Fig. 14a and b, respectively. For both flow field designs, the electrolyte flow can be forced through the porous electrode and adjacent flow channels; however, for the SFF design only a small fraction of the electrolyte reactants actually penetrates into the porous electrode driven by pressure gradients, while for the IFF all of the electrolyte reactants are forced through the porous electrode. The optimum flow field depends on the several aspects of the system, such as the electrode materials and the electrolytes chosen. For example, a VRFB with a SFF showed lower overpotentials due to a better electrolyte distribution over the electrode surface and a higher round trip efficiency at the optimum flow rate when compared with a RFB without flow field structure.[377] On the other hand, the use of an IFF bipolar plate over multiple layers of carbon paper electrode can improve the cell performance, due to the fact that thinner electrodes are enabled to be used instead of carbon felt or graphite felt electrodes, which consequently leads to smaller ohmic losses.[378] In addition, carbon paper electrodes also have a large surface area to volume ratio that reduces kinetic and mass transport losses.

Other flow fields, such as parallel flow field (PFF), spiral flow field (SpFF), tubular flow field (TFF) and circular flow field (CFF) have also been tested for RFB applications.[11] More recently, the equal path length (EPL) and aspect ratio (AR) flow field designs have been evolved based on the IFF design, demonstrating higher cell performance. For enhancing the localized mass transfer in the porous electrode, a corrugated flow field (CorFF) was designed that leads to higher limiting current density and peak power density. Marschewski *et al.* reported[379] an innovative tapered, microscale-interdigitated flow field (T-IFF) fabricated by 3D printing. In this approach, the flow battery supplies power but its fluid also carries waste heat from the microprocessors, which allowed to reach an output normalized limiting current density of > 17 500 mA cm^{-2} mol^{-1} and a peak power density of 1.4 W cm^{-2}. One of the highest power density achieved so far was *ca.* 2.6 W cm^{-2} for a 5 cm^{2} VRFB cell with a SFF structure and carbon paper electrode.[380] A summary of the limiting current density and peak power density achieved in RFBs with the various flow field designs is reported elsewhere.[11]

7.2.3 Flow dynamic modelling. Multi-dimensional models and simulations are time and cost saving tools used for easily understanding how to improve the cell performance, such as current density and power density, as well as for optimizing flow distributions within the porous electrode to achieve uniformly localized current distributions. As the electrolyte flows through the flow fields and over the porous electrode, forced convection (due to pressure gradient), diffusion (due to concentration gradient) and migration (due to potential gradient) terms have to be considered.[381] From the aspect of fluid dynamic modelling, the Nernst–Planck equation and the charge conservation equations should be used for describing the charge transport; the mass conservation and electrolyte flow are based on the continuity and momentum conservation equations.[382] The Butler–Volmer equation needs to be applied to describe the electrochemical reaction kinetics.

Computational fluid dynamics (CFD) modelling may be more efficient to optimize flow fields prior to experimental testing, simulating of the electrolyte flow transport through the flow field and porous electrode in RFBs.[383] Chakrabarti *et al.* reviewed the modelling electrode processes in RFBs and concluded that it is essential to understand the kinetic and

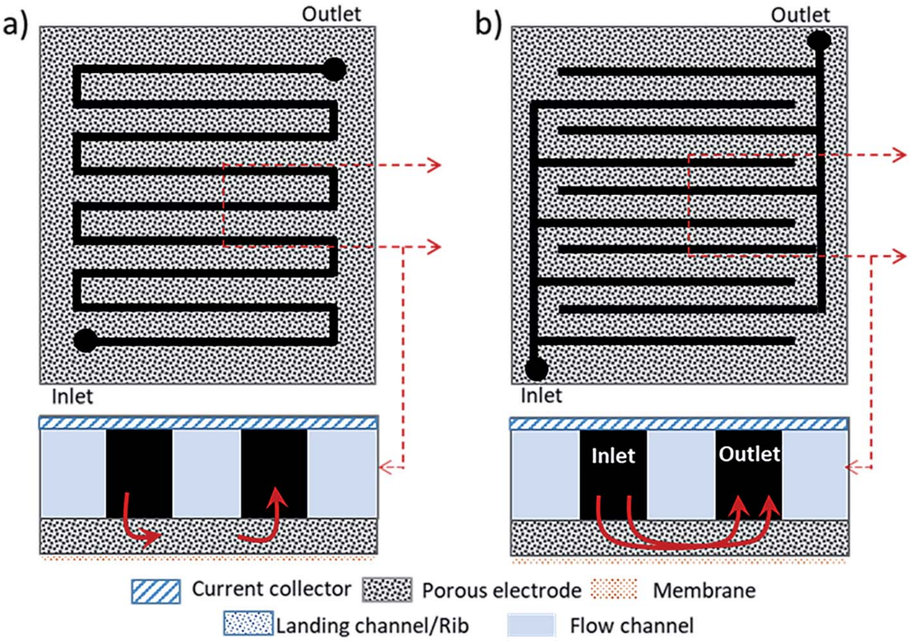

Fig. 14 Cross section views of the flow channels over the porous electrode using: (a) serpentine flow field (IFF); and (b) interdigitated flow field (IFF) (adapted from ref. 11).

mass transport phenomena in the porous electrodes, but also that multiscale approaches are needed to enable optimisation across the relevant length scales.[384] Recently, Delgado *et al.*[382] developed a 2D-dynamic phenomenological modelling of a VRFB using an AEM. It was demonstrated that the concentration overpotentials during charging and discharging steps are not equal owing to a mismatch between the state of charge and the state of discharge; the current density had a higher contribution than the flow rate. Moreover, these results showed that positioning the distribution channels close to the membrane allows a concentration overpotential reduction of up to 3.9%.[382]

7.3. Membraneless cell designs

As previously mentioned, the reliability of the IEMs is one of the main disadvantages of the RFBs, *i.e.* they need to be chemically and mechanically stable to meet the ionic conductivity and selectivity requirements. Moreover, the membrane and the electrolyte are usually the most expensive components of these systems, with an expected cost reduction of *ca.* 20–40% for IEM-free cell designs.[385] Membraneless cells are based on a fluid–fluid interface across which selective ion exchange must occur with minimal reactant crossover; thus, design challenges involving fluid flow and species transport have to be addressed to achieve efficient and selective ion exchange with minimal crossover. Most of the previous works on membraneless flow cells have involved investigations of electrochemical cell designs, such as microfluidic fuel cells, which present scalability and stackability as current issues. The designs reported to date are: (i) single-phase co-laminar flow (SLF); (ii) flowing electrolytes separated by a flowing stream of a supporting electrolyte (FSE); (iii) multiphase co-laminar flow (MLF); (iv)

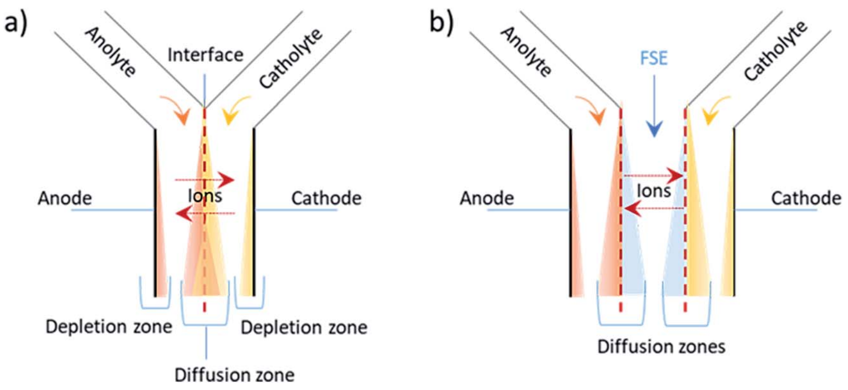

Fig. 15 Schematics of membraneless flow cell with: (a) a single-phase co-laminar design; and (b) a flowing separating electrolyte regime design (adapted from ref. 387).

membraneless hybrid flow batteries (MHFB); and (v) ionically inert solid separators (IISS).

The SFL is the most studied membraneless design; the anolyte and catholyte flow laminarly side-by-side through parallel micro-channels under laminar flux, which minimizes electrolyte mixing under the adequate fluidodynamic conditions. In these microdevices, power density, ranging from 40 mW cm^{-2} employing flow-by electrodes to up to 750 mW cm^{-2} for optimized flow-through electrodes, is mainly limited by the low flow rates that are necessary to maintain the laminar flow. The Y-shaped channel shape design (Fig. 15a) was first reported by Ferrigno *et al.*[386] with vanadium aqueous electrolyte solutions, but more chemistries consisting of iron-based active species supported in ionic liquid electrolytes,[387] as well as using non-aqueous electrolytes have been demonstrated.[388,389] For VRFBs, Kjeang *et al.* showed a CE of *ca.* 50% and the highest discharge power densities of up to 300 mW cm^{-2} with a two-inlet/two-outlet cell.[390] Despite the advancements, the reactant crossover/cross-contamination and self-discharge, always present in these co-laminar microbatteries, are responsible for the low coulombic efficiencies (<50%) and low reactant conversion (<20%) that limit the potential use of SLF designs.[376] Moreover, their scalability is limited by the compulsory microfluidic design, which restricts their practical applications to a series of commodities and small power utilities.

Designs with multiphase reactants and those including a flowing separating electrolyte stream, *i.e.* MLF and FSE designs respectively, reduce reactant crossover through the implementation of a counter-flow pattern (Fig. 15b), which leads to improve performances. A good example is the Braff's hydrogen–bromine membraneless RFB that uses an aqueous hydrogen bromide solution as the FSE design showed a round-trip voltage efficiency of 92% at 25% of peak power density (795 mW cm^{-2}).[391]

MHFBs that are not constrained to microscale design principles based on the immiscibility of redox electrolytes have been recently reported. The proof-of-concept was demonstrated by Navalpotro *et al.*[392] using one acidic solution and one ionic liquid, both containing quinoid species. This biphasic system exhibited an open circuit voltage of 1.4 V, a stable discharge plateau at 0.9 V and a power density of 1.98 mW cm^{-2}.[391] The versatility of this concept was demonstrated by using different aqueous-nonaqueous immiscible electrolytes (neutral aqueous, butanone, PC, *etc.*), different redox organic molecules (anthraquinones, TEMPOs),[376] and more abundant, less toxic and less expensive battery chemistries (ionic liquids/Na_2SO_4 and poly(ethylene glycol)/Na_2SO_4). Although the crossover can be suppressed by choosing species with adequate partitioning, the self-discharge at the interface is inherent to this technology and constitutes one of the most important challenges. Another challenge is the RFB operation under flowing conditions, since commonly used filter press reactors are not appropriate within these configurations.[376] Therefore, alternative reactor designs should be developed to demonstrate if this membrane-free approach might become a real alternative.

Further improvements and increased adoption of low-cost IISS as the scalability and stackability do not require cell assembly that differ much from typical RFB designs with IEMs. The main purpose of such separators is not ion exchange but aiding the separation between the reactants and the FSE or reactant-to-reactant liquid–liquid interface in the case of a co-laminar flow design. Escalante-Garćıa *et al.*[261] used a Daramic® microporous separator to evaluate the performance of a non-aqueous V(acac)$_3$ RFB (active area of 5 cm^2), achieving 73% CE and 68% EE against 91% CE and 80% EE when is used a pre-treated Nafion® 1035 membrane. Following the power output improvements, scale-up attempts capable of recharging and recirculation of the same electrolyte streams for multiple cycles have been limiting the potential of the membraneless RFB designs.

7.4. Large-scale flow batteries

For achieving larger cell voltage, power and capacity, the development of large-scale flow batteries with multi-stack designs are required, as well as the optimization of manifolds and channel ducts. Increasing electrolyte volume stored in the external tanks and size of cell stacks, either cell number (voltage) or cell area (current) will lead to larger power and energy.[11] For example, an aqueous-based RFB stack reaching 15 kW was designed with 120 cells (with an electrode area of 1500 cm^2) displaying a nominal current density of 60 mA cm^{-2} and a single cell voltage of *ca.* 1.4 V.[393] A commercial prototype of a 40 kW (225 W L^{-1}) VRFB stack was developed by Vionx Energy Corporation. In the next subsections, it will be discussed the three main factors for designing large-scale flow battery stacks: flow distribution, shunt current loss and pump loss.

7.4.1 Flow pattern. The optimization of the flow distribution is even more essential for large-scale applications. CFD is a powerful tool to simulate the uniformity of flow distribution, as discussed in Section 7.2. The goal of optimizing flow distributions by modelling is to easily increase the utilization of the porous electrode area and, consequently, improve the electrochemical performance of RFB stacks. Factors to be considered in the cell design are flow channel width and depth, landing dimensions and porous electrode properties, such as permeability, wettability and thickness; fluid properties, such as composition, temperature and flow rate, are also important.[11] Operational optimization of flow rates will also contribute to ensure reduced pumping power while preserving electric performance.[394] From the aspect of electrochemistry, the electrolyte flow distributions also affect the ion concentration distributions and diffusion boundary layers associated with the mass transfer limiting current densities.[11] Kim *et al.*[229] conducted a CFD analysis on a single flow frame and on 20 and 40 cell stacks (using the same flow frame design) for optimizing the flow distribution within the porous electrode and then achieving uniformly localized current distributions. Despite cells near the inlet and outlet ports tend to have slightly larger flows as the number of cells increase, it was validated an uniform fluid flow through each cell in both cell stack assemblies, showing a maximum variation < 0.25% of the ideal flow rate. Also, longer and narrower port channel allows to have a more uniform flow distribution, but higher pressures drops.

7.4.2 Shunt currents. Redox flow cells are connected electrically in series with a bipolar plate, *i.e.* an anode current corrector on one side and a cathode current collector on the other side, and they are fed electrolyte in parallel from a common manifold channel. Since electrolytes are conductive, they are prone to shunt (leakage) currents, *i.e.* electric currents along the distribution and flow channels, which produce additional losses in current and voltage efficiencies and power, thereby decreasing the cell performance. Research efforts also demonstrated that shunt currents can cause unwanted side reactions, including corrosion and gas generation. Several dynamic models, based on mass balance, energy balance and electric circuit, have been used to investigate different parameters of the battery system.[393,395,396] Understanding the distribution of shunt currents allows more accurate predictions about the stack performance, while provides an insight into battery design and optimization. Kaminski *et al.*[397] reported that the maximum shunt current in the stack manifold occurs at the center cell in the stack and its distribution t is related to the design of the anode and cathode cell compartments. Therefore, shunt currents are affected by dimensions and layouts of manifold components, cell voltage, applied current, conductivity of electrolyte and number of cells in the stack.[11] During standby, shunt current and its associated internal discharge reactions can generate heat and increase stack temperature, potentially leading to thermal precipitation in the positive half-cell that could block the channels and membranes and thus lower battery performance.[398] For reducing the effect of shunt current on stack efficiency and temperature, it is desirable to have longer length and smaller cross-sectional area channels. However, it is generally recognized that extending the path of electrolyte flow in the manifold and port channels, *e.g.* designing longer and thinner ducts, is detrimental to increase the pumping losses (resulting from increased pressure drops). Therefore, the trade-off among minimization of shunt currents, pumping losses and flow distributions needs to take into account for an optimal design.

7.4.3 Stack and tank sizing. Compared to other electrochemical storage technologies, in RFBs the power conversion is separated from the energy storage units, thus allowing for independent power and energy sizing. The power directly depends on the charge/discharge current and on the voltage that is generated between the electrodes of the stack; the maximum power value is reached when both current and voltage are maximum. This means that the power is related to the size of the electrochemical cells stack and it can be increased connecting more cells in series or parallel. Then, the maximum voltage needed for the stack is given by the product of the number of cells connected in series and the cell voltage, which can be obtained from the Nernst equation.[399] On the other hand, the energy capacity depends on the volume of the tanks and, consequently, on the concentration of the electrolyte solutions. This feature allows for virtually unlimited capacity of RFBs by using more electrolyte volume and larger storage tanks, which makes them suitable when storage times longer than 4–6 h are required.[394] The energy of present designs ranges from 102 W h to 107 W h. However, the reversible nature of the RFB reactions, enabling the same cell to operate as converter of electricity into chemical energy and *vice versa*, as well as the handling and storing RFB's liquid electrolytes (instead of managing hydrogen gas as in fuel cells), allow the use of two low cost tanks. One tank contains the positive electrolyte (catholyte) and the other contains the negative electrolyte (anolyte). Only two pumps are needed for circulating the electrolytes between the two tanks and the cell electrodes, making the system a closed circuit. The electrolyte tanks should contain the same amount of liquid, but the oxidation state of each species will depend on the reaction that takes place in the cell during the operation of the system. As long as there are species that can be transformed, the battery can continue the process of charging or discharging. Therefore, this configuration also avoids self-discharge and the cells can be left completely discharged for long periods with no ill effects.[393,394] Moreover, rapid refueling by solution exchange is possible, in case of need, and furthermore, they require low maintenance.

7.4.4 Stack performance and limitation. In the design of large-scale flow battery stacks aiming at high cell performance and even durability, trade-offs are to be made among achieving uniform flow distribution, minimizing pump and shunt current losses. Few studies on the design of large-scale stacks have been reported in literature. To date, two examples of kW-scale flow battery stack systems presented are aqueous-based and suspension-based.[400] The first work on aqueous vanadium RFB stacks was done by Skyllas-Kazacos *et al.*,[401] who demonstrated a 1.33 kW stack based on 10-cells with an electrode area of 1500 cm^2 and an applied current density of 80 mA cm^{-2}. Recently, Pacific Northwest National Laboratory (PNNL)[229] developed a 1.1 kW VRFB stack (15-cells) achieving a higher stack energy efficiency by utilizing mixed electrolytes of hydrochloric acid and sulfuric acid, an active electrode area of 780 cm^2 and an applied current density of 80 mA cm^{-2}. Larger electrode area and more cells in the stacks were reported by Zhao *et al.*,[402] Park *et al.*[403] and Wu *et al.*[404] for the vanadium stacks and power in the range of 5–10 kW. Research programs currently underway aim at reducing the cost and size of RFB systems, while improving their power density, to make them commercially competitive. Various patents on flow fields, bipolar plates and stacks used in RFBs have been filled and contribute to commercialization effects all over the world.[11]

7.5. Applications and installations

RFBs are a good choice for stationary applications that require large stored energy, such as: (i) inter-stational storage; (ii) load levelling function, storing the surplus energy during off-peak demand periods, and using it during periods of high demand of energy; (iii) uninterruptible power supply (UPS) in case of failure of the main power source; (iv) support systems in renewable energy installations, such as wind or solar, during periods of high energy demand; (v) electric or hybrid vehicles, especially those of large dimensions due to its low energy density (*e.g.* buses and maritime vehicles such as boats, ships or submarines); and (vi) storage applications that require a full charge from an initial, empty state to full load.

VRFBs have reached effective commercialization in the 80s;[394] nowadays, 26 companies are producing this technology and several plants have been installed globally, according to Vanitec website.[405] Among the world largest VRFBs are: (i) 5 MW/10 MW h system launched in China by Rongke Power (RKP) in 2012;[406] (ii) the Minami Hayakita Substation in Japan, rated 15 MW and 60 MW h and built for Hokkaido Electric Power Inc. in 2015;[407] and (iii) the energy storage station at Fraunhofer ICT in Germany rating 2 MW and 20 MW h (2019).[408] The largest project so far results from the collaboration of the RKP and the Dalian Institute (DICP-RKP group) of China. This VRFB demonstration consists of a power capacity of 200 MW (ten units rated at 20 MW) and an electricity storage capacity of 800 MW h.[409] Table 4 summarizes the main existing VRFB installations across the globe.

Present research aims at electrolytes capable of increased energy density, membranes with higher proton conductivity and lower ions crossover, porous electrodes capable of better hydraulic performance. Therefore, other redox chemistries have been proposed for flow and hybrid batteries, such as zinc-based RFBs (ZBFBs), displaying high operating OCV (*ca.* 1.58 V) that have been scaled-up into industrial systems.[40] Among them, zinc-bromide flow battery is the most investigated and successfully commercialized. Ensync Energy Systems (US) manufactured a 2 MW/2 MW h system for load leveling service in 2004 and Toyota Motors (Japan) and Fiat (Italy) are using Sn–Br batteries to power electric vehicles.[410] ZBFB pilot systems are capable of charge/discharge durations up to 10 h, a performance comparable to commercial VRFBs and can operate at current densities up to 80 mA cm^{-2}, with energy efficiencies around 80%. However, they are not cheaper than equivalent VRFBs due to expensive sequestering agents needed to avoid toxic bromine vapor emissions.[376] In this sense, employing sustainable redox active organic molecules based on Earth-abundant elements as C, H, O, N, S is a promising for large scale applications. Kemiwatt, Jena Batteries, Green Energy Storage and CMBlu European companies are focused on the development of aqueous organic redox flow batteries (AORFBs). Kemiwatt working on quinone-based electrolyte and Jena Batteries employing pyridine-based anolyte have successfully tested demonstrators on kW scale (20–100 kW and 400 kW h), while aiming for MW scale.[376] TEMPO derivatives and iron(II) complexes as ferrocenes or ferrocyanide have been employed as the catholyte counterpart.[164] Viability of AORFB will be highly dependent on active material's cost and high stability. The wide range of materials available, complemented by high-throughput screening and computational investigations, could result in the optimization of new chemistries for RFBs.

8. Economic aspects

RFB technology possesses the potential to occupy the main position of static energy storage systems. To reach this status, it is necessary to adapt their development to the market guidelines in terms of cost/performance. As a standard, scientific community uses as an indicator the price (in USD generally) invested per kWh of capacity of the battery ($\$\ \mathrm{kW\,h^{-1}}$). The USA Department of Energy, through the inform Grid Energy Storage, fixed a long-term system capital cost target of $\$150\ \mathrm{kW\,h^{-1}}$, with a good enough stability to spend less than 10 $\$\cdot$kW per h per cycle.[416] This objective was established for a battery with a system efficiency over 80% and cycle life of more than 5000 cycles. The large working lifetime and cyclability already reported[417] clearly surpass these values, making this technology potentially more attractive for grid energy storage.

In order to clarify the main factors that determine RFB prices, authors have developed a series of mathematical models.[59,334,418,419] Even with different points of view and considerations, common elements are included in all the provided models, including electrolyte, cell and stacking, control components and installation. The focus is mainly set on the most variable cost of chemicals and materials, as well as for the design and the stacking. The following paragraphs summarize the more remarkable aspects of each component.

8.1. Electrolyte components

Models divide the total price of the electrolytes into three different sources:[26,59] redox-active species, solvent and supporting electrolyte. Redox-active species have received special attention, because of all the considerations needed for its cost evaluation. While prices are set on $\$\ \mathrm{kg^{-1}}$, a low molar mass implies a higher number of active units per kg, reducing the cost for the same number of moles. Similar reasoning is applied

Table 4 Main existing installations of VRFBs in the world

Installation	Place	Energy density/MW h	Power density/kW	Application	Year/ref.
Kashima-Kita Electric power	Japan	0.8	200	Load-leveling	1996/(ref. 411)
Kansai Electric	Japan	1.6	200	Load-leveling	2000/(ref. 412)
Kansai Electric	Japan	6	4 000	Peak-shaving and UPS	2005/(ref. 413)
RKP	China	10	5 000	—	2012/(ref. 406)
Hokkaido Electric power	Japan	60	15 000	Grid integration of wind renewable energy	2016/(ref. 407)
Frauhofer project	Germany	20	2 000	Testing purposes	2019/(ref. 408)
UniEnergy technologies	US-WA	8	2 000	—	2020/(ref. 414)
DICP-RKP	China	800	200 000	—	2021/(ref. 415)

to the number of exchanged electrons. A molecule which exchanges 2 electrons per reaction will decrease to the half the price per mole of electrons when compared with 1-electron processes. Solubility also appears as a determinant factor, but in this case, affecting the total mass of electrolyte. A greater value of solubility will reduce the solvent needed for the same number of active species.

The other two components, solvent and supporting electrolytes, are intimately linked. New solvents as DESs and ILs are still in development and will not be considered for cost comparisons. Since water presents basically no additional cost to the entire price of the system, there is a great difference when using non-aqueous media. Even for lower-price organic solvents, as PC, would add \$45−50 kW h^{-1} to the material cost.[44] Supporting salts need a good solubility and conductivity in the selected media, determined by the solvent selection. Low-cost compounds such as NaCl or H_2SO_4 can be used for aqueous media, with variations in electrolyte cheaps in comparison to other cost contributions.[420] However, for non-aqueous solvents, salt costs can be higher than the rest of the components of the electrolytes (\$20 kg^{-1}) because of the use of fluorinated anions as PF_6^- and $N(SO_2CF_3)_2^-$.[44]

After considering all the different parameters, Darling *et al.*[59] designed a graphical adaptation of their model that summarizes the requisites that must satisfy a proposed electrolyte to be economically suitable for the development of RFBs based on its chemistry (Fig. 16). It represents the allowable chemical cost (\$ kg^{-1}) *vs.* the OCP (V). The price of the reactor is incorporated into the graph by the addition of the lines $ca \cdot R$ (\$ $m\Omega^{-1}$). Each point of the line is calculated for a total value of the system of \$120 kW h^{-1}, under the target price fixed by USA DE of \$150 kW h^{-1}. Shaded triangles mark the regions where the electrolytes are economically promissory for aqueous (blue) and non-aqueous (green) systems.

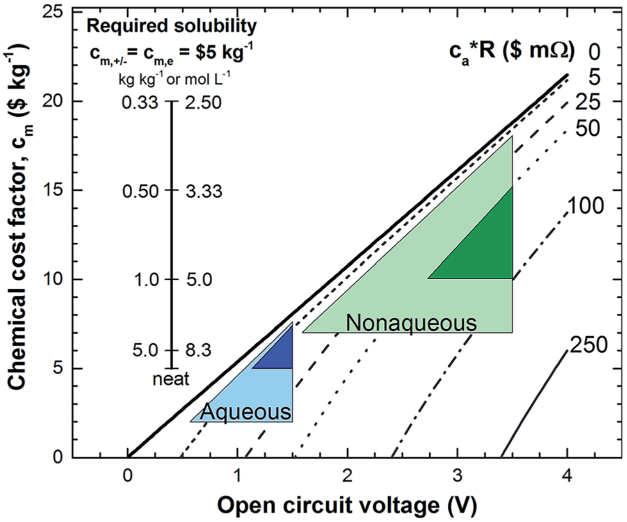

Fig. 16 Allowable chemical cost factor on an active material basis (in \$ kg^{-1}) *versus* OCP for a range of reactor costs (caR in \$ mU^{-1}). All points on a line give a system price of \$120 per kW per h. The region $U < 1.5$ V is considered to be available to aqueous systems. The dark shaded triangles are considered to have a higher likelihood of achievability compared to the larger lighter shaded triangles. The leftmost inset vertical scale shows the required solubility (in mol L^{-1}) of a nonaqueous active species when solvent and solute cost \$5 kg^{-1}. The rightmost inset vertical scale on the right shows the molar concentration, assuming specific volumes of 1 L kg^{-1}. Extracted from ref. 59.

The graph remarks the main limitation of each system. For aqueous electrolytes, the stability of water is limited to around 1.5–1.7 for most favourable cases as Zn–Br_2 or lead–acid batteries. Therefore, the price of electrolyte should be reduced for the same energy. A practical guideline for a reasonable cost for aqueous systems is \$2 kg^{-1}. Higher voltages are restricted to non-aqueous solvents, which cost is higher than water. The model predicted that a minimum of 2 V (preferably 2.7 V, dark green triangle) for a non-aqueous electrolyte to be potentially considered for their implementation in RFBs, appearing this region on the right side of the Fig. 16.

8.2. Cell and stacking

Revised models[26,59] relate the cost of the cell to the area of the reactor, including bipolar plates, electrodes and membranes. The final price of a system is referred to the energy that is able to storage and supply, which is clearly affected by the area-specific resistance associated with the cell components. Cost also involves all the terms on which energy depends as OCP, discharge VE, system efficiency during discharge, which includes losses external to the cell as pumping or other equipment, and discharge time.

Regarding the building materials, great effort is invested in the development of low-cost IEM. However, their cost still supposes around \$20 kW h^{-1} (assuming \$500 m^{-2}, 0.5 W cm^{-2}, and 5 h capacity),[421] due to the standard use of Nafion® as membrane. Incorporation of lower-cost reinforcement can dilute the economic impact of this material. It is estimated that by reducing the price of membrane materials from \$1000 m^{-2}, a price that can be easily reached by Nafion® membranes, to \$100 m^{-2} the total capital cost can be reduced in more than 75%.[44] Exchange of Nafion® by SPEEK-based membrane could decrease by 2.5 the price of the system. This reduction could be more pronounced when using SEPM, leading to a price one order of magnitude below .[422]

Electrodes are basically constituted by different morphological carbon, which price causes less economic impact when compared with IEM. However, the use of a good-performance electrocatalyst can increase the cost of this part of the cell, especially when using noble metals. Concern is mitigated due to the small quantity required of the desired catalyst to provide a remarkable enhancing of system properties. Following the calculation realized by Perry *et al.*,[421] a loading of 0.1 mg cm^{-2} of a platinum-group metal alloy for a cell with power density of 0.5 W cm^{-2} and 5 h energy capacity would only add \$2 kW h^{-1} to the total price of the system.

8.3. Control components and installation

Last term considered focuses on the equipment external to the cell and its installation. It contains the flow system (pumps, pipes, fans, filters, valves), thermal regulation (heat exchangers) and control system. It also must be added costs of delivery, interconnection, and step-up transformation as part of the installation process.

Monitoring the performance of the system attracts an important part of the investment. Some authors highlight the relevance of the control of flow rate and the state-of-charge during the charge–discharge process,[423–425] being necessary to increase the equipment for that purpose. The addition of a strategy for the detection of leaking and other possible electrolyte losses is also necessary.

A particularity of the RFBs which differs from classical batteries installation is the construction of the electrolyte tanks. They can require additional supporting structures for bigger systems or specific designs for reduced indoor batteries.[426]

Generally, there is no great cost difference between the different RFB chemistries for the external components and installation, as reported by Darling *et al.*[59] as the cost for balance-of-plant components. Variations can be found for requirements derived from the cell chemistry, as an increased security control due to toxicity (bromine) or fire risks (flammable solvents); or gas-flow control (Zn–air).

9. Characterization techniques

9.1. Basic techniques

In this first section, a group of basic techniques largely employed for the evaluation of batteries performance are summarized. Exist a bast bibliography where the theoretical principles can be consulted.[427–429] In this manuscript, only the main characteristics of each technique are introduced.

9.1.1 Charge–discharge curves and cycling. The most widely used *in situ* electrochemical technique to evaluate the performance of flow batteries is the charge–discharge curves. Briefly, a constant current is applied to the system, making the voltage raise until a previously set value. This first part of the experiment is the charge. At this point, the equivalent opposite current is applied to discharge the system. Successive charge–discharge cycling gives information about C, VE, CE and EE, as well as their useful lifetime. In addition, the sensitivity of cycling behavior to current density can provide some indirect insight into limiting phenomena occurring in the battery, *e.g.* slow reaction kinetics, high ohmic loss, and poor mass transport.[430]

9.1.2 Cyclic voltammetry. Analysis of electron-exchange reactions is realized by the cyclic voltammetry (CV), thus allowing to investigate reduction and oxidation processes. This experimental method is commonly used in initial studies of new redox chemistries and has been used to assess the performance of porous electrodes for capacitive deionization.[430]

The separation between both peaks, oxidation and reduction, is defined by the number of electrons exchanged and an indicator of the electrochemical reversibility of the reaction. The higher the separation, the lower the electrochemical reversibility. It is noteworthy the possibility of chemical irreversibility, which is caused by the degradation of at least one of the species of the pair during the cycling process.

9.1.3 Conductivity measurement. Conductivity measurements can be performed *in situ* and *ex situ* to assess electronic, thermal and ionic conductivity. An elevated conductivity is required in the different components of the RFBs to avoid the ohmic losses.

The ionic conductivity is usually measured to assess the conductivity of the solution (electrolyte) as well as the conductivity of the IEM (separator). For measuring the conductivity of a liquid electrolyte, an external conductivity meter is usually used.[431] In addition, it is critical to precisely measure the thickness and the width of the samples used in the conductivity cell. The ionic conductivity of separators is usually measured using the four-electrode AC impedance technique.

9.1.4 Electrochemical impedance spectroscopy (EIS). Electrochemical impedance spectroscopy (EIS) is a powerful technique to characterize the electrical behavior of the entire system and the individual components, namely to detect/quantify the process losses, most of them proceeding at different rates. EIS is able to distinguish between the different resistance contributions, even for systems involving multiple-step reactions, parallel reactions or additional processes, such as adsorption.[432]

EIS in RFBs enables the separation of the different contributions of the components to the impedance, finding those that can be improved or presented problems. In the best of the cases, specific physical processes, as overpotentials due to charge transfer[433] or mass transport, can be differentiated. Additionally, offers the possibility to investigate the components separately from the entire dispositive or tested in half-cell systems. EIS has been applied to a variety of chemistries, including all-vanadium,[434] aqueous organic,[435] hybrid air–vanadium,[436] and non-aqueous vanadium,[437] *etc.*

9.1.5 Rotating disk electrode (RDE) voltammetry. Rotating disk electrode (RDE) voltammetry is a common technique used to study reaction mechanism behavior and mass transport characteristics, similar to stationary cyclic voltammetry. However, in RDE, the working electrode spins in the electrolyte and a laminar flow is established above the surface of the RDE. An RDE setup is an *ex situ* method and primarily uses electrode materials that are not directly useable in an operating RFB.

The mass transference can be described by the Levich equations. Considering a gradient of concentration, the equation for the limiting current for a reaction controlled by mass transfer can be obtained eqn (11):

$$i_t = 0.620nFAC^0D^{2/3}\nu^{-1/6}\omega^{1/2} \tag{11}$$

Considering the Levich equation, representation of i_{t} *vs.* $\omega^{1/2}$ leads to a straight line that passes through the origin. Deviation from the linearity reveals a kinetic limitation of the reaction in the selected electrolyte.

9.2. Polarization curves

Measurements of cell potential as a function of current density are known as polarization curves. For these experiments, the system should be in a steady state in relation to the relative concentration of redox species. These curves are determined by the cell resistance, exposing information about performance losses. Although this technique is typically used in fuel cells, where a steady state can be easily achieved, it could be employed for RFBs, where a similar state can be obtained by a constant supply of reagent during operation at a stoichiometric flow rate above that demanded by the current density.[438]

A generalized polarization curve is shown in Fig. 17; its shape is a composite of kinetic losses usually described by the Butler–Volmer model, ohmic losses obeying Ohm's law, and mass transport losses (also known as concentration polarization) described by local concentration limitation effect on reaction.[430] For low current densities, main losses possess a kinetic nature that could be a result of high reaction overpotential or electrode polarization. Ohmic processes dominate potential losses when current density takes an intermediate value; the ionic conductivity, especially through the membrane, and the internal resistances associated with contacts between the components (wire, tanks, electrodes, current collector, *etc.*) determine the slope of the straight line typical in this region. At the highest currents, losses are due to mass transport within flow fields or within an electrode structure. For systems with elevated kinetic and ohmic losses, this part of the curve cannot be appreciated.

Distribution of the different losses offers a tool to localize the source of decreasing efficiency and let a selective improvement, focused on their precedence. It is noteworthy that all of these mechanisms exist simultaneously for every current value, even when one of them is more notorious for each range of current.

9.3. Pressure drop and pump energy

One of the main concerns about RFBs, in terms of design engineering, is the control of the electrolyte flow rate. Measuring the normal operating pressure of the system, at real-time conditions, is further useful for diagnosing any deviations from the optimal operation that may affect the cell performance. Such perturbations could involve clogs associated with precipitates or contaminants in the electrolyte, leaks in the manifold or through cell materials (*e.g.* gaskets or plumbing), or issues with the pumps.

Changes in the pressure can be directly obtained. Classically, the pressure difference can be measured between the electrolyte inlet and outlet ports, with direct observation of the total pressure drop.[439] Nevertheless, more recent research introduces the use of transducers for pressure detection at several points of the system,[440] obtaining more precise information about the effect of each section on the total pressure change.

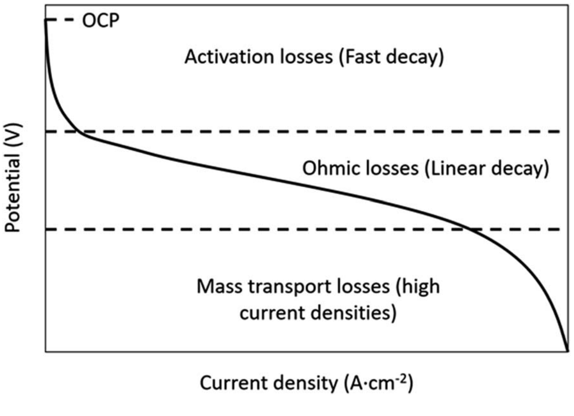

Fig. 17 Generalized polarization curve for a VRB indicating the dominant source of overpotential in each region.

Pressure drop is also an important metric for assessing the EE of the system since it will directly determine the pumping energy required during charge and discharge in conjunction with the flow rate; this relation is calculated from eqn (12):[423]

$$E_{\text{pump}} = \frac{\Delta p_{\text{total}} Q}{\alpha} t \tag{12}$$

where, Δp_{total} is the total pressure drop, which depends on the flow rate, Q is the flow rate, and α is the pump efficiency for the selected pump configuration and operational conditions.

9.4. Visualization of flow distribution

The use of the entire active surface of the electrodes is the ideal scenario during the exploitation of a RFB. The identification of electrolyte flow distribution within the cell can be performed using optical and thermal visualization techniques. Optical visualization of RFB flow distributions is an area that has been scarcely explored due to system and component limitations. Nevertheless, this is not a trivial matter since the inner part of the cell is covered by opaque components, avoiding direct flow visualization. Until a few years ago, computational modeling was the only tool available to provide information about the flow distribution.[441–444] Nowadays, a series of thermal techniques are under development employing a Reynolds analogy for the direct visualization of the electrolyte flow mixing and distribution within the electrode, through the correlation of mass transport with thermal transport.

Two different thermal approaches were proposed. First, the thermal detection using an electrolyte (or water) with differential temperature with respect of the cell. Houser *et al.*[445] replaced the membrane of a half-cell with a heat-sensitive liquid crystal sheet (temperature sensitivity range of 25–30 °C). Instead of closing the cell with the other flow field, a PVC plate was set, allowing the direct visualization of the liquid crystal changes. The detection method employed by Tanaka *et al.*[446] was the infrared thermography (IRT); a one-electrode model cell was constructed, where the carbon felt was sandwiched by clamping plates. The temperature of both electrodes and plates is controlled by thermocouples during the experiment. The hot working liquid was injected into the previously cooled cell, obtaining the flow pattern.

The second concept is the implementation of radiative techniques. Bevilacqua *et al.*[447] employed synchrotron X-ray radiography and tomography for the visualization of the flow path along carbon felt porous electrodes (Fig. 18). Due to the specific design of the cell, the effect of the compression on the flow distribution can be also addressed. The groups of Brandon and Shearing employed their knowledge on the use of time-resolved X-ray tomography for fuel cell[448] and Li-ion battery[449] electrodes for the elucidation of the electrolytes path in RFBs, obtaining 3D images of the wettability of the carbon electrodes.[450] These groups applied the benefits of the X-ray-based

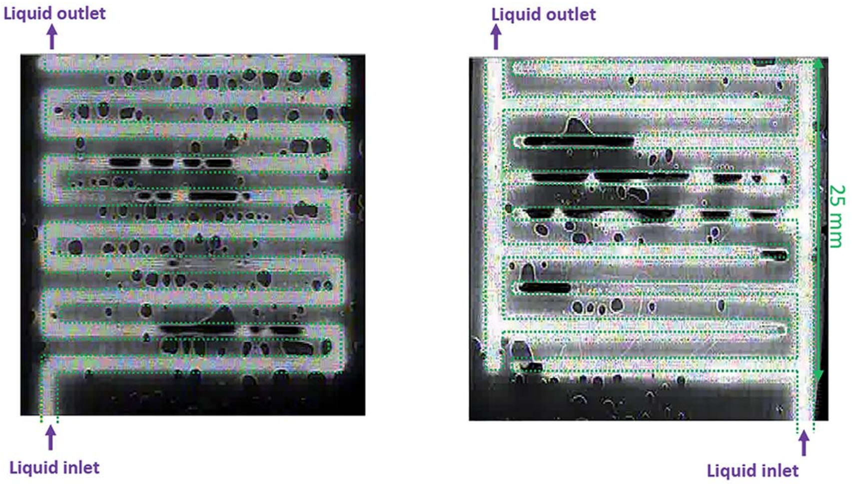

Fig. 18 Mass transport visualization showing the effect of flow field: (left) serpentine and (right) interdigitated. Extracted from ref. 456.

techniques for the direct image study of the microstructure of newly prepared electrodes,[451] determination of mass tranfer parameters[452,453] and their degradation *in situ*.[454,455] The reactor designed by Rubio-García *et al.*[456] was optimized for the use of luminol as a flow tracker. The reaction between luminol and hydrogen peroxide generates light, which can be monitored with a photodiode. To allow the pass of light, one of the electrodes is an (ITO) transparent conductor. The use of one transparent terminal is also applied by Wong *et al.*,[457] composed of a UV- transparent acrylic. Researchers take advantage of the fluorescence of AQDS for the observation of the flow by fluorescence microscopy. It is important to emphasize that this is the only example of a full RFB cell with flow visualization.

9.5. Potential distribution

Detection of polarization sources on the different components of the RFBs is the main objective of the potential distribution studies. These experiments are carried out *in situ*, while the battery is operating. A stable reference electrode is required. The potential probes are connected to the reference and then situated between the components of interest in a sandwich-like arrangement. Hwang *et al.*[458] use lugging capillaries as potential probes, that were introduced in several points of the cell for complete potential distribution. Researchers put special attention on those situated on both sides of the membrane, receiving direct information of the potential drop consequence of the resistivity of the IEM. To extract the information, a curve was plotted representing the measured potential with respect to the profile of the cell.

The group of Mench *et al.*[430,459] focused on the potential distribution on the carbon paper electrode of a VRFB. To provide a suitable surface area for electrode reactions, three layers of carbon paper were stacked and the potential was measured on the surface of each layer, introducing the potential probes on the sandwich structure. For obtaining information about the through-plane direction, a model was developed with consideration of convective, diffusive and electrophoretic fluxes.[430]

9.6. Current distribution

To obtain the best performance of a RFB, the electrode surface must be uniformly in contact with the electrolyte. The formation of homogeneities can lead to local overpotential during the charging process, with the appearance of secondary reaction as corrosion or gas evolution.[460] Measurements of current distribution provide information regarding the balance between transport and the kinetics of the electrode.[461] These techniques require the segmentation of some of the components of the cell, as the current collector or the flow field, but the obtained data can give more useful details than a simple one-dimensional performance curve.

Exist several approaches for the obtention of the current distribution. Hall effect sensors have been previously used in fuel cells[462,463] and are potentially employable for the study of RFBs. However, to the authors' knowledge, it doesn't exist a current distribution study for RFBs with this kind of detection. Hsieh *et al.*[464] substituted flow fields in a VRFB into 25 graphite segments, with each segment connected to a current shunt. Nevertheless, the resistor network technique presented problems due to increased contact resistance, low spatial resolution and relatively high cost. Clement *et al.*[465,466] employed a printed circuit board (PCB), containing the resistors embedded, which eliminates problems with electrical connections and improves the spatial resolution;[460] this technique avoids the limitations of machining a flow field. Becker *et al.*[467] employed the potential probes approach to measuring current distribution in a flow frame VRFB with carbon felt electrodes under different compressions and flow rates. A new method was introduced by Ma *et al.*[461] with the utilization of a total internal reflection (TIR)-based sensor, obtaining not only the current distribution but also a map of oxygen evolution reaction with time resolution.

9.7. Monitoring electrochemical reactions

Electrochemical behavior of the species and components of a RFB can differ from their isolated characterization if

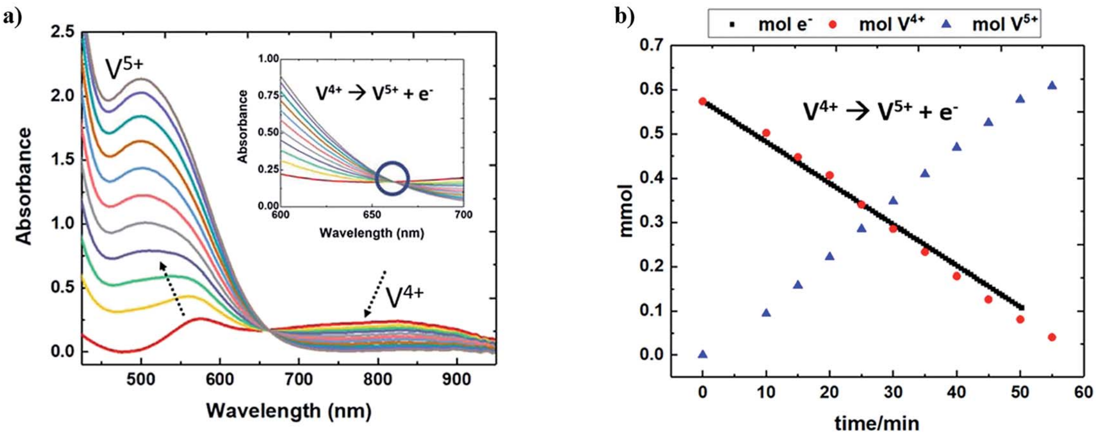

Fig. 19 (a) Monitoring of a VRFB during charge by UV-Vis. (b) Evolution of the number of moles of reduced (red) and oxidized (blue) species and the number of moles of electrons removed electrochemically (black line). Extracted from ref. 471.

compared with an operating system. Control of the reactivity inside the cell while working becomes essential. This section groups a series of auxiliary techniques to determine the chemical activity inside the battery.

Most of the active species used for electrolytes, as metal-containing or aromatics compounds, present color or absorbance in the ultraviolet (UV). Changes in their electronic configuration due to transfer-electron reactions provoke a variation in the absorption bands. Absorbance is related to the concentration of each species following the Lambert–Beer law.[468] If the bands of reduced and oxidized forms of the same redox pair are resolved in the spectrum, the continuous registration of their concentrations during the experiment is a direct measurement of the SoC of the battery. Degradation of these species can also be monitored by the detection of new species on the ultraviolet-visible (UV-Vis) spectra. Both advantages were employed by Tong *et al.*[469] during the study of quinone-containing RFBs. They were able to find the relationship between HQ and SoC by absorbance measurements. Additionally, a non-desired species, the quinhydrone dimer, was also detected, exposing its relevance to the performance of the battery. The system was modified by introducing a cross-flow cell into the flow system, coupled with UV-Vis Spectrometer. It supposes another advantage as it is no necessary modification of the cell. A similar methodology was implemented by Shin *et al.*[470] for the study of the SoC of a VRFB. In this case, instead of incorporating the cell, they used a bypass on the flow system to recirculate the flow to the spectrometer. Gokoglan *et al.*[471] change the focus, realizing the measurements directly in the tank with the help of a UV-Vis fiber-optic probe (Fig. 19). It is remarkable that the experiment was carried out in a non-aqueous media, with DMSO as the solvent, showing no interferences in the measurement wavelengths.

Raman Spectroscopy has been employed for *ex situ* monitorization of the changes in the species of RFB electrolytes. Investigations of Bauer *et al.*[472] and Jeon *et al.*[473] focused on bromine-based batteries. Kausar *et al.*[474] applied Raman studies for the determination of the different vanadium sulfate compounds during the charge of a VRFB. An alternative technique, Fourier Transform Infrared (FTIR) spectroscopy, was employed by Kautek *et al.*[475] for *in situ* investigations on the formation of Br-complexes for an operating Zn–Br_2 RFB.

Secondary reactions as decomposition of the electrolyte or degradation of the electrodes is a main concern that must be evaluated during the operation of the RFBs. Mass spectroscopy (MS) has been adapted for *in situ* analysis of gas releases from the cell. The evolution of gases is an undesired process that typically occurs on the electrode surface due to the application of elevated potentials. Sun *et al.*[476] used MS technique to quantify the hydrogen evolution on the negative carbon electrode for a VRFB, finding a linear increase of the hydrogen released with time. Liu *et al.*[477] designed an equivalent method for the positive electrode. It showed a preferred evolution of CO_2 and CO due to the corrosion of the electrode, instead of the predictable O_2 release. Kosswattaarachchi *et al.*[478] observed the evolution of the BODIPY proposed as a precursor for all-organic RFBs. The molecule breaks due to the bulk electrolysis and the fragments are identified by MS.

Some of these techniques, as Raman spectroscopy, and other classical methods used in materials sciences as scanning electron microscopy (SEM) or X-ray photoelectron spectroscopy (XPS) are applied for the characterization of electrodes after a certain operating time.[329,473,479] Potential damages or failures are analyzed *ex situ* to understand their effect on battery performance.

10. Conclusion and perspectives on RFBs

The aim of this review is to offer both the scientific and industrial community a critical overview of the RFB system together with detailed insights of their technical, scientific and economic aspects. The field of RFBs has been booming recently, particularly after the necessary advancements that made this technology competitive in the energy market. Nevertheless, several bottlenecks are yet in place and we expect to see significant improvements in the next few years. Here are presented some perspectives that might unlock the full potential of RFBs.

10.1. Use of membrane-electrode assemblies (MEAs)

Development of the IEMs is a main concern, which has been approached by the exchange of the constituent material. Researchers try to explode the similarities between fuel cells and RFBs architectures, especially of those batteries which possess a gas as one of the components, to find new tools for the improvement of their technologies. The use of IEMs is a common factor of both energy systems, with the possibility of knowledge sharing. In this sense, the use of membrane-electrode assemblies (MEAs) is presented as an alternative to the classic IEM. It is composed of a stack of an ion-permeable membrane and an electrode (or both). The electrode material is normally deposited onto the membrane surface. MEAs have been extensively studied for fuel cells[480,481] because of the accessibility of the active species and exchanged ions to both membrane and electrode and the effective removal of produced water.[482] Hosseiny *et al.*[41] explored the use of MEAs in a vanadium/air flow battery. Compared with an equivalent fuel cell, the cost of the catalyst is reduced since only the reversible air side requires it, with the vanadium reaction reversible on graphite. New patents[483,484] were registered in 2019 for the use of MEAs in RFBs with the possibility of use liquids for both half-cells, as for VRFBs. Authors suggest an improvement of the cell short and cell resistance by using of MEAs, opening a new opportunity for research on new RFB architectures.

10.2. Introduction of solid energy boosters

As described throughout the article, the total capacity of a RFB is determined by the volume of the electrolytes tanks. Improvement of electrolytes is the main strategy to maximize the effective use of this volume, obtaining maximum energy storage capacity. In 2013, Huang *et al.*[485] proposed a new concept where the former active species acts as charge carriers, furtherly known as mediators, transporting it to a solid redox active material, known as booster, that is found into the tanks. Energy storage takes place on the solid booster, as they receive the charge from the mediators. The standard potential of the redox mediator has to match the Fermi level of the redox solid booster to ensure a reversible charge transfer at the solid–liquid interface.[486] Initially, this concept was applied for Li-based RFBs with a non-aqueous media, where $LiFePO_4$ is considered the preferred booster for lithiation-delithiation processes.[485,487–489] Fan *et al.*[490] introduce the Prussian blue, a low-cost pigment, as an alternative booster for a solar-rechargeable RFB, using EV and I_2 as mediators. The first proposal of the use of mediators/boosters in aqueous media was made by Zanzola *et al.*[491] In this case, the energy storage is carried out in polyaniline, which possesses three stages of oxidation. Iron ions are used as mediators. Authors reach a three-fold improvement in volumetric capacity, compared with the electrolyte alone.

10.3. Combined systems: solar redox flow cell

Due to their adaptability, RFBs possess a great potential for more sustainable energy storage. Generally, the battery should be coupled with a conversion energy system, such as wind turbines. A further step is the development of new multiple-task or combined designs, removing the necessity of extra elements for the implementation of the batteries. In this scenario, solar redox flow cells (SRFCs) appear as emerging technologies to tackle the photovoltaic intermittency issues. Briefly, a SRFC uses based on a semiconductor–liquid junction photo-electrochemical cell to charge the redox pairs dissolved in electrolytes; they can be discharged at a RFB. Therefore, a SRFC displays the following advantages over other systems such as solar water splitting: (i) the redox energy levels of the electrolytes can be optimized to fit the energy levels of the photo-electrode, rendering the system more efficient; (ii) non-aqueous solvents can be used for improving the stability, and the stored energy density; and (iii) allows the simultaneous conversion of sunlight to an electrochemical fuel and to thermal energy; (iv) faster kinetics with lower overpotential in redox reactions; (v) no need for gas pressurization; (vi) possibility of using a closed system with no need for refueling. Due to its simplicity, compact size, and the low cost of the raw materials considered, which are earth-abundant, it is expected that the SRFC devices are very cost-effective. However, the SRFCs are still at a scientific research stage and not ready for industrialization. New chemistries using inexpensive and unlimited materials, as well as high-efficient and stable photoelectrodes have been implemented to gain an advantage in lifespan and performance values. A more detailed analysis of the principles and mechanisms involved on SRFCs can be found elsewhere.[22,492] Our group is the author of several SRFC proposal, including aqueous organic and inorganic actives species, using as photoelectrode materials as hematite or CdS.[164,493,494]

Other tandem models have been proposed in the literature. Kim *et al.*[495] designed a water deionization system coupled to a RFB. Ions from seawater migrate through the IEM, balancing the charge due to the electrochemical storage reactions. Jiang *et al.*[496] achieve the electrochemical reduction of CO_2 by its incorporation as active species in one of the half-cells of an electrochemical flow cell.

10.4. Design of new active species through molecular engineering

As described previously in the review, the use of organic molecules as active species is an interesting research topic due to its high variability in terms of redox potential and cost reduction.[171] To maximize the benefits of the use of this kind of redox pairs, it is proposed the use of molecular engineering. It approaches the design, synthesis and testing of new potential active molecules from their basial principles (interactions, redox potentials) to the construction of a complete species, optimizing each of the steps of the structure modification (variation of the redox-active group, incorporation of groups with effect on the electronic structure or solubility, *etc.*). Several authors have used employed this strategy for the selection of new candidates as redox pairs in RFBs.[497,498]

As a result of the rational design of improved structures, the bipolar molecules appear to be a solution for some of the main problems of working RFBs.[499–501] These molecules present both the negative and positive redox center as parts of the same structure. It offers the possibility of construction of symmetric RFBs, avoiding problems of species exchange. Even more, this rational design allows the assemble of more than one redox-active center of each nature per molecule, increasing the number of exchanged electrons per mole of active compound, as exposed by Winsberg *et al.*[500]

10.5. Introduction of 3D printing for component building

The design and building of the electrochemical cell are major challenges for engineers. Special effort is made on the optimization of flow architecture. The variable requirements of the flow channel demand a technological adapt for the construction of battery components. In this sense, 3D-printing techniques are presented as the solution because of their cost efficiency and flexibility for the design. Computational studies allow the optimization of the flow channel, giving the path for the 3D print, independently of its complexity. The as-prepared components met all the requirements for a future normalized usage, as is described in the bibliography.[379,502–504]

10.6. Composite electrolytes: combining RFBs

Nowadays, technologies following the principles of the flow batteries, as VRFBs, are commercially implemented as energy storage systems. Taking advantage of all the knowledge of these kind of chemistries, new derived electrolytes has been proposed. These composite fluids aim to exploit the different benefits of each energy storage mechanism, combining classical all-liquid RFBs with active species of the hybrid batteries. The presence of C nanoparticles, which are the base of the slurries used in semi-solid flow batteries, reduces the ohmic resistance, increasing the VE and EE compared with a commercial VRFB.[505] An increase of the energy density has been found when other redox active ions, as Mn[506] or Fe,[507] are incorporated to the V electrolytes. This strategy is not only applicable to the VRFBs. Other active species suffer equivalent effects when other carbonaceous materials (*i.e.* graphene) are suspended in the media,[508] opening a broad range possibilities for RFBs improvement.

Acronym list

acac	Acetylacetonate
ACN	Acetonitrile
AEM	Anion-exchange membranes
AIEM	Amphoteric ion-exchange membranes
AQ	Anthraquinone
AQDS	Anthraquinone-2,6-disulfonate
AR	Aspect ratio
bpy	2,2′-Bipyridine
BQ	Benzoquinone
BTMAP	Bis(3-trimethylammonio)propyl
CE	Coulombic efficiency
CEM	Cation-exchange membrane
CF	Carbon felt
CFD	Computational fluid dynamics
CFF	Circular flow field
CNT	Carbon nanotubes
CNW	Carbon nanowalls
CorFF	Corrugated flow field
Cp	Cyclopentadienyl anion
CV	Cyclic voltammetry
DBMMB	2,5-Di-terc-butyl-1-methoxy-4-[2′-methoxyethoxy] benzene
DES	Deep eutectic solvents
DMAEMA	Dimethylaminoethyl methacrylate
DMF	*N*,*N*-Dymethylformamide
DMPZ	5,10-Dihydro-5,10-dimethyl phenazine
DS	Degree of sulfonation
DVB	Divinylbenzene
EC	Ethylene carbonate
EE	Energy efficiency
EEC	Equivalent electrical circuits
EIS	Electrochemical impedance spectroscopy
EPDM	Ethylene-propylene-diene-monomer
EPL	Equal path length
Fc	Ferrocene
FcN	Quaternary ammonium-functionalized ferrocene
Fe-TEA	Triethanolamine-iron
FPAE	Fluorinated poly(arylene ether)
FSE	Flowing electrolytes separated by a flowing stream of a supporting electrolyte
GO	Graphene oxide
HQ	Hydroquinone
IEM	Ion-exchange membrane
IFF	Interdigitated flow field
IISS	Ionically inert solid separators
IL	Ionic liquid
ITO	Iron tin oxide
MEA	Membrane-electrode assemblies
MHFB	Membraneless hybrid flow batteries
MLF	Multiphase co-laminar flow
MS	Mass spectroscopy
MV	4,4-Dimethyl bipyridinium; methyl viologen
MWCNT	Multi-wall CNTs
NARFB	Non-aqueous redox flow battery
NASA	National Aeronautics and Space Administration
NHE	Normal hydrogen electrode
NMePh	*N*-Methylphthalimide
NQ	Naphthoquinone
OCP	Open-circuit potential
PAEK	Poly(aryl ether ketone)
PAES	Poly(aryl ether sulfone)
PAN	Poly(acrylonitrile)
PBI	Poly(benzimidazole)
PC	Propylene Carbonate
PCB	Printed circuit board
PE	Polyethylene
PEEK	Poly(ether ether ketone)

PEM	Proton-exchange membranes
PFF	Parallel flow field
POM	Polyoxometalate
PP	Polypropylene
PTFE	Polytetrafluoroethylene
PVDF	Poly(vinylidene fluoride)
RDE	Rotating disk electrode
RFB	Redox flow battery
SEM	Scanning electron microscopy
SEPM	Size-exclusion porous membranes
SFF	Serpentine flow field
SHE	Standard hydrogen electrode
SLF	Single-phase co-laminar flow
SoC	State-of-charge
SPEEK	Sulfonated-PEEK
SpFF	Spiral flow field
SRFC	Solar redox flow cells
TBA	Tetrabutylammonium
TEA	Tetraethylammonium
TEMPO	2,2,6,6-Tetramethyl-1-piperidinyloxy
TEMPOL	4-Hydroxy-TEMPO
Tf	Triflate; trifluoromethanesulfonate
TFF	Tubular flow field
TFSI	Bis(trifluoromethanesulfonyl)imide
T-IFF	Microscale-interdigitated flow field
TIR	Total internal reflection
UPS	Uninterruptible power supply
VRFB	Vanadium redox flow battery
XPS	X-Ray photoelectron spectroscopy

Conflicts of interest

There are no conflicts of interest to declare.

Acknowledgements

This work was financially supported by: project PTDC/EQU-EQU/30510/2017 – POCI-01-0145-FEDER-030510 – Sunflow "Solar energy storage into redox flow batteries" funded by FEDER funds through COMPETE2020 – Programa Operacional Competitividade e Internacionalização (POCI) and by National funds (PIDDAC) through FCT/MCTES. J. Azevedo and P. Dias would like to acknowledge the Portuguese Foundation for Science and Technology (FCT) for funding (CEECIND/03937/2017 and CEECIND/02862/2018, respectively).

References

1 Energy Information Administration US, *International Energy Outlook 2019*, 2019, available from: http://www.informaworld.com/openurl?genre=article&doi=10.1080/01636609609550217&magic=crossref.

2 Z. Yang, J. Zhang, C. W. M. Kintner-Meyer, X. Lu, D. Choi, *et al.*, Electrochemical energy storage for green grid, *Chem. Rev.*, 2011, **111**(5), 3577–3613.

3 R. Todd, D. Wu, J. A. Dos Santos Girio, M. Poucand and A. J. Forsyth, Supercapacitor-based energy management for future aircraft systems, *Conf Proc – IEEE Appl Power Electron Conf Expo – APEC.*, 2010, 1306–1312.

4 E. Faggioli, P. Rena, V. Danel, X. Andrieu, R. Mallant and H. Kahlen, Supercapacitors for the energy management of electric vehicles, *J. Power Sources*, 1999, **84**(2), 261–269.

5 *Development of Sodium-Ion Batteries for Grid-Scale Energy Storage*, ECS Meet Abstr, 2016, available from: https://iopscience.iop.org/article/10.1149/MA2016-03/1/71.

6 H. S. Hirsh, Y. Li, D. H. S. Tan, M. Zhang, E. Zhao and Y. S. Meng, Sodium-Ion Batteries Paving the Way for Grid Energy Storage, *Adv. Energy Mater.*, 2020, **10**(32), 2001274, available from: https://onlinelibrary.wiley.com/doi/10.1002/aenm.202001274.

7 M. Pehl, A. Arvesen, F. Humpenöder, A. Popp, E. G. Hertwich and G. Luderer, Understanding future emissions from low-carbon power systems by integration of life-cycle assessment and integrated energy modelling, *Nat. Energy*, 2017, **2**(12), 939–945, available from: http://www.nature.com/articles/s41560-017-0032-9.

8 B. Bolund, H. Bernhoff and M. Leijon, Flywheel energy and power storage systems, *Renew. Sustain. Energy Rev.*, 2007, **11**(2), 235–258.

9 T. Mathews, Flywheel Based Kinetic Energy Recovery Systems (Kers) Integrated in Vehicles, *Int. J. Eng. Sci. Technol.*, 2013, **5**(9), 1694–1699.

10 H. Ibrahim, A. Ilinca and J. Perron, Energy storage systems-Characteristics and comparisons, *Renew. Sustain. Energy Rev.*, 2008, **12**(5), 1221–1250.

11 X. Ke, J. M. Prahl, J. I. D. Alexander, J. S. Wainright, T. A. Zawodzinski and R. F. Savinell, Rechargeable redox flow batteries: flow fields, stacks and design considerations, *Chem. Soc. Rev.*, 2018, **47**(23), 8721–8743.

12 R. Belu, *Energy Storage, Grid Integration, Energy Economics, and the Environment*, CRC Press, 2019, p.376.

13 J. Noack, N. Roznyatovskaya, T. Herr and P. Fischer, The Chemistry of Redox-Flow Batteries, *Angew. Chem. Int. Ed.*, 2015, **54**(34), 9776–9809.

14 J. Sheng, A. Mukhopadhyay, W. Wang and H. Zhu, Recent advances in the selective membrane for aqueous redox flow batteries, *Mater. Today Nano*, 2019, **7**, 100044, DOI: 10.1016/j.mtnano.2019.100044.

15 H. Prifti, A. Parasuraman, S. Winardi, T. M. Lim and M. Skyllas-Kazacos, Membranes for redox flow battery applications, *Membranes*, 2012, **2**(2), 275–306.

16 M. Guarnieri, A. Trovò, A. D'Anzi and P. Alotto, Developing vanadium redox flow technology on a 9-kW 26-kWh industrial scale test facility: Design review and early experiments, *Appl. Energy*, 2018, **230**, 1425–1434, DOI: 10.1016/j.apenergy.2018.09.021.

17 C. Minke, T. Hickmann, A. R. Dos Santos, U. Kunz and T. Turek, Cost and performance prospects for composite bipolar plates in fuel cells and redox flow batteries, *J. Power Sources*, 2016, **305**, 182–190, DOI: 10.1016/j.jpowsour.2015.11.052.

18 K. J. Kim, M. S. Park, Y. J. Kim, J. H. Kim, S. X. Dou and M. Skyllas-Kazacos, A technology review of electrodes and reaction mechanisms in vanadium redox flow batteries, *J. Mater. Chem. A*, 2015, **3**(33), 16913–16933.

19 G. Kear, A. A. Shah and F. C. Walsh, Development of the all-vanadium redox flow battery for energy storage: a review of technological, financial and policy aspects, *Int. J. Energy Res.*, 2011, **36**(11), 1105–1120.

20 H. Abdi, R. Rasouli Nezhad and M. Salehimaleh, Fuel Cells, in *Distributed Generation Systems*, Elsevier, 2017, pp. 221–300, available from: https://linkinghub.elsevier.com/retrieve/pii/B9780128042083000054.

21 Z. Melhem, *Electricity Transmission, Distribution and Storage Systems*, Elsevier, 2013, p. 512.

22 K. Wedege, D. Bae, W. A. Smith, A. Mendes and A. Bentien, Solar Redox Flow Batteries with Organic Redox Couples in Aqueous Electrolytes: A Minireview, *J. Phys. Chem. C*, 2018, **122**(45), 25729–25740.

23 E. Wikner and T. Thiringer, Extending battery lifetime by avoiding high SOC, *Appl. Sci.*, 2018, **8**(10), 1825, DOI: 10.3390/app8101825.

24 P. Prochazka, D. Cervinka, J. Martis, R. Cipin and P. Vorel, Li-ion battery deep discharge degradation, *ECS Trans.*, 2016, **74**(1), 31–36.

25 G. Ning, B. Haran and B. N. Popov, Capacity fade study of lithium-ion batteries cycled at high discharge rates, *J. Power Sources*, 2003, **117**(1–2), 160–169.

26 R. Dmello, J. D. Milshtein, F. R. Brushett and K. C. Smith, Cost-driven materials selection criteria for redox flow battery electrolytes, *J. Power Sources*, 2016, **330**, 261–272.

27 X. Sun, H. Hao, P. Hartmann, Z. Liu and F. Zhao, Supply risks of lithium-ion battery materials: An entire supply chain estimation, *Mater. Today Energy*, 2019, **14**, 100347, DOI: 10.1016/j.mtener.2019.100347.

28 T. Yamanaka, Y. Takagishi, Y. Tozuka and T. Yamaue, Modeling lithium ion battery nail penetration tests and quantitative evaluation of the degree of combustion risk, *J. Power Sources*, 2019, **416**, 132–140, DOI: 10.1016/j.jpowsour.2019.01.055.

29 *Lithium Overpotential and Dendrite Formation*, ECS Meet Abstr, 2015, available from: https://iopscience.iop.org/article/10.1149/MA2015-01/2/387.

30 M. Wang, Y. Shi, D. J. Noelle, A. V. Le, H. Yoon, H. Chung, *et al.*, Internal short circuit mitigation of high-voltage lithium-ion batteries with functional current collectors, *RSC Adv.*, 2017, **7**(72), 45662–45667, DOI: 10.1039/c7ra08277k.

31 A. H. Whitehead, T. J. Rabbow, M. Trampert and P. Pokorny, Critical safety features of the vanadium redox flow battery, *J. Power Sources*, 2017, **351**, 1–7, DOI: 10.1016/j.jpowsour.2017.03.075.

32 P. Gottesfeld, Commentary health risks from climate fix: The downside of energy storage batteries, *Environ. Res.*, 2019, **178**, 108677, DOI: 10.1016/j.envres.2019.108677.

33 E. Glogic, A. Adán-Más, G. Sonnemann, M. D. F. Montemor, L. Guerlou-Demourgues and S. B. Young, Life cycle assessment of emerging Ni-Co hydroxide charge storage electrodes: Impact of graphene oxide and synthesis route, *RSC Adv.*, 2019, **9**(33), 18853–18862.

34 C. J. Rydh, Environmental assessment of vanadium redox and lead-acid batteries for stationary energy storage, *J. Power Sources*, 1999, **80**(1), 21–29.

35 A. K. Manohar, K. M. Kim, E. Plichta, M. Hendrickson, S. Rawlings and S. R. Narayanan, A high efficiency iron-chloride redox flow battery for large-scale energy storage, *J. Electrochem. Soc.*, 2016, **163**(1), A5118–A5125.

36 T.-S. Chen, S.-L. Huang, Z.-Y. Ye, Y.-S. Lin and C.-P. Li, A novel Fe (II/0) redox couple with key components for the V/Fe redox flow battery, *J. Electroanal. Chem.*, 2019, **850**, 113396, DOI: 10.1016/j.jelechem.2019.113396.

37 Y. K. Zeng, T. S. Zhao, X. L. Zhou, L. Wei and Y. X. Ren, A novel iron-lead redox flow battery for large-scale energy storage, *J. Power Sources*, 2017, **346**, 97–102, DOI: 10.1016/j.jpowsour.2017.02.018.

38 Z. Na, S. Xu, D. Yin and L. Wang, A cerium-lead redox flow battery system employing supporting electrolyte of methanesulfonic acid, *J. Power Sources*, 2015, **295**, 28–32, DOI: 10.1016/j.jpowsour.2015.06.115.

39 P. K. Leung, C. Ponce-De-León, C. T. J. Low and F. C. Walsh, Zinc deposition and dissolution in methanesulfonic acid onto a carbon composite electrode as the negative electrode reactions in a hybrid redox flow battery, *Electrochim. Acta*, 2011, **56**(18), 6536–6546, DOI: 10.1016/j.electacta.2011.04.111.

40 A. Khor, P. Leung, M. R. Mohamed, C. Flox, Q. Xu, L. An, *et al.*, Review of zinc-based hybrid flow batteries: From fundamentals to applications, *Mater. Today Energy*, 2018, **8**, 80–108.

41 S. S. Hosseiny, M. Saakes and M. Wessling, A polyelectrolyte membrane-based vanadium/air redox flow battery, *Electrochem. Commun.*, 2011, **13**(8), 751–754, DOI: 10.1016/j.elecom.2010.11.025.

42 J. Grosse Austing, C. Nunes Kirchner, L. Komsiyska and G. Wittstock, Investigation of crossover processes in a unitized bidirectional vanadium/air redox flow battery, *J. Power Sources*, 2016, **306**, 692–701, DOI: 10.1016/j.jpowsour.2015.12.052.

43 Y. G. Zhu, C. Jia, J. Yang, F. Pan, Q. Huang and Q. Wang, Dual redox catalysts for oxygen reduction and evolution reactions: Towards a redox flow Li-O_2 battery, *Chem. Commun.*, 2015, **51**(46), 9451–9454.

44 G. L. Soloveichik, Flow Batteries: Current Status and Trends, *Chem. Rev.*, 2015, **115**(20), 11533–11558.

45 H. Chen and Y. C. Lu, A High-Energy-Density Multiple Redox Semi-Solid-Liquid Flow Battery, *Adv. Energy Mater.*, 2016, **6**(8), 1–9.

46 F. Pan and Q. Wang, Redox species of redox flow batteries: A review, *Molecules*, 2015, **20**(11), 20499–20517.

47 J. D. Milshtein, J. L. Barton, T. J. Carney, J. A. Kowalski, R. M. Darling and F. R. Brushett, Towards low resistance nonaqueous redox flow batteries, *J. Electrochem. Soc.*, 2017, **164**(12), A2487–A2499.

48 T. M. Tseng, R. H. Huang, C. Y. Huang, K. L. Hsueh and F. S. Shieu, A kinetic study of the platinum/carbon anode

catalyst for vanadium redox flow battery, *J. Electrochem. Soc.*, 2013, **160**(4), 690–696.

49 B. Sun and M. Skyllas-Kazacos, Chemical modification of graphite electrode materials for vanadium redox flow battery application-part II. Acid treatments, *Electrochim. Acta*, 1992, **37**(13), 2459–2465.

50 D. Bae, B. Seger, P. C. K. Vesborg, O. Hansen and I. Chorkendorff, Strategies for stable water splitting via protected photoelectrodes, *Chem. Soc. Rev.*, 2017, **46**(7), 1933–1954, available from: http://xlink.rsc.org/?DOI=C6CS00918B.

51 L. F. Arenas, C. Ponce de León and F. C. Walsh, Engineering aspects of the design, construction and performance of modular redox flow batteries for energy storage, *J. Energy Storage*, 2017, **11**, 119–153, DOI: 10.1016/j.est.2017.02.007.

52 J. L. Barton, J. D. Milshtein, J. J. Hinricher and F. R. Brushett, Quantifying the impact of viscosity on mass-transfer coefficients in redox flow batteries, *J. Power Sources*, 2018, **399**, 133–143, DOI: 10.1016/j.jpowsour.2018.07.046.

53 Q. Xu, T. S. Zhao and C. Zhang, Effects of SOC-dependent electrolyte viscosity on performance of vanadium redox flow batteries, *Appl. Energy*, 2014, **130**, 139–147.

54 I. Geoffroy, P. Willmann, K. Mesfar, B. Carré and D. Lemordant, Electrolytic characteristics of ethylene carbonate-diglyme-based electrolytes for lithium batteries, *Electrochim. Acta*, 2000, **45**(13), 2019–2027.

55 Y. Wen, Y. Xu, J. Cheng, G. Cao and Y. Yang, Investigation on the stability of electrolyte in vanadium flow batteries, *Electrochim. Acta*, 2013, **96**, 268–273, DOI: 10.1016/j.electacta.2013.02.091.

56 C. Wiberg, T. J. Carney, F. Brushett, E. Ahlberg and E. Wang, Dimerization of 9,10-anthraquinone-2,7-Disulfonic acid (AQDS), *Electrochim. Acta*, 2019, **317**, 478–485, DOI: 10.1016/j.electacta.2019.05.134.

57 X. Wei, W. Xu, J. Huang, L. Zhang, E. Walter, C. Lawrence, *et al.*, Radical Compatibility with Nonaqueous Electrolytes and Its Impact on an All-Organic Redox Flow Battery, *Angew. Chem. Int. Ed.*, 2015, **54**(30), 8684–8687.

58 M. Skyllas-Kazacos, C. Menictas and M. Kazacos, Thermal stability of concentrated V(V) electrolytes in the vanadium redox cell, *J. Electrochem. Soc.*, 1996, **143**(4), 86–88.

59 R. M. Darling, K. G. Gallagher, J. A. Kowalski, S. Ha and F. R. Brushett, Pathways to low-cost electrochemical energy storage: A comparison of aqueous and nonaqueous flow batteries, *Energy Environ. Sci.*, 2014, **7**(11), 3459–3477.

60 A. D. Curzons, D. C. Constable and V. L. Cunningham, Solvent selection guide: a guide to the integration of environmental, health and safety criteria into the selection of solvents, *Clean Technol. Environ. Policy*, 1999, **1**(2), 82–90.

61 M. Bartolozzi, Development of redox flow batteries. A historical bibliography, *J. Power Sources*, 1989, **27**(3), 219–234.

62 L. I. Krishtalik, pH-dependent redox potential: How to use it correctly in the activation energy analysis, *Biochim. Biophys. Acta Bioenerg.*, 2003, **1604**(1), 13–21.

63 J. Zhang, G. Jiang, P. Xu, A. Ghorbani Kashkooli, M. Mousavi, A. Yu, *et al.*, An all-aqueous redox flow battery with unprecedented energy density, *Energy Environ. Sci.*, 2018, **11**(8), 2010–2015.

64 J. Luo, W. Wu, C. Debruler, B. Hu, M. Hu and T. L. Liu, A 1.51 v pH neutral redox flow battery towards scalable energy storage, *J. Mater. Chem. A*, 2019, **7**(15), 9130–9136.

65 P. Singh, Application of non-aqueous solvents to batteries, *J. Power Sources*, 1984, **11**(1–2), 135–142. available from: https://linkinghub.elsevier.com/retrieve/pii/0378775384800798.

66 A. A. Shinkle, T. J. Pomaville, A. E. S. Sleightholme, L. T. Thompson and C. W. Monroe, Solvents and supporting electrolytes for vanadium acetylacetonate flow batteries, *J. Power Sources*, 2014, **248**, 1299–1305, DOI: 10.1016/j.jpowsour.2013.10.034.

67 B. Chakrabarti, J. Rubio-Garcia, E. Kalamaras, V. Yufit, F. Tariq, C. T. J. Low, *et al.*, Evaluation of a Non-Aqueous Vanadium Redox Flow Battery Using a Deep Eutectic Solvent and Graphene-Modified Carbon Electrodes via Electrophoretic Deposition, *Batteries*, 2020, **6**(3), 38, available from: https://www.mdpi.com/2313-0105/6/3/38.

68 T. Fuchigami, M. Atobe and S. Inagi, *Fundamentals and Applications of Organic Electrochemistry: Synthesis, Materials, Devices*, John Wiley & Sons, 2015, p. 238.

69 T. Herr, P. Fischer, J. Tübke, K. Pinkwart and P. Elsner, Increasing the energy density of the non-aqueous vanadium redox flow battery with the acetonitrile-1,3-dioxolane-dimethyl sulfoxide solvent mixture, *J. Power Sources*, 2014, **265**, 317–324, DOI: 10.1016/j.jpowsour.2014.04.141.

70 W. J. Peppel, Preparation and Properties of the Alkylene Carbonates, *Ind Eng Chem*, 1958, **50**(5), 767–770.

71 P. Patnaik, *A Comprehensive Guide to the Hazardous Properties of Chemical Substances*, John Wiley & Sons, 3rd edn, 2007, p. 1059, available from: https://www.wiley.com/en-us/A+Comprehensive+Guide+to+the+Hazardous+Properties+of+Chemical+Substances%2C+3rd+Edition-p-9780471714583.

72 W. van Schalkwijk and B. Scrosati, *Advances in Lithium-Ion Batteries*, Springer Science & Business Media; 2007, p. 513.

73 D. Lloyd, T. Vainikka, M. Ronkainen and K. Kontturi, Characterisation and application of the Fe(II)/Fe(III) redox reaction in an ionic liquid analogue, *Electrochim. Acta*, 2013, **109**, 843–851, DOI: 10.1016/j.electacta.2013.08.013.

74 D. Lloyd, T. Vainikka and K. Kontturi, The development of an all copper hybrid redox flow battery using deep eutectic solvents, *Electrochim. Acta*, 2013, **100**, 18–23, DOI: 10.1016/j.electacta.2013.03.130.

75 A. Ejigu, P. A. Greatorex-Davies and D. A. Walsh, Room temperature ionic liquid electrolytes for redox flow batteries, *Electrochem. Commun.*, 2015, **54**, 55–59, DOI: 10.1016/j.elecom.2015.01.016.

76 M. J. Earle and K. R. Seddon, Ionic liquids: Green solvents for the future, *ACS Symp. Ser.*, 2002, **819**(7), 10–25.

77 M. Freemantle, Designer Solvents: Ionic liquids may boost clean technology development, *Chem. Eng. News*, 1998, **76**(13), 32–37. available from: http://pubs.acs.org/doi/abs/10.1021/cen-v076n013.p032.

78 K. N. Marsh, J. A. Boxall and R. Lichtenthaler, Room temperature ionic liquids and their mixtures - A review, *Fluid Phase Equil.*, 2004, **219**(1), 93–98.

79 M. H. Chakrabarti, F. S. Mjalli, I. M. Alnashef, M. A. Hashim, M. A. Hussain, L. Bahadori, *et al.*, Prospects of applying ionic liquids and deep eutectic solvents for renewable energy storage by means of redox flow batteries, *Renew. Sustain. Energy Rev.*, 2014, **30**, 254–270, DOI: 10.1016/j.rser.2013.10.004.

80 G. García, S. Aparicio, R. Ullah and M. Atilhan, Deep eutectic solvents: Physicochemical properties and gas separation applications, *Energy Fuels*, 2015, **29**(4), 2616–2644.

81 Q. Zhang, K. De Oliveira Vigier, S. Royer and F. Jérôme, Deep eutectic solvents: Syntheses, properties and applications, *Chem. Soc. Rev.*, 2012, **41**(21), 7108–7146.

82 S. Schaltin, Y. Li, N. R. Brooks, J. Sniekers, I. F. J. Vankelecom, K. Binnemans, *et al.*, Towards an all-copper redox flow battery based on a copper-containing ionic liquid, *Chem. Commun.*, 2016, **52**(2), 414–417, DOI: 10.1039/c5cc06774j.

83 L. Bahadori, M. A. Hashim, N. S. A. Manan, F. S. Mjalli, I. M. Alnashef, N. P. Brandon, *et al.*, Investigation of ammonium- And phosphonium-based deep eutectic solvents as electrolytes for a non-aqueous all-vanadium redox cell, *J. Electrochem. Soc.*, 2016, **163**(5), A632–A638.

84 Y. Wang and H. Zhou, A green and cost-effective rechargeable battery with high energy density based on a deep eutectic catholyte, *Energy Environ. Sci.*, 2016, **9**(7), 2267–2272, DOI: 10.1039/c6ee00902f.

85 C. Zhang, Y. Ding, L. Zhang, X. Wang, Y. Zhao, X. Zhang, *et al.*, A Sustainable Redox-Flow Battery with an Aluminum-Based, Deep-Eutectic-Solvent Anolyte, *Angew. Chem. Int. Ed.*, 2017, **56**(26), 7454–7459.

86 L. Zhang, C. Zhang, Y. Ding, K. Ramirez-Meyers and G. Yu, A Low-Cost and High-Energy Hybrid Iron-Aluminum Liquid Battery Achieved by Deep Eutectic Solvents, *Joule*, 2017, **1**(3), 623–633, DOI: 10.1016/j.joule.2017.08.013.

87 C. Zhang, Z. Niu, Y. Ding, L. Zhang, Y. Zhou, X. Guo, *et al.*, Highly Concentrated Phthalimide-Based Anolytes for Organic Redox Flow Batteries with Enhanced Reversibility, *Chem*, 2018, **4**(12), 2814–2825, DOI: 10.1016/j.chempr.2018.08.024.

88 Y. Wang, Z. Niu, Q. Zheng, C. Zhang, J. Ye, G. Dai, *et al.*, Zn-based eutectic mixture as anolyte for hybrid redox flow batteries, *Sci. Rep.*, 2018, **8**(1), 8–15, DOI: 10.1038/s41598-018-24059-x.

89 Y. Ding, C. Zhang, L. Zhang, H. Wei, Y. Li and G. Yu, Insights into hydrotropic solubilization for hybrid ion redox flow batteries, *ACS Energy Lett.*, 2018, **3**(11), 2641–2648.

90 Q. Xu, L. Y. Qin, Y. N. Ji, P. K. Leung, H. N. Su, F. Qiao, *et al.*, A deep eutectic solvent (DES) electrolyte-based vanadium-iron redox flow battery enabling higher specific capacity and improved thermal stability, *Electrochim. Acta*, 2019, **293**, 426–431.

91 K. Gong, Q. Fang, S. Gu, S. F. Y. Li and Y. Yan, Nonaqueous redox-flow batteries: Organic solvents, supporting electrolytes, and redox pairs, *Energy Environ. Sci.*, 2015, **8**(12), 3515–3530.

92 B. Li and J. Liu, Progress and directions in low-cost redox-flow batteries for large-scale energy storage, *Natl. Sci. Rev.*, 2017, **4**(1), 91–105.

93 C. Zhang, L. Zhang, Y. Ding, S. Peng, X. Guo, Y. Zhao, *et al.*, Progress and prospects of next-generation redox flow batteries, *Energy Storage Materials*, 2018, **15**, 324–350, DOI: 10.1016/j.ensm.2018.06.008.

94 Y.-W. D. Chen, Solution Redox Couples for Electrochemical Energy Storage, *J. Electrochem. Soc.*, 1981, **128**(7), 1460.

95 Anon. *NASA Redox Storage System Development Project Calendar Year 1982*, NASA Technical Memorandum, 1983.

96 M. Skyllas-Kazacos, M. Rychcik, R. G. Robins and A. G. Fane, New All-Vanadium Redox Flow Cell, *J. Electrochem. Soc.*, 1986, **133**(5), 1057–1058.

97 M. Skyllas-Kazakos, All vanadium batteries and additives, H01M 10/36, 10/44, 10/46H01M 10/02, 4/38/ 4,487H01M 4/96, 2/14, WO 89/05526, 1989.

98 C. Choi, S. Kim, R. Kim, Y. Choi, S. Kim and H. Jung, A review of vanadium electrolytes for vanadium redox flow batteries, *Renew. Sustain. Energy Rev.*, 2017, **69**, 263–274, DOI: 10.1016/j.rser.2016.11.188.

99 A. Tang, J. Bao and M. Skyllas-Kazacos, Dynamic modelling of the effects of ion diffusion and side reactions on the capacity loss for vanadium redox flow battery, *J. Power Sources*, 2011, **196**(24), 10737–10747, DOI: 10.1016/j.jpowsour.2011.09.003.

100 J. Rubio-Garcia, A. Kucernak, D. Zhao, D. I. Li, K. F. Fahy, V. Yufit, *et al.*, Hydrogen/manganese hybrid redox flow battery (in press), *J. Phys. Energy*, 2018, **1**, 015006, DOI: 10.1088/2515-7655/aaee17.

101 L. Wei, H. R. Jiang, Y. X. Ren, M. C. Wu, J. B. Xu and T. S. Zhao, Investigation of an aqueous rechargeable battery consisting of manganese tin redox chemistries for energy storage, *J. Power Sources*, 2019, **437**, 226918.

102 Y. Dong, H. Kaku, H. Miyawaki, R. Tatsumi, K. Moriuchi and T. Shigematsu, Titanium-manganese electrolyte for redox flow battery, *SEI Tech. Rev.*, 2017, (84), 35–40.

103 P. K. Leung, C. Ponce De León and F. C. Walsh, An undivided zinc-cerium redox flow battery operating at room temperature (295 K), *Electrochem. Commun.*, 2011, **13**(8), 770–773, DOI: 10.1016/j.elecom.2011.04.011.

104 G. Nikiforidis, L. Berlouis, D. Hall and D. Hodgson, Impact of electrolyte composition on the performance of the zinc-cerium redox flow battery system, *J. Power Sources*, 2013, **243**, 691–698, DOI: 10.1016/j.jpowsour.2013.06.045.

105 P. K. Leung, M. R. Mohamed, A. A. Shah, Q. Xu and M. B. Conde-Duran, A mixed acid based vanadium-

cerium redox flow battery with a zero-gap serpentine architecture, *J. Power Sources*, 2015, **274**, 651–658.

106 A. Dinesh, S. Olivera, K. Venkatesh, M. S. Santosh, M. G. Priya, Inamuddin, *et al.*, Iron-based flow batteries to store renewable energies, *Environ. Chem. Lett.*, 2018, **16**(3), 683–694, DOI: 10.1007/s10311-018-0709-8.

107 M. C. Tucker, A. Phillips and A. Z. Weber, All-Iron Redox Flow Battery Tailored for Off-Grid Portable Applications, *ChemSusChem*, 2015, **8**(23), 3996–4004.

108 Y. Zhao, L. Wang and H. R. Byon, High-performance rechargeable lithium-iodine batteries using triiodide/iodide redox couples in an aqueous cathode, *Nat. Commun.*, 2013, **4**, 1896–1897, DOI: 10.1038/ncomms2907.

109 Z. Li, G. Weng, Q. Zou, G. Cong and Y. C. Lu, A high-energy and low-cost polysulfide/iodide redox flow battery, *Nano Energy*, 2016, **30**, 283–292, DOI: 10.1016/j.nanoen.2016.09.043.

110 A. Khataee, J. Azevedo, P. Dias, D. Ivanou, E. Dražević, A. Bentien, *et al.*, Integrated design of hematite and dye-sensitized solar cell for unbiased solar charging of an organic-inorganic redox flow battery, *Nano Energy*, 2019, **62**, 832–843, DOI: 10.1016/j.nanoen.2019.06.001.

111 W. Lee, A. Permatasari, B. W. Kwon and Y. Kwon, Performance evaluation of aqueous organic redox flow battery using anthraquinone-2,7-disulfonic acid disodium salt and potassium iodide redox couple, *Chem. Eng. J.*, 2019, **358**(2018), 1438–1445, DOI: 10.1016/j.cej.2018.10.159.

112 J. Yu, L. Fan, R. Yan, M. Zhou and Q. Wang, Redox Targeting-Based Aqueous Redox Flow Lithium Battery, *ACS Energy Lett.*, 2018, **3**(10), 2314–2320.

113 F. Yu, L. Pang, X. Wang, E. R. Waclawik, F. Wang, K. Ostrikov, *et al.*, Aqueous alkaline–acid hybrid electrolyte for zinc-bromine battery with 3V voltage window, *Energy Storage Materials*, 2019, **19**, 56–61, DOI: 10.1016/j.ensm.2019.02.024.

114 S. Bae, J. Lee and D. S. Kim, The effect of Cr3+-Functionalized additive in zinc-bromine flow battery, *J. Power Sources*, 2019, **413**(2018), 167–173.

115 H. S. Yang, J. H. Park, H. W. Ra, C. S. Jin and J. H. Yang, Critical rate of electrolyte circulation for preventing zinc dendrite formation in a zinc-bromine redox flow battery, *J. Power Sources*, 2016, **325**, 446–452, DOI: 10.1016/j.jpowsour.2016.06.038.

116 B. Li, Z. Nie, M. Vijayakumar, G. Li, J. Liu, V. Sprenkle, *et al.*, Ambipolar zinc-polyiodide electrolyte for a high-energy density aqueous redox flow battery, *Nat. Commun.*, 2015, **6**, 1–8, DOI: 10.1038/ncomms7303.

117 P. K. Leung, T. Martin, A. A. Shah, M. A. Anderson and J. Palma, Membrane-less organic-inorganic aqueous flow batteries with improved cell potential, *Chem. Commun.*, 2016, **52**(99), 14270–14273.

118 Q. Zhao, W. Huang, Z. Luo, L. Liu, Y. Lu, Y. Li, *et al.*, High-capacity aqueous zinc batteries using sustainable quinone electrodes, *Sci. Adv.*, 2018, **4**, eaao1761, DOI: 10.1126/sciadv.aao1761.

119 M. Bockelmann, U. Kunz and T. Turek, Electrically rechargeable zinc-oxygen flow battery with high power density, *Electrochem. Commun.*, 2016, **69**, 24–27, DOI: 10.1016/j.elecom.2016.05.013.

120 Y. H. Wen, J. Cheng, S. Q. Ning and Y. S. Yang, Preliminary study on zinc-air battery using zinc regeneration electrolysis with propanol oxidation as a counter electrode reaction, *J. Power Sources*, 2009, **188**(1), 301–307.

121 V. Caramia and B. Bozzini, Materials science aspects of zinc-air batteries: A review, *Mater. Renew. Sustain. Energy*, 2014, **3**, 28, DOI: 10.1007/s40243-014-0028-3.

122 X. Wei, W. Xu, M. Vijayakumar, L. Cosimbescu, T. Liu, V. Sprenkle, *et al.*, TEMPO-based catholyte for high-energy density nonaqueous redox flow batteries, *Adv. Mater.*, 2014, **26**(45), 7649–7653.

123 M. Yu, W. D. McCulloch, D. R. Beauchamp, Z. Huang, X. Ren and Y. Wu, Aqueous Lithium-Iodine Solar Flow Battery for the Simultaneous Conversion and Storage of Solar Energy, *J. Am. Chem. Soc.*, 2015, **137**(26), 8332–8335.

124 Y. Zhao and H. R. Byon, High-Performance Lithium-Iodine Flow Battery, *Nat. Commun.*, 2013, **4**, 1896, DOI: 10.1038/ncomms2907.

125 M. Genovese and K. Lian, Polyoxometalate modified inorganic-organic nanocomposite materials for energy storage applications: A review, *Curr. Opin. Solid State Mater. Sci.*, 2015, **19**(2), 126–137, DOI: 10.1016/j.cossms.2014.12.002.

126 N. I. Gumerova and A. Rompel, Synthesis, structures and applications of electron-rich polyoxometalates, *Nat. Rev. Chem.*, 2018, **2**, 0112, DOI: 10.1038/s41570-018-0112.

127 H. Wang, S. Hamanaka, Y. Nishimoto, S. Irle, T. Yokoyama, H. Yoshikawa, *et al.*, In Operando X-ray Absorption Fine Structure Studies of Polyoxometalate Molecular Cluster Batteries: Polyoxometalates as Electron Sponges, *J. Am. Chem. Soc.*, 2012, **134**, 4918–4924.

128 Q. Li, L. Zhang, J. Dai, H. Tang, Q. Li, H. Xue, *et al.*, Polyoxometalate-based materials for advanced electrochemical energy conversion and storage, *Chem. Eng J.*, 2018, **351**, 441–461, DOI: 10.1016/j.cej.2018.06.074.

129 Y. Ji, L. Huang, J. Hu, C. Streb and Y. Song, Polyoxometalate-functionalized nanocarbon materials for energy conversion, energy storage and sensor systems, *Energy Environ. Sci.*, 2015, **8**, 776–789, DOI: 10.1039/c4ee03749a.

130 K. Kume, N. Kawasaki, H. Wang, T. Yamada, H. Yoshikawa and K. Awaga, Enhanced capacitor effects in polyoxometalate/graphene nanohybrid materials; a synergetic approach to high performance energy storages, *J. Mater. Chem. A*, 2014, **2**, 3801–3807.

131 S. Herrmann, C. Ritchie and C. Streb, Polyoxometalate - Conductive polymer composites for energy conversion, energy storage and nanostructured sensors, *Dalt. Trans*, 2015, **44**(16), 7092–7104.

132 S. Herrmann, N. Aydemir, F. Nägele, D. Fantauzzi, T. Jacob, J. Travas-Sejdic, *et al.*, Enhanced Capacitive Energy Storage in Polyoxometalate-Doped Polypyrrole, *Adv. Funct. Mater.*, 2017, **27**(25), 1–8.

133 P. Gómez-Romero, K. Cuentas-Gallegos, M. Lira-Cantú and N. Casañ-Pastor, Hybrid nanocomposite materials for energy storage and conversion applications, *J. Mater. Sci.*, 2005, **40**(6), 1423–1428.

134 H. D. Pratt, N. S. Hudak, X. Fang and T. M. Anderson, A polyoxometalate flow battery, *J. Power Sources*, 2013, **236**, 259–264, DOI: 10.1016/j.jpowsour.2013.02.056.

135 H. D. Pratt III, W. R. Pratta, X. Fang, N. S. Hudaka and T. M. Anderson, Mixed-Metal,Structural,and Substitution Effects ofPolyoxometalates on Electrochemical Behavior in a Redox Flow Battery, *Electrochim. Acta*, 2014, **138**, 210–214.

136 H. D. Pratt and T. M. Anderson, Mixed addenda polyoxometalate "solutions" for stationary energy storage, *Dalt Trans*, 2013, **42**(44), 15650–15655.

137 J. J. J. Chen and M. A. Barteau, Molybdenum polyoxometalates as active species for energy storage in non-aqueous media, *J. Energy Storage*, 2017, **13**, 255–261, DOI: 10.1016/j.est.2017.07.017.

138 L. E. Vangelder, A. M. Kosswattaarachchi, P. L. Forrestel, T. R. Cook and E. M. Matson, Polyoxovanadate-Alkoxide clusters as multi-electron charge carriers for symmetric non-Aqueous redox flow batteries, *Chem Sci*, 2018, **9**(6), 1692–1699.

139 T. Feng, H. Wang, Y. Liu, J. Zhang, Y. Xiang and S. Lu, A redox flow battery with high capacity retention using 12-phosphotungstic acid/iodine mixed solution as electrolytes, *J. Power Sources*, 2019, **436**, 226831, DOI: 10.1016/j.jpowsour.2019.226831.

140 J. Friedl, M. V. Holland-Cunz, F. Cording, F. L. Pfanschilling, C. Wills, W. McFarlane, *et al.*, Asymmetric polyoxometalate electrolytes for advanced redox flow batteries, *Energy Environ. Sci.*, 2018, **11**(10), 3010–3018, available from: http://xlink.rsc.org/?DOI=C8EE00422F.

141 J. Friedl, F. L. Pfanschilling, M. V. Holland-Cunz, R. Fleck, B. Schricker, H. Wolfschmidt, *et al.*, A polyoxometalate redox flow battery: functionality and upscale, *Clean Energy*, 2019, **3**(4), 278–287, available from: https://academic.oup.com/ce/article/3/4/278/5550272.

142 G. A. Lawrance, *Introduction to Coordination Chemistry*, John Wiley & Sons, 2013, p. 304.

143 G. B. Adams, *US Pat.*, 4180623, 1979, available from: https://linkinghub.elsevier.com/retrieve/pii/0375650585900112.

144 Y. Matsuda, K. Tanaka, M. Okada, Y. Takasu, M. Morita and T. Matsumura-Inoue, A rechargeable redox battery utilizing ruthenium complexes with non-aqueous organic electrolyte, *J Appl Electrochem*, 1988, **18**(6), 909–914.

145 P. J. Cappillino, H. D. Pratt, N. S. Hudak, N. C. Tomson, T. M. Anderson and M. R. Anstey, Application of Redox Non-Innocent Ligands to Non-Aqueous Flow Battery Electrolytes, *Adv. Energy Mater.*, 2014, **4**(1), 2–6.

146 I. A. Popov, N. Mehio, T. Chu, B. L. Davis, R. Mukundan, P. Yang, *et al.*, Impact of Ligand Substitutions on Multielectron Redox Properties of Fe Complexes Supported by Nitrogenous Chelates, *ACS Omega*, 2018, **3**(11), 14766–14778.

147 E. Wiberg, A. F. Holleman and N. Wiberg, *Inorganic Chemistry*, Academic Press, 2001, p. 1884.

148 P. A. Vigato, V. Peruzzo and S. Tamburini, The evolution of β-diketone or β-diketophenol ligands and related complexes, *Coord. Chem. Rev.*, 2009, **253**(7–8), 1099–1201.

149 P. J. Cabrera, X. Yang, J. A. Suttil, K. L. Hawthorne, R. E. M. Brooner, M. S. Sanford, *et al.*, Complexes containing redox noninnocent ligands for symmetric, multielectron transfer nonaqueous redox flow batteries, *J. Phys. Chem. C*, 2015, **119**(28), 15882–15889.

150 A. A. Shinkle, A. E. S. Sleightholme, L. T. Thompson and C. W. Monroe, Electrode kinetics in non-aqueous vanadium acetylacetonate redox flow batteries, *J. Appl. Electrochem.*, 2011, **41**(10), 1191–1199.

151 Q. Liu, A. E. S. Sleightholme, A. A. Shinkle, Y. Li and L. T. Thompson, Non-aqueous vanadium acetylacetonate electrolyte for redox flow batteries, *Electrochem. Commun.*, 2009, **11**(12), 2312–2315, DOI: 10.1016/j.elecom.2009.10.006.

152 J. A. Suttil, J. F. Kucharyson, I. L. Escalante-Garcia, P. J. Cabrera, B. R. James, R. F. Savinell, *et al.*, Metal Acetylacetonate Complexes for High Energy Density Non-Aqueous Redox Flow Batteries, *J. Mater. Chem. A*, 2015, **3**, 7929–7938.

153 Q. Liu, A. A. Shinkle, Y. Li, C. W. Monroe, L. T. Thompson and A. E. S. Sleightholme, Non-aqueous chromium acetylacetonate electrolyte for redox flow batteries, *Electrochem. Commun.*, 2010, **12**(11), 1634–1637, DOI: 10.1016/j.elecom.2010.09.013.

154 A. E. S. Sleightholme, A. A. Shinkle, Q. Liu, Y. Li, C. W. Monroe and L. T. Thompson, Non-aqueous manganese acetylacetonate electrolyte for redox flow batteries, *J. Power Sources*, 2011, **196**(13), 5742–5745, DOI: 10.1016/j.jpowsour.2011.02.020.

155 T. Yamamura, Y. Shiokawa, H. Yamana and H. Moriyama, Electrochemical investigation of uranium β-diketonates for all-uranium redox flow battery, *Electrochim. Acta*, 2002, **48**(1), 43–50.

156 C. M. Elliott and E. J. Hershenhart, Electrochemical and Spectral Investigations of Ring-Substituted Bipyridine Complexes of Ruthenium, *J. Am. Chem. Soc.*, 1982, **104**(26), 7519–7526.

157 S. M. Laramie, J. D. Milshtein, T. M. Breault, F. R. Brushett and L. T. Thompson, Performance and cost characteristics of multi-electron transfer, common ion exchange non-aqueous redox flow batteries, *J. Power Sources*, 2016, **327**, 681–692, DOI: 10.1016/j.jpowsour.2016.07.015.

158 L. Meda, F. Oldani, G. Tozzola, S. Caramori, E. Benazzi, V. Cristino, *et al.*, Searching for new redox-complexes\in organic flow batteries, *Solid State Ionics*, 2018, **317**(2017), 142–148, DOI: 10.1016/j.ssi.2018.01.017.

159 P. J. Cabrera, X. Yang, J. A. Suttil, R. E. M. Brooner, L. T. Thompson and M. S. Sanford, Evaluation of Tris-Bipyridine Chromium Complexes for Flow Battery Applications: Impact of Bipyridine Ligand Structure on Solubility and Electrochemistry, *Inorg. Chem.*, 2015, **54**(21), 10214–10223.

160 V. V. Strelets, Sandwich and bent sandwich complexes. Electrochemical studies, *Coord. Chem. Rev.*, 1992, **114**(1), 1–60.

161 D. Astruc, Why is Ferrocene so Exceptional?, *Eur. J. Inorg. Chem.*, 2017, **2017**(1), 6–29.

162 S. Yousefinejad, F. Honarasa and A. Solhjoo, On the Solubility of Ferrocene in Nonaqueous Solvents, *J. Chem. Eng. Data.*, 2016, **61**(1), 614–621.

163 B. Hu, C. Debruler, Z. Rhodes, T. Liu, B. Hu, C. Debruler, *et al.*, A Long Cycling Aqueous Organic Redox Flow Battery (AORFB) towards Sustainable and Safe Energy Storage, *J Am Chem Soc*, 2017, **139**(3), 1207–1214.

164 K. Wedege, J. Azevedo, A. Khataee, A. Bentien and A. Mendes, Direct Solar Charging of an Organic–Inorganic, Stable, and Aqueous Alkaline Redox Flow Battery with a Hematite Photoanode, *Angew. Chem. Int. Ed.*, 2016, **55**(25), 7142–7147.

165 H. S. Kim, S. Hwang, J. Mun, H. Park, J. H. Ryu and S. M. Oh, Counter anion effects on the energy density of Ni(II)-chelated tetradentate azamacrocyclic complex cation as single redox couple for non-aqueous flow batteries, *Electrochim. Acta*, 2019, **308**(Ii), 227–230.

166 S. Hwang, H. Kim, J. H. Ryu and S. M. Oh, Ni(II)-chelated thio-crown complex as a single redox couple for non-aqueous flow batteries, *Electrochem. Commun.*, 2017, **85**(Ii), 36–39, DOI: 10.1016/j.elecom.2017.10.015.

167 M. H. Chakrabarti, R. A. W. Dryfe and E. P. L. Roberts, Evaluation of electrolytes for redox flow battery applications, *J. Chem. Soc. Pakistan*, 2007, **29**(4), 294–300.

168 Z. Li, S. Li, S. Liu, K. Huang, D. Fang, F. Wang, *et al.*, Electrochemical properties of an all-organic redox flow battery using 2,2,6,6-tetramethyl-1-piperidinyloxy and N-Methylphthalimide, *Electrochem Solid-State Lett.*, 2011, **14**(12), 1–4.

169 R. H. Thomson, *Naturally Occurring Quinones*, Elsevier, 2012, p. 742.

170 R. A. Larson and E. J. Weber, *Reaction Mechanisms in Environmental Organic Chemistry*, CRC Press, 1994, p. 448.

171 K. Wedege, E. Dražević, D. Konya and A. Bentien, Organic Redox Species in Aqueous Flow Batteries: Redox Potentials, Chemical Stability and Solubility, *Sci. Rep.*, 2016, **6**, 1–13, DOI: 10.1038/srep39101.

172 T. J. Carney, S. J. Collins, J. S. Moore and F. R. Brushett, Concentration-Dependent Dimerization of Anthraquinone Disulfonic Acid and Its Impact on Charge Storage, *Chem. Mater.*, 2017, **29**(11), 4801–4810, available from: https://pubs.acs.org/doi/10.1021/acs.chemmater.7b00616.

173 B. Yang, L. Hoober-Burkhardt, S. Krishnamoorthy, A. Murali, G. K. S. Prakash and S. R. Narayanan, High-Performance Aqueous Organic Flow Battery with Quinone-Based Redox Couples at Both Electrodes, *J. Electrochem. Soc.*, 2016, **163**(7), A1442–A1449, available from: https://iopscience.iop.org/article/10.1149/2.1371607jes.

174 L. Hoober-Burkhardt, S. Krishnamoorthy, B. Yang, A. Murali, A. Nirmalchandar, G. K. S. Prakash, *et al.*, A New Michael-Reaction-Resistant Benzoquinone for Aqueous Organic Redox Flow Batteries, *J. Electrochem. Soc.*, 2017, **164**(4), A600–A607, available from: https://iopscience.iop.org/article/10.1149/2.0351704jes.

175 J. B. Gerken, C. W. Anson, Y. Preger, P. G. Symons, J. D. Genders, Y. Qiu, *et al.*, Comparison of Quinone-Based Catholytes for Aqueous Redox Flow Batteries and Demonstration of Long-Term Stability with Tetrasubstituted Quinones, *Adv. Energy Mater.*, 2020, **10**(20), 2000340, available from: https://onlinelibrary.wiley.com/doi/10.1002/aenm.202000340.

176 S. Er, C. Suh, M. P. Marshak and A. Aspuru-Guzik, Computational design of molecules for an all-quinone redox flow battery, *Chem. Sci.*, 2015, **6**(2), 885–893.

177 P. Hu, H. Lan, X. Wang, Y. Yang, X. Liu, H. Wang, *et al.*, Renewable-lawsone-based sustainable and high-voltage aqueous flow battery, *Energy Storage Materials*, 2019, **19**, 62–68, DOI: 10.1016/j.ensm.2018.10.017.

178 L. Tong, M.-A. Goulet, D. P. Tabor, E. F. Kerr, D. De Porcellinis, E. M. Fell, *et al.*, Molecular Engineering of an Alkaline Naphthoquinone Flow Battery, *ACS Energy Lett.*, 2019, **4**(8), 1880–1887, DOI: 10.1021/acsenergylett.9b01321.

179 M. Miroshnikov, K. Kato, G. Babu, K. P. Divya, L. M. Reddy Arava, P. M. Ajayan, *et al.*, A common tattoo chemical for energy storage: Henna plant-derived naphthoquinone dimer as a green and sustainable cathode material for Li-ion batteries, *RSC Adv.*, 2018, **8**(3), 1576–1582, DOI: 10.1039/c7ra12357d.

180 Y. Liu, S. Lu, S. Chen, H. Wang, J. Zhang and Y. Xiang, A Sustainable Redox Flow Battery with Alizarin-Based Aqueous Organic Electrolyte, *ACS Appl. Energy Mater*, 2019, **2**(4), 2469–2474.

181 L. Tong, Y. Jing, R. G. Gordon and M. J. Aziz, Symmetric All-Quinone Aqueous Battery, *ACS Appl. Energy Mater*, 2019, **2**(6), 4016–4021.

182 T. Liu, X. Wei, Z. Nie, V. Sprenkle and W. Wang, A Total Organic Aqueous Redox Flow Battery Employing a Low Cost and Sustainable Methyl Viologen Anolyte and 4-HO-TEMPO Catholyte, *Adv. Energy Mater.*, 2016, **6**(3), 1501449, DOI: 10.1002/aenm.201501449.

183 T. Janoschka, N. Martin, M. D. Hager and U. S. Schubert, An Aqueous Redox-Flow Battery with High Capacity and Power: The TEMPTMA/MV System, *Angew Chemie. Int Ed.*, 2016, **55**(46), 14427–14430.

184 B. Hu and T. L. Liu, Two electron utilization of methyl viologen anolyte in nonaqueous organic redox flow battery, *J. Energy Chem.*, 2018, **27**(5), 1326–1332.

185 C. Debruler, B. Hu, J. Moss, J. Luo and T. L. Liu, A Sulfonate-Functionalized Viologen Enabling Neutral Cation Exchange, Aqueous Organic Redox Flow Batteries toward Renewable Energy Storage, *ACS Energy. Lett.*, 2018, **3**(3), 663–668.

186 C. L. Bird and A. T. Kuhn, Electrochemistry of the viologens, *Chem. Soc. Rev.*, 1981, **10**(1), 49–82.

187 C. DeBruler, B. Hu, J. Moss, X. Liu, J. Luo, Y. Sun, *et al.*, Designer Two-Electron Storage Viologen Anolyte Materials for Neutral Aqueous Organic Redox Flow Batteries, *Chem*, 2017, **3**(6), 961–978.

188 E. S. Beh, D. De Porcellinis, R. L. Gracia, K. T. Xia, R. G. Gordon and M. J. Aziz, A neutral pH aqueous organic- organometallic redox flow battery with extremely high capacity retention, *ACS Energy Lett*, 2017, **2**(3), 639–644.

189 Y. Liu, M. A. Goulet, L. Tong, Y. Liu, Y. Ji, L. Wu, *et al.*, A Long-Lifetime All-Organic Aqueous Flow Battery Utilizing TMAP-TEMPO Radical, *Chem*, 2019, **5**(7), 1861–1870, DOI: 10.1016/j.chempr.2019.04.021.

190 W. Li, E. Kerr, M. A. Goulet, H. C. Fu, Y. Zhao, Y. Yang, *et al.*, A Long Lifetime Aqueous Organic Solar Flow Battery, *Adv. Energy Mater.*, 2019, **1900918**, 1–8.

191 J. Huang, Z. Yang, V. Murugesan, E. Walter, A. Hollas, B. Pan, *et al.*, Spatially Constrained Organic Diquat Anolyte for Stable Aqueous Flow Batteries, *ACS Energy Lett*, 2018, **3**(10), 2533–2538.

192 F. R. Brushett, J. T. Vaughey and A. N. Jansen, An all-organic non-aqueous lithium-ion redox flow battery, *Adv. Energy Mater.*, 2012, **2**(11), 1390–1396.

193 A. Hollas, X. Wei, V. Murugesan, Z. Nie, B. Li, D. Reed, *et al.*, A biomimetic high-capacity phenazine-based anolyte for aqueous organic redox flow batteries, *Nat. Energy*, 2018, **3**(6), 508–514, DOI: 10.1038/s41560-018-0167-3.

194 G. Kwon, S. Lee, J. Hwang, H. S. Shim, B. Lee, M. H. Lee, *et al.*, Multi-redox Molecule for High-Energy Redox Flow Batteries, *Joule*, 2018, **2**(9), 1771–1782, DOI: 10.1016/j.joule.2018.05.014.

195 W. Lee, B. W. Kwon and Y. Kwon, Effect of Carboxylic Acid-Doped Carbon Nanotube Catalyst on the Performance of Aqueous Organic Redox Flow Battery Using the Modified Alloxazine and Ferrocyanide Redox Couple, *ACS Appl. Mater. Interfaces.*, 2018, **10**(43), 36882–36891.

196 J. B. Gilroy, S. D. J. McKinnon, B. D. Koivisto and R. G. Hicks, Electrochemical studies of verdazyl radicals, *Org. Lett.*, 2007, **9**(23), 4837–4840.

197 G. D. Charlton, S. M. Barbon, J. B. Gilroy and C. A. Dyker, A bipolar verdazyl radical for a symmetric all-organic redox flow-type battery, *J. Energy. Chem.*, 2019, 52–56, DOI: 10.1016/j.jechem.2018.09.020.

198 H. Karoui, F. L. Moigne, O. Ouari and P. Tordo, Nitroxide Radicals: Properties, Synthesis and Applications, *Stable Radicals: Fundamentals and Applied Aspects of Odd-Electron Compounds*, 2010. vol. 12, pp. 173–229.

199 B. P. Soule, F. Hyodo, K. Matsumoto, N. L. Simone, J. A. Cook, M. C. Krishna, *et al.*, The chemistry and biology of nitroxide compounds, *Free. Radic. Biol. Med.*, 2007, **42**(11), 1632–1650.

200 J. Winsberg, T. Hagemann, T. Janoschka, M. D. Hager and U. S. Schubert, Redox-Flow Batteries: From Metals to Organic Redox-Active Materials, *Angew. Chem. Int. Ed.*, 2017, **56**(3), 686–711.

201 M. J. F. Fernandez and H. Sato, Solvent effect on (2,2,6,6-Tetramethylpiperidine-1-yl)oxyl (TEMPO): A RISM-SCF-SEDD study, *Theor. Chem. Acc.*, 2011, **130**(2–3), 299–304.

202 A. Orita, M. G. Verde, M. Sakai and Y. S. Meng, The impact of pH on side reactions for aqueous redox flow batteries based on nitroxyl radical compounds, *J. Power Sources*, 2016, **321**, 126–134, DOI: 10.1016/j.jpowsour.2016.04.136.

203 Z. Chang, D. Henkensmeier and R. Chen, One-Step Cationic Grafting of 4-Hydroxy-TEMPO and its Application in a Hybrid Redox Flow Battery with a Crosslinked PBI Membrane, *ChemSusChem*, 2017, **10**(16), 3193–3197.

204 Z. Chang, D. Henkensmeier and R. Chen, Shifting redox potential of nitroxyl radical by introducing an imidazolium substituent and its use in aqueous flow batteries, *J. Power Sources*, 2019, **418**, 11–16, DOI: 10.1016/j.jpowsour.2019.02.028.

205 H. seung Kim, K. J. Lee, Y. K. Han, J. H. Ryu and S. M. Oh, A comparative study on the solubility and stability of p-phenylenediamine-based organic redox couples for non-aqueous flow batteries, *J. Power Sources*, 2017, **348**, 264–269, DOI: 10.1016/j.jpowsour.2017.03.019.

206 X. Wei, W. Duan, J. Huang, L. Zhang, B. Li, D. Reed, *et al.*, A High-Current, Stable Nonaqueous Organic Redox Flow Battery, *ACS Energy Lett.*, 2016, **1**(4), 705–711.

207 J. Huang, L. Cheng, R. S. Assary, P. Wang, Z. Xue, A. K. Burrell, *et al.*, Liquid catholyte molecules for nonaqueous redox flow batteries, *Adv. Energy Mater.*, 2015, **5**(6), 1–6.

208 L. Zhang, Z. Zhang, P. C. Redfern, L. A. Curtiss and K. Amine, Molecular engineering towards safer lithium-ion batteries: A highly stable and compatible redox shuttle for overcharge protection, *Energy Environ. Sci.*, 2012, **5**(8), 8204–8207.

209 J. Zhang, J. Huang, L. A. Robertson, I. A. Shkrob and L. Zhang, Comparing calendar and cycle life stability of redox active organic molecules for nonaqueous redox flow batteries, *J. Power Sources*, 2018, **397**, 214–222, DOI: 10.1016/j.jpowsour.2018.07.001.

210 X. Xing, Q. Liu, W. Xu, W. Liang, J. Liu, B. Wang, *et al.*, All-Liquid Electroactive Materials for High Energy Density Organic Flow Battery, *ACS Appl. Energy Mater*, 2019, **2**(4), 2364–2369.

211 P. Leung, T. Martin, M. Liras, A. M. Berenguer, R. Marcilla, A. Shah, *et al.*, Cyclohexanedione as the negative electrode reaction for aqueous organic redox flow batteries, *Appl. Energy*, 2017, **197**, 318–326.

212 M. Burgess, J. S. Moore and J. Rodríguez-López, Redox Active Polymers as Soluble Nanomaterials for Energy Storage, *Acc. Chem. Res.*, 2016, **49**(11), 2649–2657.

213 J. B. Flanagan, S. Margel, A. J. Bard and F. C. Anson, Electron Transfer to and from Molecules Containing Multiple, Noninteracting Redox Centers. Electrochemical Oxidation of Poly(vinylferrocene), *J. Am. Chem. Soc.*, 1978, **100**(13), 4248–4253.

214 T. Janoschka, N. Martin, U. Martin, C. Friebe, S. Morgenstern, H. Hiller, *et al.*, An aqueous, polymer-based redox-flow battery using non-corrosive, safe, and low-cost materials, *Nature*, 2015, **527**(7576), 78–81.

215 A. M. Schwenke, T. Janoschka, C. Stolze, N. Martin, S. Hoeppener and U. S. Schubert, Microwave-assisted preparation of carbon nanofiber-functionalized graphite

felts as electrodes for polymer-based redox-flow batteries, *J. Power Sources*, 2016, **335**, 155–161, DOI: 10.1016/j.jpowsour.2016.09.121.

216 T. Janoschka, S. Morgenstern, H. Hiller, C. Friebe, K. Wolkersdörfer, B. Häupler, *et al.*, Synthesis and characterization of TEMPO- and viologen-polymers for water-based redox-flow batteries Received, *Polym. Chem.*, 2015, **6**, 7801–7811.

217 V. A. Iyer, J. K. Schuh, E. C. Montoto, V. Pavan Nemani, S. Qian, G. Nagarjuna, *et al.*, Assessing the impact of electrolyte conductivity and viscosity on the reactor cost and pressure drop of redox-active polymer flow batteries, *J. Power Sources*, 2017, **361**, 334–344.

218 J. Winsberg, S. Muench, T. Hagemann, S. Morgenstern, T. Janoschka, M. Billing, *et al.*, Polymer/zinc hybrid-flow battery using block copolymer micelles featuring a TEMPO corona as catholyte, *Polym. Chem.*, 2016, **7**(9), 1711–1718.

219 J. Winsberg, T. Janoschka, S. Morgenstern, T. Hagemann, S. Muench, G. Hauffman, *et al.*, Poly(TEMPO)/Zinc Hybrid-Flow Battery: A Novel, "green," High Voltage, and Safe Energy Storage System, *Adv. Mater.*, 2016, **28**(11), 2238–2243.

220 J. Winsberg, T. Hagemann, S. Muench, C. Friebe, B. Häupler, T. Janoschka, *et al.*, Poly(boron-dipyrromethene)-A Redox-Active Polymer Class for Polymer Redox-Flow Batteries, *Chem. Mater.*, 2016, **28**(10), 3401–3405.

221 K. Hatakeyama-Sato, T. Nagano, S. Noguchi, Y. Sugai, J. Du, H. Nishide, *et al.*, Hydrophilic Organic Redox-Active Polymer Nanoparticles for Higher Energy Density Flow Batteries, *ACS Appl Polym. Mater.*, 2019, **1**(2), 188–196.

222 G. Minton and L. Lue, The influence of excluded volume and excess ion polarisability on the capacitance of the electric double layer, *Mol. Phys.*, 2016, **114**(16–17), 2477–2491.

223 M. Venturi, Q. G. Mulazzani and M. Z. Hoffman, Radiolytically-induced one-electron reduction of methyl viologen in aqueous solution. Stability of the radical cation in acidic and highly alkaline media(1), *Radiat. Phys. Chem.*, 1984, **23**(1–2), 229–236.

224 Q. Cheng, W. Fan, Y. He, P. Ma, S. Vanka, S. Fan, *et al.*, Photorechargeable High Voltage Redox Battery Enabled by Ta3N5 and GaN/Si Dual-Photoelectrode, *Adv. Mater.*, 2017, **29**(26), 1–8.

225 K. Lin, R. Gómez-Bombarelli, E. S. Beh, L. Tong, Q. Chen, A. Valle, *et al.*, A redox-flow battery with an alloxazine-based organic electrolyte, *Nat. Energy*, 2016, **1**(9), 1–8.

226 K. Lin, Q. Chen, M. R. Gerhardt, L. Tong, S. B. Kim, L. Eisenach, *et al.*, Alkaline quinone flow battery, *Science*, 2015, **349**(6255), 1529–1532.

227 H. Vafiadis and M. Skyllas-Kazacos, Evaluation of membranes for the novel vanadium bromine redox flow cell, *J. Membr. Sci.*, 2006, **279**(1–2), 394–402.

228 S. Kim, M. Vijayakumar, W. Wang, J. Zhang, B. Chen, Z. Nie, *et al.*, Chloride supporting electrolytes for all-vanadium redox flow batteries, *Phys. Chem. Chem. Phys.*, 2011, **13**(40), 18186–18193.

229 S. Kim, E. Thomsen, G. Xia, Z. Nie, J. Bao, K. Recknagle, *et al.*, 1 kW/1 kWh advanced vanadium redox flow battery utilizing mixed acid electrolytes, *J. Power Sources*, 2013, **237**, 300–309.

230 K. M. Kadish and J. Q. Ding, Resistance of Nonaqueous Solvent Systems Contalnlng Tetraalkylammonium Salts, *Anal. Chem.*, 1984, **56**(9), 1741–1744, DOI: 10.1021/ac00273a051.

231 Y. Marcus, Tetraalkylammonium ions in aqueous and non-aqueous solutions, *J. Solut. Chem.*, 2008, **37**(8), 1071–1098.

232 M. Kerner and P. Johansson, Pyrrolidinium fsi and TFSI-based polymerized ionic liquids as electrolytes for high-temperature lithium-ion batteries, *Batteries*, 2018, **4**(1), 10, DOI: 10.3390/batteries4010010.

233 A. Guerfi, M. Dontigny, P. Charest, M. Petitclerc, M. Lagacé, A. Vijh, *et al.*, Improved electrolytes for Li-ion batteries: Mixtures of ionic liquid and organic electrolyte with enhanced safety and electrochemical performance, *J. Power Sources*, 2010, **195**(3), 845–852.

234 D. Zhang, Q. Liu, X. Shi and Y. Li, Tetrabutylammonium hexafluorophosphate and 1-ethyl-3-methyl imidazolium hexafluorophosphate ionic liquids as supporting electrolytes for non-aqueous vanadium redox flow batteries, *J. Power ources*, 2012, **203**, 201–205, DOI: 10.1016/j.jpowsour.2011.10.136.

235 B. Schwenzer, J. Zhang, S. Kim, L. Li, J. Liu and Z. Yang, Membrane development for vanadium redox flow batteries, *ChemSusChem*, 2011, **4**(10), 1388–1406.

236 R. Ye, D. Henkensmeier, S. J. Yoon, Z. Huang, D. K. Kim, Z. Chang, *et al.*, Redox Flow Batteries for Energy Storage: A Technology Review, *J. Electrochem. Energy Convers. Storage*, 2018, **15**(1), 010801, DOI: 10.1115/1.4037248.

237 A. Trovò, F. Picano and M. Guarnieri, Comparison of energy losses in a 9 kW vanadium redox flow battery, *J. Power Sources*, 2019, **440**, 227144.

238 C. Youn, S. A. Song, K. Kim, J. Y. Woo, Y. W. Chang and S. N. Lim, Effect of nitrogen functionalization of graphite felt electrode by ultrasonication on the electrochemical performance of vanadium redox flow battery, *Mater. Chem. Phys.*, 2019, **237**, 121873, DOI: 10.1016/j.matchemphys.2019.121873.

239 J. Qiu, B. Huang, Y. Liu, D. Chen and Z. Xie, Glucose-derived hydrothermal carbons as energy storage booster for vanadium redox flow batteries, *J. Energy. Chem.*, 2019, DOI: 10.1016/j.jechem.2019.09.030.

240 Y. Yang, Y. Zhang, L. Tang, T. Liu, J. Huang, S. Peng, *et al.*, Investigations on physicochemical properties and electrochemical performance of sulfate-chloride mixed acid electrolyte for vanadium redox flow battery, *J. Power Sources*, 2019, **434**, 226719, DOI: 10.1016/j.jpowsour.2019.226719.

241 Z. N. Duan, Z. G. Qu, Q. Wang and J. J. Wang, Structural modification of vanadium redox flow battery with high electrochemical corrosion resistance, *Appl. Energy*, 2019, **250**, 1632–1640.

242 M. A. Aziz, S. I. Hossain and S. Shanmugam, Hierarchical oxygen rich-carbon nanorods: Efficient and durable electrode for all-vanadium redox flow batteries, *J. Power Sources*, 2020, **445**(2019), 227329, DOI: 10.1016/j.jpowsour.2019.227329.

243 M. B. Karimi, F. Mohammadi and K. Hooshyari, Recent approaches to improve Nafion performance for fuel cell applications: A review, *Int. J. Hydrogen Energy*, 2019, DOI: 10.1016/j.ijhydene.2019.09.096.

244 A. Khataee, D. Pan, J. S. Olsson, P. Jannasch and R. W. Lindström, Asymmetric cycling of vanadium redox flow batteries with a poly(arylene piperidinium)-based anion exchange membrane, *J. Power Sources*, 2021, **483**, 229202, available from: https://linkinghub.elsevier.com/retrieve/pii/S0378775320314920.

245 X. Teng, J. Dai, J. Su, Y. Zhu, H. Liu and Z. Song, A high performance polytetrafluoroethene/Nafion composite membrane for vanadium redox flow battery application, *J. Power Sources*, 2013, **240**, 131–139.

246 X. Teng, Y. Zhao, J. Xi, Z. Wu, X. Qiu and L. Chen, Nafion/organic silica modified TiO2 composite membrane for vanadium redox flow battery via in situ sol-gel reactions, *J. Membr. Sci.*, 2009, **341**(1–2), 149–154.

247 J. Xi, Z. Wu, X. Qiu and L. Chen, Nafion/SiO2 hybrid membrane for vanadium redox flow battery, *J. Power Sources*, 2007, **166**(2), 531–536.

248 N. Wang, S. Peng, D. Lu, S. Liu, Y. Liu and K. Huang, Nafion/TiO 2 hybrid membrane fabricated via hydrothermal method for vanadium redox battery, *J. Solid State Electrochem.*, 2012, **16**(4), 1577–1584.

249 R. T. S. Muthu-Lakshmi, V. Choudhary and I. K. Varma, Sulphonated poly(ether ether ketone): Synthesis, *J. Mater. Sci.*, 2005, **40**, 629–636.

250 Z. Mai, H. Zhang, X. Li, C. Bi and H. Dai, Sulfonated poly(tetramethydiphenyl ether ether ketone) membranes for vanadium redox flow battery application, *J. Power Sources*, 2011, **196**(1), 482–487, DOI: 10.1016/j.jpowsour.2010.07.028.

251 Z. Li, W. Dai, L. Yu, J. Xi, X. Qiu and L. Chen, Sulfonated poly(ether ether ketone)/mesoporous silica hybrid membrane for high performance vanadium redox flow battery, *J. Power Sources*, 2014, **257**, 221–229, DOI: 10.1016/j.jpowsour.2014.01.127.

252 W. Dai, L. Yu, Z. Li, J. Yan, L. Liu, J. Xi, *et al.*, Sulfonated Poly(Ether Ether Ketone)/Graphene composite membrane for vanadium redox flow battery, *Electrochim. Acta*, 2014, **132**, 200–207, DOI: 10.1016/j.electacta.2014.03.156.

253 D. Cai and M. Song, Recent advance in functionalized graphene/polymer nanocomposites, *J. Mater. Chem.*, 2010, **20**(37), 7906–7915.

254 M. Fang, K. Wang, H. Lu, Y. Yang and S. Nutt, Covalent polymer functionalization of graphene nanosheets and mechanical properties of composites, *J. Mater. Chem.*, 2009, **19**(38), 7098–7105.

255 Q. Luo, H. Zhang, J. Chen, D. You, C. Sun and Y. Zhang, Preparation and characterization of Nafion/SPEEK layered composite membrane and its application in vanadium redox flow battery, *J. Membr. Sci.*, 2008, **325**(2), 553–558.

256 T. Mohammadi and M. Skyllas-Kazacos, Preparation of sulfonated composite membrane for vanadium redox flow battery applications, *J. Membr. Sci.*, 1995, **107**(1–2), 35–45.

257 B. Tian, C. W. Yan and F. H. Wang, Proton conducting composite membrane from Daramic/Nafion for vanadium redox flow battery, *J. Membr. Sci.*, 2004, **234**(1–2), 51–54.

258 D. Chen, S. Kim, L. Li, G. Yang and M. A. Hickner, Stable fluorinated sulfonated poly(arylene ether) membranes for vanadium redox flow batteries, *RSC Adv.*, 2012, **2**(21), 8087–8094.

259 H. S. Choi, Y. H. Oh, C. H. Ryu and G. J. Hwang, Characteristics of the all-vanadium redox flow battery using anion exchange membrane, *J. Taiwan Inst. Chem. Eng.*, 2014, **45**(6), 2920–2925, DOI: 10.1016/j.jtice.2014.08.032.

260 P. K. Leung, Q. Xu, T. S. Zhao, L. Zeng and C. Zhang, Preparation of silica nanocomposite anion-exchange membranes with low vanadium-ion crossover for vanadium redox flow batteries, *Electrochim. Acta*, 2013, **105**, 584–592.

261 I. L. Escalante-García, J. S. Wainright, L. T. Thompson and R. F. Savinell, Performance of a non-aqueous vanadium acetylacetonate prototype redox flow battery: Examination of separators and capacity decay, *J. Electrochem. Soc.*, 2015, **162**(3), A363–A372.

262 G. J. Hwang and H. Ohya, Crosslinking of anion exchange membrane by accelerated electron radiation as a separator for the all-vanadium redox flow battery, *J. Membr. Sci.*, 1997, **132**(1), 55–61.

263 S. Yun, J. Parrondo and V. Ramani, A vanadium-cerium redox flow battery with an anion-exchange membrane separator, *Chempluschem*, 2015, **80**(2), 412–421.

264 B. Zhang, S. Zhang, Z. Weng, G. Wang, E. Zhang, P. Yu, *et al.*, Quaternized adamantane-containing poly(aryl ether ketone) anion exchange membranes for vanadium redox flow battery applications, *J. Power Sources*, 2016, **325**, 801–807, DOI: 10.1016/j.jpowsour.2016.06.101.

265 X. G. Jian, C. Yan, H. M. Zhang, S. H. Zhang, C. Liu and P. Zhao, Synthesis and characterization of quaternized poly(phthalazinone ether sulfone ketone) for anion-exchange membrane, *Chinese Chem Lett*, 2007, **18**(10), 1269–1272.

266 S. Zhang, B. Zhang, G. Zhao and X. Jian, Anion exchange membranes from brominated poly(aryl ether ketone) containing 3,5-dimethyl phthalazinone moieties for vanadium redox flow batteries, *J. Mater. Chem. A*, 2014, **2**(9), 3083–3091.

267 S. Zhang, C. Yin, D. Xing, D. Yang and X. Jian, Preparation of chloromethylated/quaternized poly(phthalazinone ether ketone) anion exchange membrane materials for vanadium redox flow battery applications, *J. Membr. Sci.*, 2010, **363**(1–2), 243–249, DOI: 10.1016/j.memsci.2010.07.046.

268 D. Chen, M. A. Hickner, E. Agar and E. C. Kumbur, Optimized anion exchange membranes for vanadium

redox flow batteries, *ACS Appl. Mater. Interfaces*, 2013, **5**(15), 7559–7566.

269 F. Zhang, H. Zhang and C. Qu, A dication cross-linked composite anion-exchange membrane for all-vanadium flow battery applications, *ChemSusChem*, 2013, **6**(12), 2290–2298.

270 M. S. Cha, H. Y. Jeong, H. Y. Shin, S. H. Hong, T. H. Kim, S. G. Oh, *et al.*, Crosslinked anion exchange membranes with primary diamine-based crosslinkers for vanadium redox flow battery application, *J. Power Sources*, 2017, **363**, 78–86, DOI: 10.1016/j.jpowsour.2017.07.068.

271 J. Ren, Y. Dong, J. Dai, H. Hu, Y. Zhu and X. Teng, A novel chloromethylated/quaternized poly(sulfone)/poly(vinylidene fluoride) anion exchange membrane with ultra-low vanadium permeability for all vanadium redox flow battery, *J. Membr. Sci.*, 2017, **544**, 186–194, DOI: 10.1016/j.memsci.2017.09.015.

272 S. G. Park, N. S. Kwak, C. W. Hwang, H. M. Park and T. S. Hwang, Synthesis and characteristics of aminated vinylbenzyl chloride-co-styrene-co-hydroxyethyl acrylate anion-exchange membrane for redox flow battery applications, *J. Membr. Sci.*, 2012, **423–424**, 429–437, DOI: 10.1016/j.memsci.2012.08.040.

273 S. Maurya, S. H. Shin, M. K. Kim, S. H. Yun and S. H. Moon, Stability of composite anion exchange membranes with various functional groups and their performance for energy conversion, *J. Membr. Sci.*, 2013, **443**, 28–35, DOI: 10.1016/j.memsci.2013.04.035.

274 C. W. Hwang, H. M. Park, C. M. Oh, T. S. Hwang, J. Shim and C. S. Jin, Synthesis and characterization of vinylimidazole-co-trifluoroethylmethacrylate-co-divinylbenzene anion-exchange membrane for all-vanadium redox flow battery, *J. Membr. Sci.*, 2014, **468**, 98–106, DOI: 10.1016/j.memsci.2014.05.050.

275 C. Zhou, Y. Hu, Z. Yang, T. Yuan, J. Huang, P. Li, *et al.*, Facile synthesis and characterization of urushiol analogues from tung oil via ultraviolet photocatalysis, *Prog. Org. Coatings.*, 2018, **120**, 240–251, DOI: 10.1016/j.porgcoat.2018.03.015.

276 S. J. Gong, D. Kim, E. Cho, S. S. Hwang and J. Won, A Chitosan/Urushi Anion Exchange Membrane for a Non–aqueous Redox Flow Battery, *ChemistrySelect*, 2017, **2**(5), 1843–1849.

277 E. Cho and J. Won, Novel composite membrane coated with a poly(diallyldimethylammonium chloride)/urushi semi-interpenetrating polymer network for non-aqueous redox flow battery application, *J. Power Sources*, 2016, **335**, 12–19, DOI: 10.1016/j.jpowsour.2016.10.020.

278 A. Bhattarai, A. H. Whitehead, R. Schweiss, G. G. Scherer, M. Skyllas-Kazacos, N. Wai, *et al.*, Anomalous Behavior of Anion Exchange Membrane during Operation of a Vanadium Redox Flow Battery, *ACS Appl. Energy Mater.*, 2019, **2**(3), 1712–1719, available from: https://pubs.acs.org/doi/10.1021/acsaem.8b01816.

279 T. Mohammadi and M. Skyllas Kazacos, Modification of anion-exchange membranes for vanadium redox flow battery applications, *J. Power Sources*, 1996, **63**(2), 179–186.

280 S. Liu, L. Wang, D. Li, B. Liu, J. Wang and Y. Song, Novel amphoteric ion exchange membranes by blending sulfonated poly(ether ether ketone)/quaternized poly(ether imide) for vanadium redox flow battery applications, *J. Mater. Chem. A*, 2015, **3**(34), 17590–17597, DOI: 10.1039/c5ta04351d.

281 J. Dai, Y. Dong, P. Gao, J. Ren, C. Yu, H. Hu, *et al.*, A sandwiched bipolar membrane for all vanadium redox flow battery with high coulombic efficiency, *Polymer*, 2018, **140**, 233–239, DOI: 10.1016/j.polymer.2018.02.051.

282 R. Gan, Y. Ma, S. Li, F. Zhang and G. He, Facile fabrication of amphoteric semi-interpenetrating network membranes for vanadium flow battery applications, *J. Energy Chem.*, 2018, **27**(4), 1189–1197, DOI: 10.1016/j.jechem.2017.09.017.

283 X. Yan, C. Zhang, Y. Dai, W. Zheng, X. Ruan and G. He, A novel imidazolium-based amphoteric membrane for high-performance vanadium redox flow battery, *J. Membr. Sci.*, 2017, **544**(April), 98–107, DOI: 10.1016/j.memsci.2017.09.025.

284 P. P. Sharma, A. Paul, D. N. Srivastava and V. Kulshrestha, Semi-Interpenetrating Network-Type Cross-Linked Amphoteric Ion-Exchange Membrane Based on Styrene Sulfonate and Vinyl Benzyl Chloride for Vanadium Redox Flow Battery, *ACS Omega*, 2018, **3**(8), 9872–9879.

285 N. M. Vargas-Barbosa, G. M. Geise, M. A. Hickner and T. E. Mallouk, Assessing the utility of bipolar membranes for use in photoelectrochemical water-splitting cells, *ChemSusChem*, 2014, **7**(11), 3017–3020.

286 D. A. Vermaas, M. Sassenburg and W. A. Smith, Photo-assisted water splitting with bipolar membrane induced pH gradients for practical solar fuel devices, *J. Mater. Chem. A*, 2015, **3**(38), 19556–19562.

287 J. Balster, D. Stamatialis and M. Wessling, Electro-catalytic membrane reactors and the development of bipolar membrane technology, *Chem. Eng. Process Process Intensif.*, 2004, **43**(9), 1115–1127, available from: https://linkinghub.elsevier.com/retrieve/pii/S0255270104000558.

288 C. Fernandez-Gonzalez, A. Dominguez-Ramos, R. Ibañez and A. Irabien, Electrodialysis with Bipolar Membranes for Valorization of Brines, *Sep. Purif. Rev.*, 2016, **45**(4), 275–287, available from: http://www.tandfonline.com/doi/full/10.1080/15422119.2015.1128951.

289 A. Khataee, K. Wedege, E. Dražević and A. Bentien, Differential pH as a method for increasing cell potential in organic aqueous flow batteries, *J. Mater. Chem. A*, 2017, **5**(41), 21875–21882.

290 C. Noh, M. Jung, D. Henkensmeier, S. W. Nam and Y. Kwon, Vanadium Redox Flow Batteries Using meta-Polybenzimidazole-Based Membranes of Different Thicknesses, *ACS Appl Mater Interfaces*, 2017, **9**(42), 36799–36809.

291 J. B. Liao, M. Z. Lu, Y. Q. Chu and J. L. Wang, Ultra-low vanadium ion diffusion amphoteric ion-exchange membranes for all-vanadium redox flow batteries, *J. Power Sources*, 2015, **282**, 241–247.

292 A. Chromik, A. R. dos Santos, T. Turek, U. Kunz, T. Häring and J. Kerres, Stability of acid-excess acid-base blend

membranes in all-vanadium redox-flow batteries, *J. Membr. Sci.*, 2015, **476**, 148–155, DOI: 10.1016/j.memsci.2014.11.036.

293 D. Chen, X. Chen, L. Ding and X. Li, Advanced acid-base blend ion exchange membranes with high performance for vanadium flow battery application, *J. Membr. Sci.*, 2018, **553**, 25–31, DOI: 10.1016/j.memsci.2018.02.039.

294 F. J. Oldenburg, E. Nilsson, T. J. Schmidt and L. Gubler, Tackling Capacity Fading in Vanadium Redox Flow Batteries with Amphoteric Polybenzimidazole/Nafion Bilayer Membranes, *ChemSusChem*, 2019, **12**(12), 2620–2627.

295 Z. Xia, L. Ying, J. Fang, Y. Y. Du, W. M. Zhang, X. Guo, *et al.*, Preparation of covalently cross-linked sulfonated polybenzimidazole membranes for vanadium redox flow battery applications, *J. Membr. Sci.*, 2017, **525**(2016), 229–239.

296 J. Yuan, C. Yu, J. Peng, Y. Wang, J. Ma, J. Qiu, *et al.*, Facile synthesis of amphoteric ion exchange membrane by radiation grafting of sodium styrene sulfonate and N,N-dimethylaminoethyl methacrylate for vanadium redox flow battery, *J. Polym. Sci. Part A. Polym. Chem.*, 2013, **51**(24), 5194–5202.

297 G. Hu, Y. Wang, J. Ma, J. Qiu, J. Peng, J. Li, *et al.*, A novel amphoteric ion exchange membrane synthesized by radiation-induced grafting α-methylstyrene and N,N-dimethylaminoethyl methacrylate for vanadium redox flow battery application, *J. Membr. Sci.*, 2012, **407–408**, DOI: 10.1016/j.memsci.2012.03.042.

298 J. Ma, Y. Wang, J. Peng, J. Qiu, L. Xu, J. Li, *et al.*, Designing a new process to prepare amphoteric ion exchange membrane with well-distributed grafted chains for vanadium redox flow battery, *J. Membr. Sci.*, 2012, **419–420**, 1–8, DOI: 10.1016/j.memsci.2012.04.034.

299 J. Qiu, M. Li, J. Ni, M. Zhai, J. Peng, L. Xu, *et al.*, Preparation of ETFE-based anion exchange membrane to reduce permeability of vanadium ions in vanadium redox battery, *J. Membr. Sci.*, 2007, **297**(1–2), 174–180.

300 J. Qiu, J. Zhang, J. Chen, J. Peng, L. Xu, M. Zhai, *et al.*, Amphoteric ion exchange membrane synthesized by radiation-induced graft copolymerization of styrene and dimethylaminoethyl methacrylate into PVDF film for vanadium redox flow battery applications, *J. Membr. Sci.*, 2009, **334**(1–2), 9–15.

301 J. Qiu, M. Zhai, J. Chen, Y. Wang, J. Peng, L. Xu, *et al.*, Performance of vanadium redox flow battery with a novel amphoteric ion exchange membrane synthesized by two-step grafting method, *J. Membr. Sci.*, 2009, **342**(1–2), 215–220.

302 S. Liu, D. Li, L. Wang, H. Yang, X. Han and B. Liu, Ethylenediamine-functionalized graphene oxide incorporated acid-base ion exchange membranes for vanadium redox flow battery, *Electrochim. Acta*, 2017, **230**, 204–211, DOI: 10.1016/j.electacta.2017.01.170.

303 L. Cao, Q. Sun, Y. Gao, L. Liu and H. Shi, Novel acid-base hybrid membrane based on amine-functionalized reduced graphene oxide and sulfonated polyimide for vanadium redox flow battery, *Electrochim. Acta*, 2015, **158**, 24–34, DOI: 10.1016/j.electacta.2015.01.159.

304 S. Liu, L. Wang, Y. Ding, B. Liu, X. Han and Y. Song, Novel sulfonated poly(ether ether keton)/polyetherimide acid-base blend membranes for vanadium redox flow battery applications, *Electrochim. Acta*, 2014, **130**, 90–96, DOI: 10.1016/j.electacta.2014.02.144.

305 Z. Li, W. Dai, L. Yu, L. Liu, J. Xi, X. Qiu, *et al.*, Properties investigation of sulfonated poly(ether ether ketone)/polyacrylonitrile acid-base blend membrane for vanadium redox flow battery application, *ACS Appl. Mater. Interfaces*, 2014, **6**(21), 18885–18893.

306 R. Niu, L. Kong, L. Zheng, H. Wang and H. Shi, Novel graphitic carbon nitride nanosheets/sulfonated poly(ether ether ketone) acid-base hybrid membrane for vanadium redox flow battery, *J. Membr. Sci.*, 2017, **525**(2016), 220–228, DOI: 10.1016/j.memsci.2016.10.049.

307 Y. Wang, S. Wang, M. Xiao, S. Song, D. Han, M. A. Hickner, *et al.*, Amphoteric ion exchange membrane synthesized by direct polymerization for vanadium redox flow battery application, *Int. J. Hydrogen Energy*, 2014, **39**(28), 16123–16131, DOI: 10.1016/j.ijhydene.2014.04.049.

308 S. C. Chieng, M. Kazacos and M. Skyllas-Kazacos, Preparation and evaluation of composite membrane for vanadium redox battery applications, *J. Power Sources*, 1992, **39**(1), 11–19.

309 S. C. Chieng, M. Kazacos and M. Skyllas-Kazacos, Modification of Daramic, microporous separator, for redox flow battery applications, *J. Membr. Sci.*, 1992, **75**(1–2), 81–91.

310 X. L. Zhou, T. S. Zhao, L. An, Y. K. Zeng and L. Wei, Modeling of ion transport through a porous separator in vanadium redox flow batteries, *J. Power Sources*, 2016, **327**, 67–76.

311 H. Zhang, H. Zhang, X. Li, Z. Mai and J. Zhang, Nanofiltration (NF) membranes: The next generation separators for all vanadium redox flow batteries (VRBs)?, *Energy Environ. Sci.*, 2011, **4**(5), 1676–1679.

312 J. Cao, H. Zhang, W. Xu and X. Li, Poly(vinylidene fluoride) porous membranes precipitated in water/ethanol dual-coagulation bath: The relationship between morphology and performance in vanadium flow battery, *J. Power Sources*, 2014, **249**, 84–91, DOI: 10.1016/j.jpowsour.2013.10.069.

313 B. M. Weckhuysen and J. Yu, Recent advances in zeolite chemistry and catalysis, *Chem. Soc. Rev.*, 2015, **44**(20), 7022–7024, DOI: 10.1039/c5cs90100f.

314 P. J. Bereciartua, C. Á, A. Corma, J. L. Jordá, M. Palomino, F. Rey, *et al.*, Control of zeolite framework flexibility and pore topology for separation of ethane and ethylene, *Science*, 2017, **358**(6366), 1068–1071.

315 R. Yang, Z. Xu, S. Yang, I. Michos, L. F. Li, A. P. Angelopoulos, *et al.*, Nonionic zeolite membrane as potential ion separator in redox-flow battery, *J. Membr. Sci.*, 2014, **450**, 12–17, DOI: 10.1016/j.memsci.2013.08.048.

316 Z. Yuan, X. Zhu, M. Li, W. Lu, X. Li and H. Zhang, A Highly Ion-Selective Zeolite Flake Layer on Porous Membranes for

Flow Battery Applications, *Angew. Chem. Int. Ed.*, 2016, **55**(9), 3058–3062.

317 P. Arévalo-Cid, J. Isasi and F. Martín-Hernández, Comparative study of core-shell nanostructures based on amino-functionalized Fe3O4@SiO2 and CoFe2O4@SiO2 nanocomposites, *J. Alloys Compd*, 2018, **766**, 609–618.

318 X. Wei, B. Li and W. Wang, Porous polymeric composite separators for redox flow batteries, *Polym. Rev.*, 2015, **55**(2), 247–272.

319 H. Zhang, H. Zhang, X. Li, Z. Mai and W. Wei, Silica modified nanofiltration membranes with improved selectivity for redox flow battery application, *Energy Environ. Sci.Energy Environ. Sci.*, 2012, **5**(4), 6299–6303.

320 X. Wei, Z. Nie, Q. Luo, B. Li, B. Chen, K. Simmons, *et al.*, Nanoporous polytetrafl uoroethylene/silica composite separator as a high-performance all-vanadium redox flow battery membrane, *Adv. Energy Mater.*, 2013, **3**(9), 1215–1220.

321 L. Yan, D. Li, S. Li, Z. Xu, J. Dong, W. Jing, *et al.*, Balancing Osmotic Pressure of Electrolytes for Nanoporous Membrane Vanadium Redox Flow Battery with a Draw Solute, *ACS Appl Mater Interfaces*, 2016, **8**(51), 35289–35297.

322 A. Bhattarai, N. Wai, R. Schweiss, A. Whitehead, T. M. Lim and H. H. Hng, Advanced porous electrodes with flow channels for vanadium redox flow battery, *J. Power Sources*, 2017, **341**, 83–90, DOI: 10.1016/j.jpowsour.2016.11.113.

323 M. Moore and M. C. Robert, An Analysis of the Contributions of Current Density and Voltage Efficiency to the Capital Costs of an All Vanadium Redox-Flow Battery, *J Chem Eng Process Technol*, 2016, **7**, 2, DOI: 10.4172/2157-7048.1000288.

324 P. Zhang, T. Yuan, Y. Pang, C. Peng, J. Yang, Z. F. Ma, *et al.*, Influence of current density on graphite anode failure in lithium-ion batteries, *J. Electrochem. Soc.*, 2019, **166**(3), A5489–A5495.

325 R. Banerjee, N. Bevilacqua, A. Mohseninia, B. Wiedemann, F. Wilhelm, J. Scholta, *et al.*, Carbon felt electrodes for redox flow battery: Impact of compression on transport properties, *J. Energy Storage*, 2019, **26**, 100997, DOI: 10.1016/j.est.2019.100997.

326 N. Gurieff, V. Timchenko and C. Menictas, Variable porous electrode compression for redox flow battery systems, *Batteries*, 2018, **4**(4), 1–10.

327 L. Eifert, Z. Jusys, R. J. Behm and R. Zeis, Side reactions and stability of pre-treated carbon felt electrodes for vanadium redox flow batteries: A DEMS study, *Carbon*, 2019; available from: https://www.sciencedirect.com/science/article/abs/pii/S0008622319311546%0Ahttps://linkinghub.elsevier.com/retrieve/pii/S0008622319311546.

328 L. Eifert, R. Banerjee, Z. Jusys and R. Zeis, Characterization of carbon felt electrodes for vanadium redox flow batteries: Impact of treatment methods, *J. Electrochem. Soc.*, 2018, **165**(11), A2577–A2586.

329 H. Liu, Q. Xu, C. Yan and Y. Qiao, Corrosion behavior of a positive graphite electrode in vanadium redox flow battery, *Electrochim. Acta*, 2011, **56**(24), 8783–8790, DOI: 10.1016/j.electacta.2011.07.083.

330 I. Derr, M. Bruns, J. Langner, A. Fetyan, J. Melke and C. Roth, Degradation of all-vanadium redox flow batteries (VRFB) investigated by electrochemical impedance and X-ray photoelectron spectroscopy: Part 2 electrochemical degradation, *J. Power Sources*, 2016, **325**, 351–359, DOI: 10.1016/j.jpowsour.2016.06.040.

331 I. Derr, A. Fetyan, K. Schutjajew and C. Roth, Electrochemical analysis of the performance loss in all vanadium redox flow batteries using different cut-off voltages, *Electrochim. Acta*, 2017, **224**, 9–16; available from: https://linkinghub.elsevier.com/retrieve/pii/S0013468616325919.

332 M. Cecchetti, A. Casalegno and M. Zago, Local potential measurement through reference electrodes in vanadium redox flow batteries: Evaluation of overpotentials and electrolytes imbalance, *J. Power Sources*, 2018, **400**, 218–224, available from: https://linkinghub.elsevier.com/retrieve/pii/S0378775318308929.

333 T. Greese and G. Reichenauer, Anode kinetics degradation in vanadium redox flow batteries – Reversible inhibition of the V2+/V3+-reaction due to V(II)-adsorption, *J. Power Sources*, 2021, **500**, 229958, available from: https://linkinghub.elsevier.com/retrieve/pii/S0378775321004894.

334 A. Crawford, V. Viswanathan, D. Stephenson, W. Wang, E. Thomsen, D. Reed, *et al.*, Comparative analysis for various redox flow batteries chemistries using a cost performance model, *J. Power Sources*, 2015, **293**, 388–399, DOI: 10.1016/j.jpowsour.2015.05.066.

335 J. Melke, P. Jakes, J. Langner, L. Riekehr, U. Kunz, Z. Zhao-Karger, *et al.*, Carbon materials for the positive electrode in all-vanadium redox flow batteries, *Carbon*, 2014, **78**, 220–230, DOI: 10.1016/j.carbon.2014.06.075.

336 Z. González, S. Vizireanu, G. Dinescu, C. Blanco and R. Santamaría, Carbon nanowalls thin films as nanostructured electrode materials in vanadium redox flow batteries, *Nano Energy*, 2012, **1**(6), 833–839.

337 Y. Munaiah, S. Suresh, S. Dheenadayalan, V. K. Pillai and P. Ragupathy, Comparative Electrocatalytic performance of single-walled and multiwalled carbon nanotubes for zinc bromine redox flow batteries, *J. Phys. Chem. C*, 2014, **118**(27), 14795–14804.

338 S. Zhong, C. Padeste, M. Kazacos and M. Skyllas-Kazacos, Comparison of the physical, chemical and electrochemical properties of rayon- and polyacrylonitrile-based graphite felt electrodes, *J. Power Sources*, 1993, **45**(1), 29–41.

339 M. Ulaganathan, A. Jain, V. Aravindan, S. Jayaraman, W. C. Ling, T. M. Lim, *et al.*, Bio-mass derived mesoporous carbon as superior electrode in all vanadium redox flow battery with multicouple reactions, *J. Power Sources*, 2015, **274**, 846–850, DOI: 10.1016/j.jpowsour.2014.10.176.

340 M. C. Ribadeneyra, L. Grogan, H. Au, P. Schlee, S. Herou, T. Neville, *et al.*, Lignin-derived electrospun freestanding carbons as alternative electrodes for redox flow batteries,

Carbon, 2020, **157**, 847–56, available from: https://linkinghub.elsevier.com/retrieve/pii/S000862231931139X.

341 D. Aaron, C. N. Sun, M. Bright, A. B. Papandrew, M. M. Mench and T. A. Zawodzinski, In situ kinetics studies in all-vanadium redox flow batteries, *ECS Electrochem. Lett.*, 2013, **2**(3), 2013–2015.

342 N. Roznyatovskaya, J. Noack, K. Pinkwart and J. Tübke, Aspects of electron transfer processes in vanadium redox-flow batteries, *Curr. Opin. Electrochem.*, 2020, **19**, 42–48, DOI: 10.1016/j.coelec.2019.10.003.

343 Z. Jiang, K. Klyukin and V. Alexandrov, First-principles study of adsorption-desorption kinetics of aqueous V 2+/V 3+ redox species on graphite in a vanadium redox flow battery, *Phys. Chem. Chem. Phys.*, 2017, **19**(23), 14897–14901, DOI: 10.1039/c7cp02350b.

344 K. J. Kim, Y. J. Kim, J. H. Kim and M. S. Park, The effects of surface modification on carbon felt electrodes for use in vanadium redox flow batteries, *Mater. Chem. Phys.*, 2011, **131**(1–2), 547–553, DOI: 10.1016/j.matchemphys.2011.10.022.

345 Q. H. Liu, G. M. Grim, A. B. Papandrew, A. Turhan, T. A. Zawodzinski and M. M. Mench, High Performance Vanadium Redox Flow Batteries with Optimized Electrode Configuration and Membrane Selection, *J. Electrochem. Soc.*, 2012, **159**(8), A1246–A1252.

346 Z. González, C. Botas, P. Álvarez, S. Roldán, C. Blanco, R. Santamaría, *et al.*, Thermally reduced graphite oxide as positive electrode in Vanadium Redox Flow Batteries, *Carbon*, 2012, **50**(3), 828–834.

347 A. M. Pezeshki, J. T. Clement, G. M. Veith, T. A. Zawodzinski and M. M. Mench, High performance electrodes in vanadium redox flow batteries through oxygen-enriched thermal activation, *J. Power Sources*, 2015, **294**, 333–338, DOI: 10.1016/j.jpowsour.2015.05.118.

348 J. Kim, H. Lim, J. Y. Jyoung, E. S. Lee, J. S. Yi and D. Lee, High electrocatalytic performance of N and O atomic co-functionalized carbon electrodes for vanadium redox flow battery, *Carbon*, 2017, **111**, 592–601, DOI: 10.1016/j.carbon.2016.10.043.

349 Y. Shao, X. Wang, M. Engelhard, C. Wang, S. Dai, J. Liu, *et al.*, Nitrogen-doped mesoporous carbon for energy storage in vanadium redox flow batteries, *J. Power Sources*, 2010, **195**(13), 4375–4379, DOI: 10.1016/j.jpowsour.2010.01.015.

350 J. Wang, S. Yang, D. Guo, P. Yu, D. Li, J. Ye, *et al.*, Comparative studies on electrochemical activity of graphene nanosheets and carbon nanotubes, *Electrochem. Commun.*, 2009, **11**(10), 1892–1895, DOI: 10.1016/j.elecom.2009.08.019.

351 H. M. Tsai, S. Y. Yang, C. C. M. Ma and X. Xie, Preparation and electrochemical properties of graphene-modified electrodes for all-vanadium redox flow batteries, *Electroanalysis*, 2011, **23**(9), 2139–2143.

352 W. Li, Z. Zhang, Y. Tang, H. Bian, T. W. Ng, W. Zhang, *et al.*, Graphene-nanowall-decorated carbon felt with excellent electrochemical activity toward VO2+/VO2+ couple for all vanadium redox flow battery, *Adv. Sci.*, 2016, **3**(4), 1–7.

353 K. S. Ibrahim, Carbon nanotubes-properties and applications: a review, *Carbon Lett.*, 2013, **14**(3), 131–144.

354 W. Li, J. Liu and C. Yan, Multi-walled carbon nanotubes used as an electrode reaction catalyst for VO2+/VO2+ for a vanadium redox flow battery, *Carbon*, 2011, **49**(11), 3463–3470, DOI: 10.1016/j.carbon.2011.04.045.

355 M. Park, Y. J. Jung, J. Kim, H. I. Lee and J. Cho, Synergistic effect of carbon nanofiber/nanotube composite catalyst on carbon felt electrode for high-performance all-vanadium redox flow battery, *Nano Lett.*, 2013, **13**(10), 4833–4839.

356 S. Wang, X. Zhao, T. Cochell and A. Manthiram, Nitrogen-doped carbon nanotube/graphite felts as advanced electrode materials for vanadium redox flow batteries, *J. Phys. Chem. Lett.*, 2012, **3**(16), 2164–2167.

357 Y. Matsumoto and E. Sato, Electrocatalytic properties of transition metal oxides for oxygen evolution reaction, *Mater. Chem. Phys.*, 1986, **14**, 397–426.

358 Z. Chen, D. Higgins, A. Yu, L. Zhang and J. Zhang, A review on non-precious metal electrocatalysts for PEM fuel cells, *Energy Environ. Sci.*, 2011, **4**(9), 3167–3192.

359 Z. Chen, X. Duan, W. Wei, S. Wang and B. J. Ni, Recent advances in transition metal-based electrocatalysts for alkaline hydrogen evolution, *J. Mater. Chem. A*, 2019, **7**(25), 14971–15005.

360 W. H. Wang and X. D. Wang, Investigation of Ir-modified carbon felt as the positive electrode of an all-vanadium redox flow battery, *Electrochim. Acta*, 2007, **52**(24), 6755–6762.

361 L. Wei, T. S. Zhao, L. Zeng, X. L. Zhou and Y. K. Zeng, Copper nanoparticle-deposited graphite felt electrodes for all vanadium redox flow batteries, *Appl. Energy*, 2016, **180**, 386–391, DOI: 10.1016/j.apenergy.2016.07.134.

362 C. Flox, M. Skoumal, J. Rubio-Garcia, T. Andreu and J. R. Morante, Strategies for enhancing electrochemical activity of carbon-based electrodes for all-vanadium redox flow batteries, *Appl. Energy*, 2013, **109**, 344–351, DOI: 10.1016/j.apenergy.2013.02.001.

363 S. Zhang, X. Zhang, Y. Rui, R. Wang and X. Li, Recent advances in non-precious metal electrocatalysts for pH-universal hydrogen evolution reaction, *Green Energy Environ.*, 2020, available from: https://linkinghub.elsevier.com/retrieve/pii/S2468025720301709.

364 Q. Shi, C. Zhu, D. Du and Y. Lin, Robust noble metal-based electrocatalysts for oxygen evolution reaction, *Chem. Soc. Rev.*, 2019, **48**(12), 3181–3192, available from: http://xlink.rsc.org/?DOI=C8CS00671G.

365 K. Amini, J. Gostick and M. D. Pritzker, Metal and Metal Oxide Electrocatalysts for Redox Flow Batteries, *Adv. Funct. Mater.*, 2020, **30**(23), 1910564, available from: https://onlinelibrary.wiley.com/doi/10.1002/adfm.201910564.

366 P. C. Ghimire, R. Schweiss, G. G. Scherer, N. Wai, T. M. Lim, A. Bhattarai, *et al.*, Titanium carbide-decorated graphite felt as high performance negative electrode in vanadium redox flow batteries, *J. Mater. Chem. A*, 2018, **6**(15), 6625–6632, available from: http://xlink.rsc.org/?DOI=C8TA00464A.

367 J. Vázquez-Galván, C. Flox, J. R. Jervis, A. B. Jorge, P. R. Shearing and J. R. Morante, High-power nitrided TiO2 carbon felt as the negative electrode for all-vanadium redox flow batteries, *Carbon*, 2019, **148**, 91–104, available from: https://linkinghub.elsevier.com/retrieve/pii/S0008622319300752.

368 T. S. Chen, S. L. Huang, M. L. Chen, T. J. Tsai and Y. S. Lin, Improving electrochemical activity in a semi-V-I redox flow battery by using a C-TiO2-Pd composite electrode, *J. Nanomater.*, 2019, **2019**, 7460856, DOI: 10.1155/2019/7460856.

369 C. Yang, H. Wang, S. Lu, C. Wu, Y. Liu, Q. Tan, *et al.*, Titanium nitride as an electrocatalyst for V(II)/V(III) redox couples in all-vanadium redox flow batteries, *Electrochim. Acta*, 2015, **182**(Ii), 834–840, DOI: 10.1016/j.electacta.2015.09.155.

370 Y. Jiang, X. Feng, G. Cheng, Y. Li, C. Li, Z. He, *et al.*, Electrocatalytic activity of MnO2 nanosheet array-decorated carbon paper as superior negative electrode for vanadium redox flow batteries, *Electrochim. Acta*, 2019, **322**, 134754, available from: https://linkinghub.elsevier.com/retrieve/pii/S0013468619316251.

371 B. Li, M. Gu, Z. Nie, Y. Shao, Q. Luo, X. Wei, *et al.*, Bismuth nanoparticle decorating graphite felt as a high-performance electrode for an all-vanadium redox flow battery, *Nano Lett.*, 2013, **13**(3), 1330–1335.

372 D. J. Suárez, Z. González, C. Blanco, M. Granda, R. Menéndez and R. Santamaría, Graphite felt modified with bismuth nanoparticles as negative electrode in a vanadium redox flow battery, *ChemSusChem*, 2014, **7**(3), 914–918.

373 B. Li, M. Gu, Z. Nie, X. Wei, C. Wang, V. Sprenkle, *et al.*, Nanorod Niobium Oxide as Powerful Catalysts for an All Vanadium Redox Flow Battery, *Nano Lett.*, 2014, **14**(1), 158–165, available from: https://pubs.acs.org/doi/10.1021/nl403674a.

374 D. S. Aaron, Q. Liu, Z. Tang, G. M. Grim, A. B. Papandrew, A. Turhan, *et al.*, Dramatic performance gains in vanadium redox flow batteries through modified cell architecture, *J. Power Sources*, 2012, **206**, 450–453, available from: https://linkinghub.elsevier.com/retrieve/pii/S0378775311024451.

375 P. Leung, X. Li, C. Ponce de León, L. Berlouis, C. T. J. Low and F. C. Walsh, Progress in redox flow batteries, remaining challenges and their applications in energy storage, *RSC Adv.*, 2012, **2**(27), 10125, available from: http://xlink.rsc.org/?DOI=c2ra21342g.

376 E. Sánchez-Díez, E. Ventosa, M. Guarnieri, A. Trovò, C. Flox, R. Marcilla, *et al.*, Redox flow batteries: Status and perspective towards sustainable stationary energy storage, *J. Power Sources*, 2021, 481.

377 Q. Xu, T. S. Zhao and P. K. Leung, Numerical investigations of flow field designs for vanadium redox flow batteries, *Appl. Energy*, 2013, **105**, 47–56, available from: https://linkinghub.elsevier.com/retrieve/pii/S0306261912009324.

378 R. M. Darling and M. L. Perry, The Influence of Electrode and Channel Configurations on Flow Battery Performance, *J. Electrochem. Soc.*, 2014, **161**(9), A1381–A1387, available from: https://iopscience.iop.org/article/10.1149/2.0941409jes.

379 J. Marschewski, L. Brenner, N. Ebejer, P. Ruch, B. Michel and D. Poulikakos, 3D-printed fluidic networks for high-power-density heat-managing miniaturized redox flow batteries, *Energy Environ. Sci.*, 2017, **10**(3), 780–787.

380 R. A. Elgammal, Z. Tang, C.-N. Sun, J. Lawton and T. A. Zawodzinski, Species Uptake and Mass Transport in Membranes for Vanadium Redox Flow Batteries, *Electrochim. Acta*, 2017, **237**, 1–11, available from: https://linkinghub.elsevier.com/retrieve/pii/S0013468617306138.

381 A. Z. Weber, M. M. Mench, J. P. Meyers, P. N. Ross, J. T. Gostick and Q. Liu, Redox flow batteries: a review, *J. Appl. Electrochem.*, 2011, **41**(10), 1137–1164, available from: http://link.springer.com/10.1007/s10800-011-0348-2.

382 N. M. Delgado, R. Monteiro, M. Abdollahzadeh, P. Ribeirinha, A. Bentien and A. Mendes, 2D-dynamic phenomenological modelling of vanadium redox flow batteries – Analysis of the mass transport related overpotentials, *J. Power Sources*, 2020, **480**, 229142, available from: https://linkinghub.elsevier.com/retrieve/pii/S0378775320314361.

383 M. D. R. Kok, A. Khalifa and J. T. Gostick, Multiphysics Simulation of the Flow Battery Cathode: Cell Architecture and Electrode Optimization, *J. Electrochem. Soc.*, 2016, **163**(7), A1408–A1419, available from: https://iopscience.iop.org/article/10.1149/2.1281607jes.

384 B. K. Chakrabarti, E. Kalamaras, A. K. Singh, A. Bertei, J. Rubio-Garcia, V. Yufit, *et al.*, Modelling of redox flow battery electrode processes at a range of length scales: a review, *Sustain. Energy Fuels*, 2020, **4**(11), 5433–5468, available from: http://xlink.rsc.org/?DOI=D0SE00667J.

385 M. O. Bamgbopa, S. Almheiri and H. Sun, Prospects of recently developed membraneless cell designs for redox flow batteries, *Renew. Sustain. Energy Rev.*, 2017, **70**, 506–518, available from: https://linkinghub.elsevier.com/retrieve/pii/S1364032116310061.

386 R. Ferrigno, A. D. Stroock, T. D. Clark, M. Mayer and G. M. Whitesides, Membraneless Vanadium Redox Fuel Cell Using Laminar Flow, *J. Am. Chem. Soc.*, 2002, **124**(44), 12930–12931, available from: https://pubs.acs.org/doi/10.1021/ja020812q.

387 M. O. Bamgbopa, Y. Shao-Horn, R. Hashaikeh and S. Almheiri, Cyclable membraneless redox flow batteries based on immiscible liquid electrolytes: Demonstration with all-iron redox chemistry, *Electrochim. Acta*, 2018, **267**, 41–50, available from: https://linkinghub.elsevier.com/retrieve/pii/S0013468618303451.

388 K. Gong, F. Xu, M. G. Lehrich, X. Ma, S. Gu and Y. Yan, Exploiting Immiscible Aqueous-Nonaqueous Electrolyte Interface toward a Membraneless Redox-Flow Battery Concept, *J. Electrochem. Soc.*, 2017, **164**(12), A2590–A2593, available from: https://iopscience.iop.org/article/10.1149/2.1241712jes.

389 M. H. Chakrabarti, E. P. L. Roberts, C. Bae and M. Saleem, Ruthenium based redox flow battery for solar energy storage, *Energy Convers. Manag.*, 2011, **52**(7), 2501–2508,

available from: https://linkinghub.elsevier.com/retrieve/pii/S0196890411000367.

390 E. Kjeang, R. Michel, D. A. Harrington, N. Djilali and D. Sinton, A Microfluidic Fuel Cell with Flow-Through Porous Electrodes, *J. Am. Chem. Soc.*, 2008, **130**(12), 4000–4006, available from: https://pubs.acs.org/doi/10.1021/ja078248c.

391 S. Tominaka, S. Ohta, H. Obata, T. Momma and T. Osaka, On-Chip Fuel Cell: Micro Direct Methanol Fuel Cell of an Air-Breathing, Membraneless, and Monolithic Design, *J. Am. Chem. Soc.*, 2008, **130**(32), 10456–10457, available from: https://pubs.acs.org/doi/10.1021/ja8024214.

392 P. Navalpotro, J. Palma, M. Anderson and R. Marcilla, A Membrane-Free Redox Flow Battery with Two Immiscible Redox Electrolytes, *Angew. Chem. Int. Ed.*, 2017, **56**(41), 12460–12465.

393 Q. Ye, J. Hu, P. Cheng and Z. Ma, Design trade-offs among shunt current, pumping loss and compactness in the piping system of a multi-stack vanadium flow battery, *J. Power Sources*, 2015, **296**, 352–364, available from: https://linkinghub.elsevier.com/retrieve/pii/S0378775315300306.

394 P. Alotto, M. Guarnieri and F. Moro, Redox flow batteries for the storage of renewable energy: A review, *Renew. Sustain. Energy Rev.*, 2014, **29**, 325–335, available from: https://linkinghub.elsevier.com/retrieve/pii/S1364032113005418.

395 M. Katz, Analysis of Electrolyte Shunt Currents in Fuel Cell Power Plants, *J. Electrochem. Soc.*, 1978, **125**(4), 515–520, available from: https://iopscience.iop.org/article/10.1149/1.2131488.

396 Y.-S. Chen, S.-Y. Ho, H.-W. Chou and H.-J. Wei, Modeling the effect of shunt current on the charge transfer efficiency of an all-vanadium redox flow battery, *J. Power Sources*, 2018, **390**, 168–175, available from: https://linkinghub.elsevier.com/retrieve/pii/S0378775318303859.

397 M. Skyllas-Kazacos, J. McCann, Y. Li, J. Bao and A. Tang, The Mechanism and Modelling of Shunt Current in the Vanadium Redox Flow Battery, *ChemistrySelect*, 2016, **1**(10), 2249–2256, available from: https://onlinelibrary.wiley.com/doi/10.1002/slct.201600432.

398 A. Tang, J. McCann, J. Bao and M. Skyllas-Kazacos, Investigation of the effect of shunt current on battery efficiency and stack temperature in vanadium redox flow battery, *J. Power Sources*, 2013, **242**, 349–356, available from: https://linkinghub.elsevier.com/retrieve/pii/S0378775313008690.

399 A. Clemente and R. Costa-Castelló, Redox flow batteries: A literature review oriented to automatic control, *Energies*, 2020, **13**(17), 1–31.

400 K. C. Smith, V. E. Brunini, Y. Dong, Y.-M. Chiang and W. C. Carter, Electroactive-Zone Extension in Flow-Battery Stacks, *Electrochim. Acta*, 2014, **147**, 460–469, available from: https://linkinghub.elsevier.com/retrieve/pii/S0013468614019392.

401 M. Skyllas-Kazacos, D. Kasherman, D. R. Hong and M. Kazacos, Characteristics and performance of 1 kW UNSW vanadium redox battery, *J. Power Sources*, 1991, **35**(4), 399–404, available from: https://linkinghub.elsevier.com/retrieve/pii/0378775391800586.

402 P. Zhao, H. Zhang, H. Zhou, J. Chen, S. Gao and B. Yi, Characteristics and performance of 10kW class all-vanadium redox-flow battery stack, *J. Power Sources*, 2006, **162**(2), 1416–1420, available from: https://linkinghub.elsevier.com/retrieve/pii/S037877530601562X.

403 D.-J. Park, K.-S. Jeon, C.-H. Ryu and G.-J. Hwang, Performance of the all-vanadium redox flow battery stack, *J. Ind. Eng. Chem.*, 2017, **45**, 387–390, available from: https://linkinghub.elsevier.com/retrieve/pii/S1226086X16303860.

404 X. Wu, X. Yuan, Z. Wang, J. Liu, Y. Hu, Q. Deng, *et al.*, Electrochemical performance of 5 kW all-vanadium redox flow battery stack with a flow frame of multi-distribution channels, *J. Solid State Electrochem.*, 2017, **21**(2), 429–435, available from: http://link.springer.com/10.1007/s10008-016-3361-x.

405 Vanitec Transforming Possibilities VRFBC, *Vanadium redox flow battery companies*, 2020, available from: http://www.vanitec.org/vanadium-redox-flow-battery-vrfb-companies.

406 H. Zhang, Progress and perspectives of flow battery technologies, *Curr. Opin. Electrochem.*, 2019, **18**, 123–125, available from: https://linkinghub.elsevier.com/retrieve/pii/S2451910319300882.

407 T. Kenning. *Round-Up: 60 MWh Japan Project, Northern Ireland's 10MW Array and Imergy Goes for Africa Teleco*, Solar Media Ltd, London, UK, 2015.

408 F. Gesellschaft, *An Affordable Way to Store Clean Energy*, 2019, available from: https://www.fraunhofer.de.

409 VanadiumCorp, *Where now for the world's largest energy storage battery in China?*, 2020, available from: https://www.vanadiumcorp.com/news/industry/where-now-for-the-worlds-largest-energy-storage-battery-in-china/.

410 P. C. Butler, P. A. Eidler, P. G. Grimes, S. E. Klassen and R. C. Miles, Zinc/bromine batteries, in *Handbook of Batteries*, McGraw-Hill, New york, 3rd edn, 2002.

411 R. Chen, S. Kim and Z. Chang, Redox Flow Batteries: Fundamentals and Applications, in *Redox - Principles and Advanced Applications*, InTech, 2017, available from: http://www.intechopen.com/books/redox-principles-and-advanced-applications/redox-flow-batteries-fundamentals-and-applications.

412 N. Tokuda, M. Furuya, Y. Kikuoko, Y. Tsutui, T. Kumamoto and T. Kanno, Development of a redox flow (RF) battery for energy storage, in *Proceedings of the Power Conversion Conference-Osaka 2002* (Cat. No. 02TH8579). In: Proceedings of the Power Conversion Conference-Osaka 2002 (Cat No. 02TH8579) PCCON-02, IEEE, 2002, available from: http://ieeexplore.ieee.org/document/997539/.

413 S. E. Group. *Redox Flow Battery*, 2005, available from: https://sei-innovation.com/energy/.

414 UniEnergy techonologies, 2020, available from: https://uetechnologies.com.

415 Ltd DC thermoelectric GC, Development DRPT, *State-owned assets supervision and administration commission of the people's government of dalian*, available from: http://www.gzw.dl.gov.cn/news/view_86238.html.
416 U.S. Department of Energy, *Grid Energy Storage Report*, 2013, December, p. 67. Available from: http://energy.gov/sites/prod/files/2014/09/f18/GridEnergyStorageDecember2013.pdf.
417 D. G. Kwabi, Y. Ji and M. J. Aziz, Electrolyte Lifetime in Aqueous Organic Redox Flow Batteries: A Critical Review, *Chem. Rev.*, 2020, **120**(14), 6467–6489.
418 J. Fu, M. Zheng, X. Wang, J. Sun and T. Wang, Flow-Rate Optimization and Economic Analysis of Vanadium Redox Flow Batteries in a Load-Shifting Application, *J. Energy Eng.*, 2017, **143**(6), 1–13.
419 F. Baccino, S. Grillo, M. Marinelli, S. Massucco and F. Silvestro, Power and energy control strategies for a Vanadium Redox Flow Battery and wind farm combined system, *2011 2nd IEEE PES International Conference and Exhibition on Innovative Smart Grid Technologies*, 2011, pp. 1–8, DOI: 10.1109/ISGTEurope.2011.6162658.
420 J. D. Milshtein, R. M. Darling, J. Drake, M. L. Perry and F. R. Brushett, The critical role of supporting electrolyte selection on flow battery cost, *J. Electrochem. Soc.*, 2017, **164**(14), A3883–A3895.
421 M. L. Perry and A. Z. Weber, Advanced redox-flow batteries: A perspective, *J. Electrochem. Soc.*, 2016, **163**(1), A5064–A5067.
422 C. Minke and T. Turek, Economics of vanadium redox flow battery membranes, *J. Power Sources*, 2015, **286**, 247–257, DOI: 10.1016/j.jpowsour.2015.03.144.
423 A. Tang, J. Bao and M. Skyllas-Kazacos, Studies on pressure losses and flow rate optimization in vanadium redox flow battery, *J. Power Sources*, 2014, **248**, 154–162, DOI: 10.1016/j.jpowsour.2013.09.071.
424 M. Skyllas-Kazacos and M. Kazacos, State of charge monitoring methods for vanadium redox flow battery control, *J. Power Sources*, 2011, **196**(20), 8822–8827, DOI: 10.1016/j.jpowsour.2011.06.080.
425 X. Ma, H. Zhang, C. Sun, Y. Zou and T. Zhang, An optimal strategy of electrolyte flow rate for vanadium redox flow battery, *J. Power Sources*, 2012, **203**, 153–158, DOI: 10.1016/j.jpowsour.2011.11.036.
426 A. A. Akhil, G. Huff, A. B. Currier, J. Hernandez, D. A. Bender and B. C. Kaun, *et al.*, *DOE/EPRI Electricity Storage Handbook in Collaboration with NRECA*, 2016, available from: http://www.osti.gov/servlets/purl/1431469/.
427 S. N. Lvov, *Introduction to Electrochemical Science and Engineering*, CRC Press, 2014, p. 339.
428 A. J. Bard, L. R. Faulkner, J. Leddy and C. G. Zoski, *Electrochemical Methods: Fundamentals and Applications*, Wiley, New York, 2nd edn, 2008, p. 864.
429 R. G. Kelly, J. R. Scully, D. Shoesmith and R. G. Buchheit, *Electrochemical Techniques in Corrosion Science and Engineering*, CRC Press, 2002, p. 440.
430 Y. A. Gandomi, D. S. Aaron, T. A. Zawodzinski and M. M. Mench, In situ potential distribution measurement and validated model for all-vanadium redox flow battery, *J. Electrochem. Soc.*, 2016, **163**(1), A5188–A5201.
431 F. Rahman and M. Skyllas-Kazacos, Vanadium redox battery: Positive half-cell electrolyte studies, *J. Power Sources*, 2009, **189**(2), 1212–1219.
432 X. Yuan, H. Wang, J. Colin Sun and J. Zhang, AC impedance technique in PEM fuel cell diagnosis-A review, *Int. J. Hydrogen Energy*, 2007, **32**(17), 4365–4380.
433 C. N. Sun, F. M. Delnick, D. S. Aaron, A. B. Papandrew, M. M. Mench and T. A. Zawodzinski, Probing electrode losses in all-vanadium redox flow batteries with impedance spectroscopy, *ECS Electrochem Lett.*, 2013, **2**(5), 2013–2015.
434 C.-N. Sun, F. M. Delnick, D. S. Aaron, A. B. Papandrew, M. M. Mench and T. A. Zawodzinski, Resolving Losses at the Negative Electrode in All-Vanadium Redox Flow Batteries Using Electrochemical Impedance Spectroscopy, *J. Electrochem. Soc.*, 2014, **161**(6), A981–A988, available from: https://iopscience.iop.org/article/10.1149/2.045406jes.
435 B. Yang, L. Hoober-Burkhardt, F. Wang, G. K. Surya Prakash and S. R. Narayanan, An Inexpensive Aqueous Flow Battery for Large-Scale Electrical Energy Storage Based on Water-Soluble Organic Redox Couples, *J. Electrochem. Soc.*, 2014, **161**(9), A1371–A1380, available from: https://iopscience.iop.org/article/10.1149/2.1001409jes.
436 H. H. Dewage, V. Yufit and N. P. Brandon, Study of Loss Mechanisms Using Half-Cell Measurements in a Regenerative Hydrogen Vanadium Fuel Cell, *J. Electrochem. Soc.*, 2016, **163**(1), A5236–A5243, available from: https://iopscience.iop.org/article/10.1149/2.0301601jes.
437 A. A. Shinkle, A. E. S. Sleightholme, L. D. Griffith, L. T. Thompson and C. W. Monroe, Degradation mechanisms in the non-aqueous vanadium acetylacetonate redox flow battery, *J. Power Sources*, 2012, **206**, 490–496, available from: https://linkinghub.elsevier.com/retrieve/pii/S0378775311000620.
438 D. Aaron, Z. Tang, A. B. Papandrew and T. A. Zawodzinski, Polarization curve analysis of all-vanadium redox flow batteries, *J. Appl. Electrochem.*, 2011, **41**(10), 1175–1182.
439 S. Kumar and S. Jayanti, Effect of flow field on the performance of an all-vanadium redox flow battery, *J. Power Sources*, 2016, **307**, 782–787, DOI: 10.1016/j.jpowsour.2016.01.048.
440 X. Li, J. Xiong, A. Tang, Y. Qin, J. Liu and C. Yan, Investigation of the use of electrolyte viscosity for online state-of-charge monitoring design in vanadium redox flow battery, *Appl. Energy*, 2018, **211**(2017), 1050–1059, DOI: 10.1016/j.apenergy.2017.12.009.
441 T. Jyothi Latha and S. Jayanti, Hydrodynamic analysis of flow fields for redox flow battery applications Batteries, *J Appl lectrochem*, 2014, **44**(9), 995–1006.
442 M. Messaggi, P. Canzi, R. Mereu, A. Baricci, F. Inzoli, A. Casalegno, *et al.*, Analysis of flow field design on vanadium redox flow battery performance: Development

of 3D computational fluid dynamic model and experimental validation, *Appl. Energy*, 2018, **228**(June), 1057–1070.

443 C. Yin, Y. Gao, S. Guo and H. Tang, A coupled three dimensional model of vanadium redox flow battery for flow field designs, *Energy*, 2014, **74**(C), 886–895, DOI: 10.1016/j.energy.2014.07.066.

444 J. Q. Chen, B. G. Wang and H. L. Lv, Numerical simulation and experiment on the electrolyte flow distribution for all vanadium redox flow battery, *Adv. Mater. Res.*, 2011, **236–238**, 604–607.

445 J. Houser, J. Clement, A. Pezeshki and M. M. Mench, Influence of architecture and material properties on vanadium redox flow battery performance, *J. Power Sources*, 2016, **302**, 369–377, DOI: 10.1016/j.jpowsour.2015.09.095.

446 H. Tanaka, Y. Miyafuji, J. Fukushima, T. Tayama, T. Sugita, M. Takezawa, *et al.*, Visualization of flow patterns in a cell of redox flow battery by infrared thermography, *J. Energy Storage*, 2018, **19**, 67–72, DOI: 10.1016/j.est.2018.07.009.

447 N. Bevilacqua, L. Eifert, R. Banerjee, K. Köble, T. Faragó, M. Zuber, *et al.*, Visualization of electrolyte flow in vanadium redox flow batteries using synchrotron X-ray radiography and tomography – Impact of electrolyte species and electrode compression, *J. Power Sources*, 2019, **439**, 227071, DOI: 10.1016/j.jpowsour.2019.227071.

448 A. Bertei, V. Yufit, F. Tariq and N. P. Brandon, A novel approach for the quantification of inhomogeneous 3D current distribution in fuel cell electrodes, *J. Power Sources*, 2018, **396**, 246–256, available from: https://linkinghub.elsevier.com/retrieve/pii/S0378775318306256.

449 T. M. M. Heenan, C. Tan, J. Hack, D. J. L. Brett and P. R. Shearing, Developments in X-ray tomography characterization for electrochemical devices, *Mater Today*, 2019, **31**, 69–85, available from: https://linkinghub.elsevier.com/retrieve/pii/S1369702119303396.

450 F. Tariq, J. Rubio-Garcia, V. Yufit, A. Bertei, B. K. Chakrabarti, A. Kucernak, *et al.*, Uncovering the mechanisms of electrolyte permeation in porous electrodes for redox flow batteries through real time in situ 3D imaging, *Sustain. Energy Fuels*, 2018, **2**(9), 2068–2080, available from: http://xlink.rsc.org/?DOI=C8SE00174J.

451 M. D. R. Kok, R. Jervis, D. Brett, P. R. Shearing and J. T. Gostick, Insights into the Effect of Structural Heterogeneity in Carbonized Electrospun Fibrous Mats for Flow Battery Electrodes by X-Ray Tomography, *Small*, 2018, **14**(9), 1703616, available from: https://onlinelibrary.wiley.com/doi/10.1002/smll.201703616.

452 R. Jervis, M. D. R. Kok, J. Montagut, J. T. Gostick, D. J. L. Brett and P. R. Shearing, X-ray Nano Computed Tomography of Electrospun Fibrous Mats as Flow Battery Electrodes, *Energy Technol*, 2018, **6**(12), 2488–2500, available from: https://onlinelibrary.wiley.com/doi/10.1002/ente.201800338.

453 M. D. R. Kok, R. Jervis, T. G. Tranter, M. A. Sadeghi, D. J. L. Brett, P. R. Shearing, *et al.*, Mass transfer in fibrous media with varying anisotropy for flow battery electrodes: Direct numerical simulations with 3D X-ray computed tomography, *Chem. Eng. Sci.*, 2019, **196**, 104–115, available from: https://linkinghub.elsevier.com/retrieve/pii/S0009250918307711.

454 P. Trogadas, O. O. Taiwo, B. Tjaden, T. P. Neville, S. Yun, J. Parrondo, *et al.*, X-ray micro-tomography as a diagnostic tool for the electrode degradation in vanadium redox flow batteries, *Electrochem. Commun.*, 2014, **48**, 155–159, available from: https://linkinghub.elsevier.com/retrieve/pii/S1388248114002975.

455 R. Jervis, M. D. R. Kok, T. P. Neville, Q. Meyer, L. D. Brown, F. Iacoviello, *et al.*, In situ compression and X-ray computed tomography of flow battery electrodes, *J Energy Chem*, 2018, **27**(5), 1353–1361, available from: https://linkinghub.elsevier.com/retrieve/pii/S2095495617311956.

456 J. Rubio-Garcia, A. Kucernak and A. Charleson, Direct visualization of reactant transport in forced convection electrochemical cells and its application to redox flow batteries, *Electrochem. Commun.*, 2018, **93**, 128–132, DOI: 10.1016/j.elecom.2018.07.002.

457 A. A. Wong, M. J. Aziz and S. M. Rubinstein, Direct visualization of electrochemical reactions and comparison of commercial carbon papers in operando by fluorescence microscopy using a quinone-based flow, *ECS Trans.*, 2017, **77**(11), 153–161.

458 G. J. Hwang and H. Ohya, Preparation of cation exchange membrane as a separator for the all-vanadium redox flow battery, *J. Membr. Sci.*, 1996, **120**(1), 55–67.

459 Q. Liu, A. Turhan, T. A. Zawodzinski and M. M. Mench, In situ potential distribution measurement in an all-vanadium flow battery, *Chem. Commun.*, 2013, **49**(57), 6292–6294.

460 T. Gerber, P. Fischer, K. Pinkwart and J. Tübke, Segmented printed circuit board electrode for locally-resolved current density measurements in all-vanadium redox flow batteries, *Batteries*, 2019, **5**(2), 38, DOI: 10.3390/batteries5020038.

461 K. Ma, Y. Zhang, L. Liu, J. Xi, X. Qiu, T. Guan, *et al.*, In situ mapping of activity distribution and oxygen evolution reaction in vanadium flow batteries, *Nat. Commun.*, 2019, **10**(1), 1–11, DOI: 10.1038/s41467-019-13147-9.

462 A. B. Geiger, R. Eckl, A. Wokaun and G. G. Scherer, An Approach to Measuring Locally Resolved Currents in Polymer Electrolyte Fuel Cells, *J. Electrochem. Soc.*, 2004, **151**(3), 394–398.

463 J. J. Hwnag, W. R. Chang, R. G. Peng, P. Y. Chen and A. Su, Experimental and numerical studies of local current mapping on a PEM fuel cell, *Int. J. Hydrogen Energy*, 2008, **33**(20), 5718–5727, DOI: 10.1016/j.ijhydene.2008.07.035.

464 W. Y. Hsieh, C. H. Leu, C. H. Wu and Y. S. Chen, Measurement of local current density of all-vanadium redox flow batteries, *J. Power Sources*, 2014, **271**, 245–251, DOI: 10.1016/j.jpowsour.2014.06.081.

465 J. T. Clement, T. A. Zawodzinski and M. M. Mench, Measurement of localized current distribution in

a vanadium redox flow battery, *ECS Trans.*, 2013, **58**(37), 9–16.

466 J. T. Clement, D. S. Aaron and M. M. Mench, In situ localized current distribution measurements in all-vanadium redox flow batteries, *J. Electrochem. Soc.*, 2016, **163**(1), A5220–A5228.

467 M. Becker, N. Bredemeyer, N. Tenhumberg and T. Turek, Polarization curve measurements combined with potential probe sensing for determining current density distribution in vanadium redox-flow batteries, *J. Power Sources*, 2016, **307**, 826–833, available from: https://linkinghub.elsevier.com/retrieve/pii/S0378775316300118.

468 H.-H. Perkampus, *UV-VIS Spectroscopy and its Applications*, Springer Science & Business Media, 2013, p. 244.

469 L. Tong, Q Chen, A. A. Wong, R. Gómez-Bombarelli, A. Aspuru-Guzik, R. G. Gordon, *et al.*, UV-Vis spectrophotometry of quinone flow battery electrolyte for: In situ monitoring and improved electrochemical modeling of potential and quinhydrone formation, *Phys. Chem. Chem. Phys.*, 2017, **19**(47), 31684–31691.

470 K. H. Shin, C. S. Jin, J. Y. So, S. K. Park, D. H. Kim and S. H. Yeon, Real-time monitoring of the state of charge (SOC) in vanadium redox-flow batteries using UV–Vis spectroscopy in operando mode, *J. Energy Storage*, 2020, **27**, 101066, DOI: 10.1016/j.est.2019.101066.

471 T. C. Gokoglan, S. K. Pahari, A. Hamel, R. Howland, P. J. Cappillino and E. Agar, Operando spectroelectrochemical characterization of a highly stable bioinspired redox flow battery active material, *J. Electrochem. Soc.*, 2019, **166**(10), A1745–A1751.

472 G. Bauer, J. Drobits, C. Fabjan, H. Mikosch and P. Schuster, Raman spectroscopic study of the bromine storing complex phase in a zinc-flow battery, *J. Electroanal. Chem.*, 1997, **427**(1–2), 123–128.

473 J. D. Jeon, H. S. Yang, J. Shim, H. S. Kim and J. H. Yang, Dual function of quaternary ammonium in Zn/Br redox flow battery: Capturing the bromine and lowering the charge transfer resistance, *Electrochim. Acta*, 2014, **127**, 397–402, DOI: 10.1016/j.electacta.2014.02.073.

474 N. Kausar, R. Howe and M. Skyllas-Kazacos, Raman spectroscopy studies of concentrated vanadium redox battery positive electrolytes, *J. Appl. Electrochem.*, 2001, **31**(12), 1327–1332.

475 W. Kautek, A. Conradi, M. Sahre, C. Fabjan, J. Drobits, G. Bauer, *et al.*, In situ investigations of bromine-storing complex formation in a zinc-flow battery at gold electrodes, *J. Electrochem. Soc.*, 1999, **146**(9), 3211–3216.

476 C. N. Sun, F. M. Delnick, L. Baggetto, G. M. Veith and T. A. Zawodzinski, Hydrogen evolution at the negative electrode of the all-vanadium redox flow batteries, *J. Power Sources*, 2014, **248**, 560–564, DOI: 10.1016/j.jpowsour.2013.09.125.

477 H. Liu, Q. Xu and C. Yan, On-line mass spectrometry study of electrochemical corrosion of the graphite electrode for vanadium redox flow battery, *Electrochem. Commun.*, 2013, **28**, 58–62, DOI: 10.1016/j.elecom.2012.12.011.

478 A. M. Kosswattaarachchi, A. E. Friedman and T. R. Cook, Characterization of a BODIPY Dye as an Active Species for Redox Flow Batteries, *ChemSusChem*, 2016, **9**(23), 3317–3323.

479 C. Jia, J. Liu and C. Yan, A multilayered membrane for vanadium redox flow battery, *J. Power Sources*, 2012, **203**, 190–194, DOI: 10.1016/j.jpowsour.2011.10.102.

480 D. H. Ye and Z. G. Zhan, A review on the sealing structures of membrane electrode assembly of proton exchange membrane fuel cells, *J. Power Sources*, 2013, **231**, 285–292, DOI: 10.1016/j.jpowsour.2013.01.009.

481 E. H. Majlan, D. Rohendi, W. R. W. Daud, T. Husaini and M. A. Haque, Electrode for proton exchange membrane fuel cells: A review, *Renew. Sustain. Energy Rev.*, 2018, **89**, 117–134, DOI: 10.1016/j.rser.2018.03.007.

482 F. Barbir, A. Basile and T. N. Veziroğlu, Compendium of Hydrogen Energy, *Hydrogen Energy Conversion*, Elsevier, 2016, vol. 3, p. 328.

483 K. Noda and Y. Hiroshige, Ion exchange membrane and method of producing same, membrane electrode assembly, and redox flow battery, *US Pat.,*2019/0259509A1, 2019, vol. 1, p. 13.

484 B. T. Weber, B. A. Bartling, O. S. Yordem, J. E. Abulu, A. T. Haug and G. M. Haugen, *et al.*, Membrane electrode-assmeblies and electrochemical cells and liquid flow batteries therefrom, *US Pat.,*2019/0181461A1, 2019, vol. 1, p. 49.

485 Q. Huang, H. Li, M. Grätzel and Q. Wang, Reversible chemical delithiation/lithiation of LiFePO4: Towards a redox flow lithium-ion battery, *Phys. Chem. Chem. Phys.*, 2013, **15**(6), 1793–1797.

486 S. Gentil, D. Reynard and H. H. Girault, Aqueous organic and redox-mediated redox flow batteries: a review, *Curr. Opin. Electrochem.*, 2020, **21**, 7–13, DOI: 10.1016/j.coelec.2019.12.006.

487 M. Zhou, Q. Huang, T. N. Pham Truong, J. Ghilane, Y. G. Zhu, C. Jia, *et al.*, Nernstian-Potential-Driven Redox-Targeting Reactions of Battery Materials, *Chem*, 2017, **3**(6), 1036–1049, DOI: 10.1016/j.chempr.2017.10.003.

488 Q. Huang, J. Yang, C. B. Ng, C. Jia and Q. Wang, A redox flow lithium battery based on the redox targeting reactions between LiFePO4 and iodide, *Energy Environ. Sci.*, 2016, **9**(3), 917–921.

489 G. Li, L. Yang, X. Jiang, T. Zhang, H. Lin, Q. Yao, *et al.*, A multi-electron redox mediator for redox-targeting lithium-sulfur flow batteries, *J. Power Sources*, 2018, **378**(2017), 418–422, DOI: 10.1016/j.jpowsour.2017.11.066.

490 L. Fan, C. Jia, Y. G. Zhu and Q. Wang, Redox targeting of prussian blue: Toward low-cost and high energy density redox flow battery and solar rechargeable battery, *ACS Energy Lett.*, 2017, **2**(3), 615–621.

491 E. Zanzola, C. R. Dennison, A. Battistel, P. Peljo, H. Vrubel, V. Amstutz, *et al.*, Redox Solid Energy Boosters for Flow Batteries: Polyaniline as a Case Study, *Electrochim. Acta*, 2017, **235**, 664–671, DOI: 10.1016/j.electacta.2017.03.084.

492 L. Cao, M. Skyllas-Kazacos and D.-W. Wang, Solar Redox Flow Batteries: Mechanism, Design, and Measurement, *Adv. Sustain. Syst.*, 2018, **2**(8–9), 1800031.

493 J. Azevedo, T. Seipp, J. Burfeind, C. Sousa, A. Bentien, J. P. Araújo, *et al.*, Unbiased solar energy storage: Photoelectrochemical redox flow battery, *Nano Energy*, 2016, **22**, 396–405.

494 K. Wedege, D. Bae, E. Dražević, A. Mendes, P. C. K. Vesborg and A. Bentien, Unbiased, complete solar charging of a neutral flow battery by a single Si photocathode, *RSC Adv.*, 2018, **8**(12), 6331–6340.

495 B. Kim, J. Y. Seo and C. H. Chung, A hybrid system of capacitive deionization and redox flow battery for continuous desalination and energy storage, *J. Power Sources*, 2020, **448**(June), 227384.

496 C. Jiang, A. W. Nichols, J. F. Walzer and C. W. MacHan, Electrochemical CO2 Reduction in a Continuous Non-Aqueous Flow Cell with [Ni(cyclam)]2+, *Inorg. Chem.*, 2020, **59**(3), 1883–1892, DOI: 10.1021/acs.inorgchem.9b03171.

497 Y. Ding, C. Zhang, L. Zhang, Y. Zhou and G. Yu, Molecular engineering of organic electroactive materials for redox flow batteries, *Chem. Soc. Rev.*, 2018, **47**(1), 69–103.

498 V. Singh, S. Kim, J. Kang and H. R. Byon, Aqueous organic redox flow batteries, *Nano Res.*, 2019, **12**(9), 1988–2001.

499 T. Hagemann, J. Winsberg, B. Häupler, T. Janoschka, J. J. Gruber, A. Wild, *et al.*, A bipolar nitronyl nitroxide small molecule for an all-organic symmetric redox-flow battery, *NPG Asia Mater*, 2017, **9**, e340, DOI: 10.1038/am.2016.195.

500 J. Winsberg, C. Stolze, S. Muench, F. Liedl, M. D. Hager and U. S. Schubert, TEMPO/Phenazine Combi-Molecule: A Redox-Active Material for Symmetric Aqueous Redox-Flow Batteries, *ACS Energy Lett.*, 2016, **1**(5), 976–980.

501 Y. Zhu, F. Yang, Z. Niu, H. Wu, Y. He, H. Zhu, *et al.*, Enhanced cyclability of organic redox flow batteries enabled by an artificial bipolar molecule in neutral aqueous electrolyte, *J. Power Sources*, 2019, **417**, 83–89, DOI: 10.1016/j.jpowsour.2019.02.021.

502 A. Ambrosi and R. D. Webster, 3D-printing for aqueous and non-aqueous redox flow batteries, *Curr. Opin. Electrochem*, 2020, **20**, 28–35, DOI: 10.1016/j.coelec.2020.02.005.

503 K. Percin, A. Rommerskirchen, R. Sengpiel, Y. Gendel and M. Wessling, 3D-printed conductive static mixers enable all-vanadium redox flow battery using slurry electrodes, *J. Power Sources*, 2018, **379**(2017), 228–233.

504 L. F. Arenas, F. C. Walsh and C. P. de León, 3D-Printing of Redox Flow Batteries for Energy Storage: A Rapid Prototype Laboratory Cell, *ECS J Solid State Sci Technol*, 2015, **4**(4), P3080–P3085.

505 J. Lobato, J. Oviedo, P. Cañizares, M. A. Rodrigo and M. Millán, Impact of carbonaceous particles concentration in a nanofluidic electrolyte for vanadium redox flow batteries, *Carbon*, 2020, **156**, 287–298.

506 S. Park, H. Lee, H. J. Lee and H. Kim, New hybrid redox flow battery with high energy density using V–Mn/V–Mn multiple redox couples, *J. Power Sources*, 2020, **451**, 227746.

507 W. Wang, L. Li, Z. Nie, B. Chen, Q. Luo, Y. Shao, *et al.*, A new hybrid redox flow battery with multiple redox couples, *J. Power Sources*, 2012, **216**, 99–103.

508 Y. Zhang, W. Liu, Z. Wang, Y. M. Shen, W. Wang, Z. Chen, *et al.*, Tetrapyridophenazine/graphene composites for aqueous hybrid flow battery anodes with long cycle life, *Carbon*, 2020, **161**, 309–315.

509 X. Ke, J. M. Prahl, J. I. D. Alexander and R. F. Savinell, Mathematical Modeling of Electrolyte Flow in a Segment of Flow Channel over Porous Electrode Layered System in Vanadium Flow Battery with Flow Field Design, *Electrochim. Acta*, 2017, **223**, 124–134, available from: https://linkinghub.elsevier.com/retrieve/pii/S0013468616325579.